

Effects of radiotherapy and hyperbaric oxygen therapy on oral microcirculation

Renée Helmers

Effects of radiotherapy and hyperbaric oxygen therapy on oral microcirculation

Renée Helmers

Publication of this thesis was financially supported by:



Copyright © 2022 by Renée Helmers

All rights reserved.

ISBN/EAN: 978-94-6332-819-7

Cover design and lay-out: Ferdinand van Nispen tot Pannerden, my-thesis.nl

Cover: illustration by Jadranka Strbac

Printed by proefschriften.nl

Effects of radiotherapy and hyperbaric oxygen therapy on oral microcirculation

ACADEMISCH PROEFSCHRIFT

ter verkrijging van de graad van doctor

aan de Universiteit van Amsterdam

op gezag van de Rector Magnificus

prof. dr. ir. K.I.J. Maex

ten overstaan van een door het College voor Promoties ingestelde commissie,

in het openbaar te verdedigen in de Aula der Universiteit

op vrijdag 14 januari 2022, te 11.00 uur

door Renée Helmers

geboren te Amsterdam

PROMOTIECOMISSIE

Promotores

prof. dr. J. de Lange

Universiteit van Amsterdam

prof. dr. L.E. Smeele

Universiteit van Amsterdam

Copromotor

dr. D.M.J. Milstein

Universiteit van Amsterdam

Overige leden

prof. dr. F.R. Rozema

Universiteit van Amsterdam

prof. dr. J.G.A.M. de Visscher

Vrije Universiteit Amsterdam

prof. dr. J. Klein Nulend

Vrije Universiteit Amsterdam

prof. dr. J.P.R. van Merkesteyn

Universiteit Leiden

prof. dr. W.S. Schlack

Universiteit van Amsterdam

prof. dr. L.J.A. Stalpers

Universiteit van Amsterdam

dr. J.A.H. Lindeboom

Universiteit van Amsterdam

Faculteit der Tandheelkunde

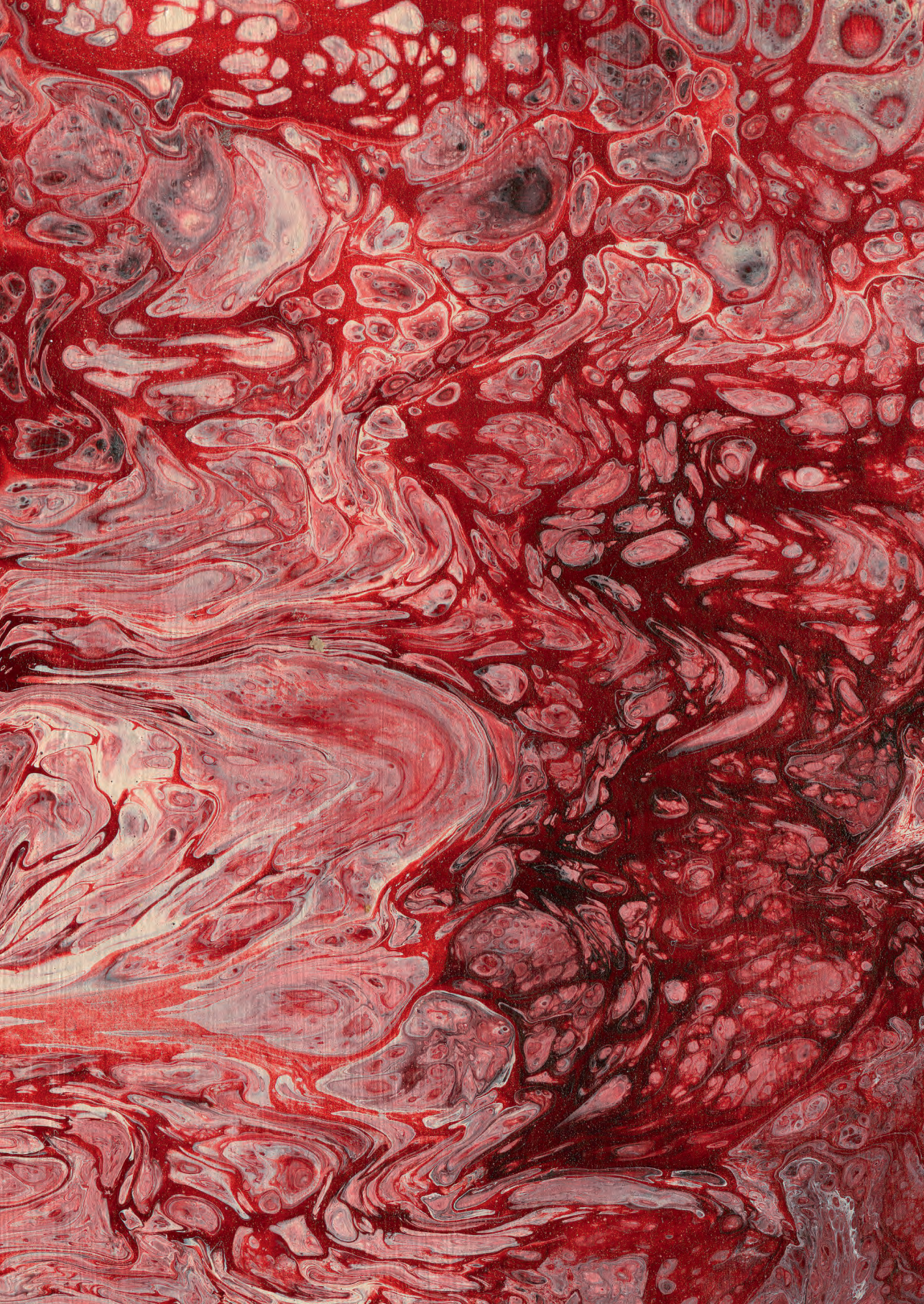
CONTENTS

CHAPTER 1	General introduction and outline of the thesis	9
PART I	PRECLINICAL STUDIES	21
CHAPTER 2	Sublingual microvascular perfusion is altered during normobaric and hyperbaric hyperoxia	23
CHAPTER 3	Hyperbaric oxygen therapy accelerates vascularization in keratinized oral mucosal surgical flaps	51
CHAPTER 4	Outcome of a rabbit model for late irradiation effects in mandibular oral mucosa and bone: a pilot study	71
PART II	CLINICAL STUDIES	93
CHAPTER 5	Patient-side appraisal of late radiation-induced oral microvascular changes	95
CHAPTER 6	Hyperbaric oxygen therapy redirects late irradiation injury in oral microcirculation towards healthy microvascular tissue state	113
CHAPTER 7	General discussion	131
CHAPTER 8	Summary	141
	Samenvatting	145
APPENDICES		149
	Contributing authors	150
	Chapter information	152
	List of publications	157
	Acknowledgements / dankwoord	159

LIST OF ABBREVIATIONS

\emptyset	diameter
\emptyset_{bv}	blood vessel diameter
$\Delta\emptyset_{bv}$	delta (change) blood vessel diameter
\emptyset_i	inner diameter
\emptyset_o	outer diameter
atm	standard atmosphere
ANOVA	analysis of variance
AVA	automated vascular analysis
AVI	audio video interleave
ATA	atmosphere absolute
BL	baseline
BMI	body mass index
CC	CytoCam
CCD	charge-coupled device
CRT	chemoradiotherapy
DBP	diastolic blood pressure
DC	direct current
DVI	digital video imaging
DOCT	Doppler optical coherence tomography
EDTA	ethylene diamine tetra-acetic acid
EU	European Union
EVG	Elastica van Gieson
FCD	functional capillary density
Fd	focal depth
FiO ₂	fraction of inspired oxygen
FOV	field of view
fps	frames per second
GA	gauge
Hb	hemoglobin
H&E	hematoxylin and eosin
HB	hyperbaric
HBO	hyperbaric oxygen
HBOT	hyperbaric oxygen therapy
HN	head and neck
HNCP(s)	head and neck cancer patient(s)

HR	heart rate
HVM	hand-held vital microscopy
IVM	intravital microscopy
HBO _m	intrabarochamber measurement
ICC	intraclass correlation coefficient
IDFI	incident dark-field imaging
IR	irradiation
iv	intravenous
LRTI	Late radiation tissue injury
LCD	liquid crystal display
LDF	lase Doppler flowmetry
LDI	laser Doppler imaging
LED	light emitting diode
MAP	mean arterial pressure
MFI	microvascular flow index
msw	meters of salt water
NB	normobaric
OPSI	orthogonal polarization spectral imaging
ORN	osteoradionecrosis
PMMA	polymethyl methacrylate
p _a CO ₂	partial pressure of carbon dioxide in arterial blood
p _a O ₂	partial pressure of oxygen in arterial blood
PPV	proportion of perfused vessels
PVD	perfused vessel density
RBC	red blood cell(s)
ROI	region of interest
RT	radiotherapy
sc	subcutaneous
SDF	sidestream dark-field
SDFI	sidestream dark-field imaging
SBP	systolic blood pressure
svOCT	speckle variance optical coherence tomography
SpO ₂	peripheral capillary oxygen saturation
sO ₂	oxygen saturation
TCD	total capillary density
TVD	total vessel density
VC	video capillaroscopy
WBC	white blood cell



The background of the entire page is a traditional marbled paper pattern. It features intricate, swirling, and cell-like designs in various shades of red, from deep crimson to light pink, interspersed with white and greyish-blue tones. The pattern is dense and organic, resembling stone or biological cells.

CHAPTER 1

GENERAL INTRODUCTION AND OUTLINE OF THE THESIS



RADIOTHERAPY SIDE EFFECTS IN HEAD AND NECK

In the Netherlands head and neck (HN) cancer has an incidence of 17 per 100,000 persons with an increasing 10-year survival rate over the last decades [the Netherlands Comprehensive Cancer Organization]. With this increasing survival rate long-term side effects of cancer treatment become more relevant as they negatively influence quality of life (QoL). Radiotherapy (RT) plays an important part in the treatment of HN malignancies and is known for inducing late side effects that develop over several months to years after treatment. Although RT regimen are aimed at protecting healthy tissue as much as possible, healthy peritumoral tissue will inevitably be affected to some extent.

Acute irradiation injury develops during the course of treatment and predominantly affects tissues with rapid cell division such as the oral mucosa, which can result in oral mucositis. Subsequent to the acute injury phase of oral mucositis, fibrin leaks into surrounding tissues driven by the release of vasoactive cytokines. Progression into the late injury state results in blockage of vascular lumen which induces tissue hypoperfusion and regional hypoxia.⁴³ It is not entirely clear if late tissue injury is caused by direct damage to mesenchymal cells, or indirectly through vascular injury or a combination of both.⁴³ In the 80's Marx proposed the 3 H's theory in which late irradiation damage in tissue is expressed in a hypovascular, hypocellular and hypoxic tissue state.^{23,24} More recent an alternative theory was proposed by Delanian et al. in which radiation-induced fibrosis caused fibroatrophy in soft tissue and bone by aberrant fibroblast activity and extracellular matrix disruption.⁹ This thesis will mainly focus on microvascular alterations associated with RT.

Late radiation tissue injury (LRTI) in the HN region usually manifests from 3–6 months after start of RT and can result in damage to salivary glands, dentition, periodontium, oral mucosa, muscles, nerves, cartilage and bone.^{7,38,43} The progress of radiation induced tissue deterioration can ultimately result in necrosis of soft tissue, cartilage and bone (osteoradionecrosis (ORN)). The definition of ORN is described as “exposed and necrotic bone associated with ulcerated or necrotic surrounding soft tissue which persists for greater than 3 months in an area that had been previously irradiated (not caused by tumor recurrence)”.³² ORN in HN cancer patients has a reported incidence of 2–22%^{27,29,39} and is a feared late complication as it could lead to mutilation and severe impairment of function. Due to the compromised health state

of the tissue surrounding the necrosis, broad resection and often extensive reconstruction are required in these advanced and clinically complicated cases. The HN region is anatomically complex with many vital structures that are important in performing everyday functions such as speech, mastication, swallowing, innervation of facial muscles and esthetics that contribute to social interaction. Inevitably, impaired function in this region has a severe impact on QoL.^{6,19}

HYPERBARIC OXYGEN THERAPY

Hyperbaric oxygen therapy (HBOT) is extensively under investigation concerning its resuscitating potential in the field of tissue repair and regeneration.^{16,31,34} HBOT is described as breathing of 100% oxygen at a pressure above 1 atmosphere absolute (ATA). Oxygen tension level in blood plasma is elevated with the purpose of mobilizing oxygen to reach hypoxic tissue and induce neoangiogenesis. HBO treatment sessions for LRTI commonly has a duration of 90–120 minutes at 2–2.4 ATA and is administered on a daily basis. Although previous studies report contradicting results on the efficacy of HBOT, its angiogenic potential has been demonstrated *in vitro* and *in vivo* studies.^{16,22,34,36,41} Furthermore, evidence of moderate quality exists in support of HBOT improving outcomes associated with LRTI.^{3,33} However, treatment protocols and the efficacy of HBOT remain a matter of debate³³ and more research to determine timing and patient selection is needed.³

Prophylactic HBOT is given if surgical intervention (e.g., tooth extraction or implant placement) is required in previously irradiated tissue. Currently no specific patient selection is considered for administration of preventive HBOT as it is not clear in which patients LRTI will develop and when. However, some risk factors are identified such as fraction dose and health-related factors.^{11,28,38} Therapeutic HBOT is administered at the time that tissue breakdown is clinically visible and the underlying pathophysiology has progressed towards critical stage. A method for visualizing *in-vivo* microvascular status could contribute to the understanding of disease progression and monitor the effects of supportive therapies. The ability to examine and observe tissue function and anatomy and to be able to quantify these observations formed the basis and the starting point of this thesis.

ORAL MICROCIRCULATION

The microcirculation consisting of the smallest vessels in the circulatory system (<100 micrometers; e.g., arterioles, capillaries, venules) serves an important function in delivering and removing constituents to and from tissues. Gas exchange (CO_2 and O_2) and management of nutrients and waste products are prerequisites for maintaining tissue health and to resist or manage pathological processes. Derangement in microcirculation can jeopardize the healing capacity and consequently result in pathologies. Interpreting early alterations diagnostically in tissue microcirculation (organ, sublingual) is an ongoing goal in a broad field of research with the aim of defining clinical targets of therapy and timing of treatments at the patient bedside. By harnessing the diagnostic value of the microcirculation, it would be possible to improve microcirculatory indices and hereby patient outcome and treatment success.^{18,37,42} An advantage of the HN region is that the oral mucosa provides a direct window into the region of interest.

The oral mucosa lines the oral cavity and has varying thicknesses in epithelium (keratinized and non-keratinized) between the different oral tissues. The underlying connective tissue (lamina propria) consists of a papillary layer and a reticular layer. Ascending arterioles extend from the reticular layer of horizontal vascular network into the papillary layer, form capillary loops that arch towards the epithelium and then continue descending down into the venous system in the reticular layer and subsequently into submucosa. The submucosa consists of loose connective and fatty tissue, larger blood and lymphatic vessels, salivary glands and nerve fibers.

Different anatomic regions and their associated microcirculation can be identified when studying the oral cavity with handheld vital microscopy (HVM). Sprouting capillary loops originating from the deeper reticular layer are organized as an array of capillary loops below the epithelial surface and in the papillary layer of the lamina propria of the oral mucosa, e.g., the lip, the gingiva [Fig. 1] and the buccal lining mucosa [Fig. 2].



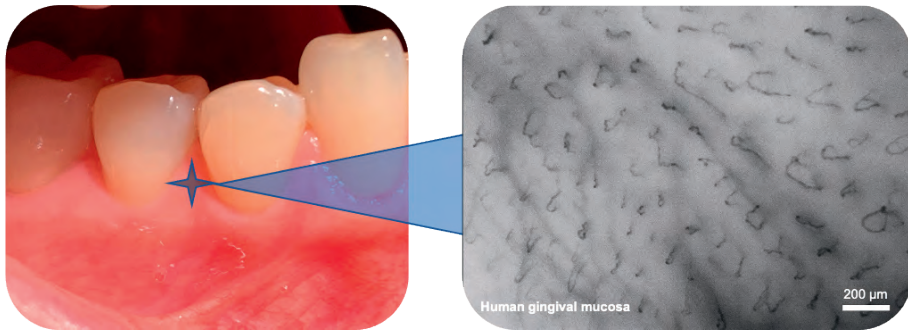


Figure 1. Handheld vital microscopy image of mandibular gingiva.

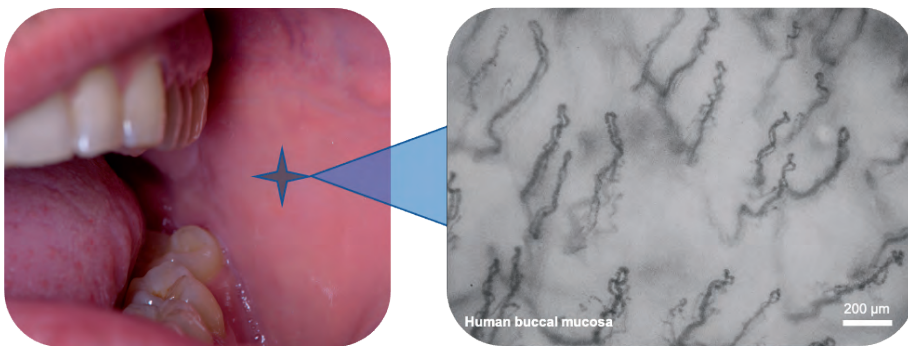


Figure 2. Handheld vital microscopy image of buccal mucosa.

In the sublingual region, capillary loops are also present but since the epithelium is thin the capillary loops are less visible and the underlying vascular bed arranged as a horizontal vascular network is visible instead in the reticular layer of the lamina propria [Fig. 3].

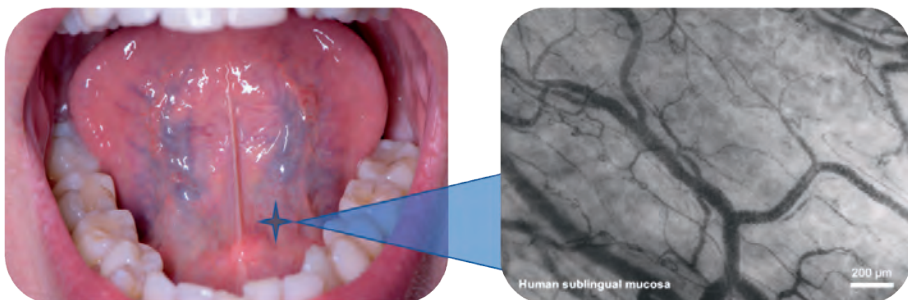


Figure 3. Handheld vital microscopy image of sublingual mucosa.

DEVELOPMENT OF BEDSIDE MICROCIRCULATION MONITORING TECHNIQUES



It is an ongoing challenge to develop suitable techniques to monitor and quantify the microcirculation at the patient-side. Several techniques exist and over the years they have assisted and facilitated clinicians and researchers with the ability to examine and investigate different aspects of the microcirculation. These established techniques range from routine static evaluation of microvascular tissue based on histology,⁴ estimation of tissue microvascular flow (e.g., laser Doppler flowmetry, laser speckle contrast imaging),^{15,40} tissue oxygenation (e.g., near-infrared spectroscopy)²¹ and direct microvascular visualization (e.g., intravital microscopy, optical coherence tomography, spectroscopy-based hand-held vital microscopy (e.g., orthogonal polarization spectral imaging, sidestream dark-field imaging, incident dark-field illumination imaging)).^{8,10,30} Bedside application and the potential to assess different microcirculatory parameters are essential for clinical evaluation of microvascular tissue overtime. HVM techniques evolved rapidly in the last 3 decades to meet clinical and diagnostic requirements associated with different medical specialties.

After introduction of incident dark-field (IDF) illumination for intravital microscopy in 1971, which provided a deeper field of illumination and visualization of erythrocytes below the surface,³⁵ devices to improve clinical applicability and image quality followed. Groner et al. developed the orthogonal polarization spectral (OPS) imaging technique (Cytoscan™, Cytometrics, Philadelphia, PA, USA).¹⁴ OPS has been validated against intravital microscopy in different settings showing significant correlation between parameters like red blood cell (RBC) velocity, vessel diameter and functional capillary density.⁵ Following OPS imaging an upgrade in the form of the sidestream dark-field (SDF) imaging device (MicroScan Video Microscope System, MicroVision Medical, Amsterdam, The Netherlands) was developed in 2007 by Goedhart et al. and again was validated against the OPS. The results of Goedhart et al. showed good comparative values for parameters like capillary diameters and RBC velocities between the two imaging devices with SDF imaging presenting a higher image quality in sublingual microcirculation versus OPS.¹³ SDF imaging used a new way of illumination by positioning LEDs at the tip and around the central light guide which prevents light reflections from tissue surface and improved contrasting. The illuminating outer core causes scattering which resulted in the illumination

of the microcirculation in the tissue. The absorption of LED lights in hemoglobin of the erythrocytes provides an image of RBCs in the microcirculation contrasted by a light background.¹³ SDF imaging also improved in clinical applicability by using low-power LED lights so that with the use of a battery pack the device is more mobile for ambulant use. Braedius Scientific introduced the third-generation device, the CytoCam (CC) Microscope System (Braedius Medical, Huizen, The Netherlands), a computer-controlled video microscopy imaging system with even higher image resolution and larger field of view.^{1,17,25} With a controllable focal depth it is easier to obtain images of different regions of interest by maintaining the right focus margin.²⁵ Additionally, the hardware of the CC offers online analyzing which brings diagnostics and analysis one step closer to realizing practical bedside application and therefore its clinical use. HVM techniques have previously been applied in oral and maxillofacial research.^{20,26}

HVM was able to enhance evaluation and examination of microcirculation heterogeneity in perfusion, microvascular density, flow and angiomorphology. These parameters collectively represent the microcirculatory state and can indicate perfusion (dys-)function. It has been proposed that heterogeneity in flow compromises O₂ distribution and therefore is less tolerated by tissues than diminished homogeneous flow in which extraction of O₂ from the blood supply is still possible.¹² For assessment of these parameters several methods were developed and validated for which consensus guidelines were established.²

OUTLINE OF THE THESIS

The aim of this thesis was to elucidate the effects of RT and HBOT independently on oral microcirculation in preclinical and clinical studies. In clinical studies the objective was to clarify aspects of LRTI in the oral microcirculation of HNCP and the subsequent resuscitating potential of HBOT. Furthermore, the feasibility of HVM (SDF and CC) in detecting RT and HBOT induced changes in the microcirculation was examined. It was hypothesized that RT elicits detectable microcirculatory derangement corresponding with a disturbed hemodynamic function and a hypovascular state. Furthermore, it was hypothesized that HBOT promotes compromised microvascular tissue towards healing or healthy microvascular tissue state.



This chapter (**Chapter 1**) provides a general introduction to ORN, RT, HBOT, the microcirculation and imaging techniques described in this thesis. In **Chapter 2** a model is presented in which the aim was to determine whether changes in the oral microcirculation of the sublingual mucosa could be measured under influence of changing normobaric and hyperbaric oxygenation settings. The hypothesis that was tested was whether the measured microcirculatory alterations were reversible. The experimental study presented in **Chapter 3** investigates the role of HBOT in advancing vascular regeneration in healing of oral mucosal flaps. A wound healing model was used to study and compare the temporal course of mucosal flap vascularization under normal and HBO conditions. In **Chapter 4** the onset of LRTI was evaluated overtime in rabbit mandibular mucosa and bone in a pilot IR model. The hypothesis was tested that cumulative IR dosages result in oral mucosal and mandibular bone histopathological changes corresponding to that of LRTI in humans.

In **Chapter 5** and **Chapter 6** two clinical studies are presented. In **Chapter 5** the pathophysiology associated with RT on the oral microcirculation is described and the clinical feasibility of patient-side assessment of late IR oral microvascular changes in HN cancer patients using the CC device was investigated. A final prospective study presents *in vivo* effects of HBOT on oral microvascular changes associated with late IR injury in HN cancer patients in **Chapter 6**. The tested hypothesis in this study was that HBOT redirects irradiated oral microcirculation parameters towards levels corresponding to healthy tissue.

All findings are presented and evaluated in the general discussion in **Chapter 7** ending with elaboration on future study perspectives. Finally, **Chapter 8** presents a general summary of this thesis in both English and Dutch.

REFERENCES

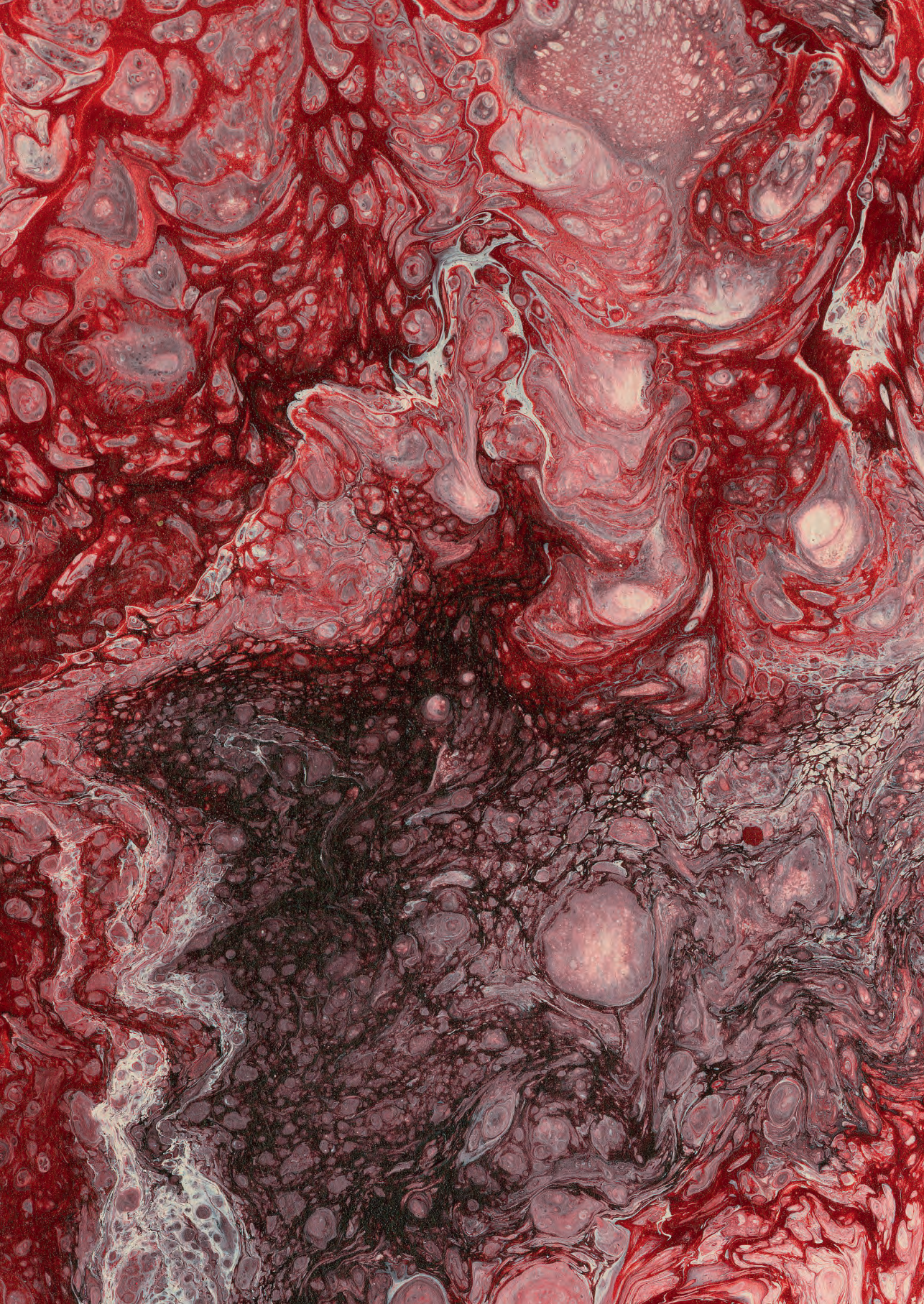
1. Aykut G, Veenstra G, Scorcella C, Ince C, Boerma C. Cytocam-IDF (incident dark field illumination) imaging for bedside monitoring of the microcirculation. *Intensive Care Med* 2015;3:40.
2. De Backer D, Hollenberg S, Boerma C, et al. How to evaluate the microcirculation: Report of a round table conference. *Crit Care* 2007;11:R101.
3. Bennett MH, Feldmeier J, Hampson NB, Smee R, Milross C. Hyperbaric oxygen therapy for late radiation tissue injury. *Cochrane Database Syst Rev* 2016;4:CD005005.
4. Bras J, de Jonge HK, van Merkesteyn JP. Osteoradionecrosis of the mandible: pathogenesis. *Am J Otolaryngol* 1990;11:244–250.
5. Cerný V, Turek Z, Parízková R. Orthogonal polarization spectral imaging. *Physiol Res* 2007;56:141–147.
6. Chang EI, Leon P, Hoffman WY, Schmidt BL. Quality of life for patients requiring surgical resection and reconstruction for mandibular osteoradionecrosis: 10-year experience at the University of California San Francisco. *Head Neck* 2012;34:207–212.
7. Cooper JS, Fu K, Marks J, Silverman S. Late effects of radiation therapy in the head and neck region. *Int J Radiation Oncology Biol Phys* 1995;31:1141–1164.
8. Davoudi B, Morrison M, Bizheva K, Yang VX, Dinniwell R, Levin W, et al. Optical coherence tomography platform for microvascular imaging and quantification: initial experience in late oral radiation toxicity patients. *J of Biomed Opt* 2013;18:76008.
9. Delanian S, Lefaix JL. The radiation-induced fibroatrophic process: Therapeutic perspective via the antioxidant pathway. *Radiother Oncol* 2004;73:119–131.
10. Dickson K, Malitan H, Lehmann C. Imaging of the Intestinal Microcirculation during Acute and Chronic Inflammation. *Biology (Basel)* 2020;9:418.
11. Dörr W. Radiobiology of tissue reactions. *Ann ICRP* 2015;44:58–68.
12. Ellis CG, Bateman RM, Sharpe MD, Sibbald WJ, Gill R. Effect of a maldistribution of microvascular blood flow on capillary O₂ extraction in sepsis. *Am J Physiol* 2002;282:H156–H164.
13. Goedhart PT, Khalilzada M, Bezemer R, Merza J, Ince C. Sidestream Dark Field (SDF) imaging: a novel stroboscopic LED ring-based imaging modality for clinical assessment of the microcirculation. *Opt Express* 2007;15:15101–15114.
14. Groner W, Winkelmann JW, Harris AG, Ince C, Bouma GJ, Messmer K. Orthogonal polarization spectral imaging: a new method for study of the microcirculation. *Nat Med* 1999;5:1209–1212.
15. Heeman W, Steenbergen W, van Dam G, Boerma EC. Clinical applications of laser speckle contrast imaging: a review. *J Biomed Opt* 2019;24:1–11.
16. Hopf HW, Gibson JJ, Angeles AP, Constant JS, Feng JJ, Rollins MD, Zamirul Hussain M, Hunt TK. Hyperoxia and angiogenesis. *Wound Repair Regen* 2005;13:558–564.
17. Hutchings SD, Watts S, Kirkman E. The Cytocam video microscope. A new method for visualizing the microcirculation using Incident Dark Field technology. *Clin Hemorheol Microcirc* 2016;62:261–271.
18. Ince C. The microcirculation is the motor of sepsis. *Crit Care* 2005;9:S13–9.
19. Jacobson AS, Zevallos J, Smith M, Lazarus CL, Husaini H, Okay D, et al. Quality of life after management of advanced osteoradionecrosis of the mandible. *Int J Oral Maxillofac Surg* 2013;42:1121–1128.
20. Lindeboom JA, Mathura KR, Ince C. Orthogonal polarization spectral (OPS) imaging and topographical characteristics of oral squamous cell carcinoma. *Oral Oncol* 2006;42:581–585.
21. Marin T, Moore J. Understanding near-infrared spectroscopy. *Adv Neonatal Care* 2011;11:382–388.
22. Marx RE, Ehler WJ, Tayapongsak P, Pierce LW. Relationship of oxygen dose to angiogenesis induction in irradiated tissue. *Am J Surg* 1990;160:519–524.
23. Marx RE, Johnson RP. Studies in the radiobiology of osteoradionecrosis and their clinical significance. *Oral Surg Oral Med Oral Pathol* 1987;64:379–390.
24. Marx RE. Osteoradionecrosis: a new concept of its pathophysiology. *J Oral Maxillofac Surg* 1983;41:283–288.

25. Milstein DM, Romay E, Ince C. A novel computer-controlled high resolution video microscopy system enables measuring mucosal subsurface focal depth for rapid acquisition of oral microcirculation video images. *Intensive Care Med* 2012;38:S271.
26. Milstein DM, Cheung YW, Ži kait L, Ince C, van den Akker HP, Lindeboom JA. An integrative approach for comparing microcirculation between normal and alveolar cleft gingiva in children scheduled for secondary bone grafting procedures. *Oral Surg Oral Med Oral Pathol Oral Radiol* 2013;115:304-309.
27. Moon DH, Moon SH, Wang K, et al. Incidence of, and risk factors for, mandibular osteoradionecrosis in patients with oral cavity and oropharynx cancers. *Oral Oncol* 2017;72:98-103.
28. Mortensen HR, Overgaard J, Specht L, Overgaard M, Johansen J, Evensen JF, Andersen LJ, Andersen E, Grau C. Prevalence and peak incidence of acute and late normal tissue morbidity in the DAHANCA 6&7 randomised trial with accelerated radiotherapy for head and neck cancer. *Radiother Oncol* 2012;103:69-75.
29. Nabil S, Samman N. Incidence and prevention of osteoradionecrosis after dental extraction in irradiated patients: a systematic review. *Int J Oral Maxillofac Surg* 2011;40:229-243.
30. Ocak I, Kara A, Ince C. Monitoring microcirculation. *Best Pract Res Clin Anaesthesiol* 2016;30:407-418.
31. Rodriguez PG, Felix FN, Woodley DT, Shim EK. The role of oxygen in wound healing: A review of the literature. *Dermatol Surg* 2008;34:1159-1169.
32. Shaw RJ, Butterworth CJ, Silcocks P, Tesfaye BT, Bickerstaff M, Jackson R, Kanatas A, Nixon P, McCaul J, Praveen P, Lowe T, Blanco-Guzman M, Forner L, Brennan P, Fardy M, Parkin R, Smerdon G, Stephenson R, Cope T, Glover M. HOPON (Hyperbaric Oxygen for the Prevention of Osteoradionecrosis): A Randomized Controlled Trial of Hyperbaric Oxygen to Prevent Osteoradionecrosis of the Irradiated Mandible After Dentoalveolar Surgery. *Int J Radiat Oncol Biol Phys* 2019;104:530-539.
33. Shaw RJ, Dhandra J. Hyperbaric oxygen in the management of late radiation injury to the head and neck. Part I: treatment. *Br J Oral Maxillofac Surg* 2011;49:2-8.
34. Sheikh AY, Rollins MD, Hopf HW, Hunt TK. Hyperoxia improves microvascular perfusion in a murine wound model. *Wound Repair Regen* 2005;13:303-308.
35. Sherman H, Klausner S, Cook WA. Incident dark-field illumination: a new method for microcirculatory study. *Angiology* 1971;22:295-303.
36. Spiegelberg L, Djasim UM, van Neck HW, Wolvius EB, van der Wal KG. Hyperbaric oxygen therapy in the management of radiation-induced injury in the head and neck region: a review of the literature. *J Oral Maxillofac Surg* 2010;68:1732-1739.
37. Spronk, P.E., Ince, C., Gardien, M.J., Mathura, K.R., Oudemans-van Straaten, H.M., and Zandstra, D.F. Nitroglycerin in septic shock after intravascular volume resuscitation. *Lancet* 2002;360:1395-1396.
38. Stone HB, Coleman CN, Anscher MS, McBride WH. Effects of radiation on normal tissue: consequences and mechanisms. *Lancet Oncol* 2003;4:529-536.
39. Strojjan P, Hutcheson KA, Eisbruch A, et al. Treatment of late sequelae after radiotherapy for head and neck cancer. *Cancer Treat Rev* 2017;59:79-92.
40. Svaltestad J, Thorsen E, Vaagbø G, Hellem S. Effect of hyperbaric oxygen treatment on oxygen tension and vascular capacity in irradiated skin and mucosa. *Int J Oral Maxillofac Surg* 2014;43:107-112.
41. Tompach PC, Lew D, Stoll JL. Cell response to hyperbaric oxygen treatment. *Int J Oral Maxillofac Surg* 1997;26:82-86.
42. Trzeciak S, Dellinger RP, Parrillo JE, Guglielmi M, Bajaj J, Abate NL, Arnold RC, Colilla S, Zanotti S, Hollenberg SM. Early microcirculatory perfusion derangements in patients with severe sepsis and septic shock: relationship to hemodynamics, oxygen transport, and survival. *Ann Emerg Med* 2007;49:88-98.
43. Vissink A, Jansma J, Spijkervet FK, Burlage FR, Coppes RP. Oral sequelae of head and neck radiotherapy. *Crit Rev Oral Biol Med* 2013;14:199-212.



PART I

PRECLINICAL STUDIES





CHAPTER 2

Sublingual microvascular perfusion is altered during normobaric and hyperbaric hyperoxia

Dan M.J. Milstein

Renée Helmers

Sanne Hackmann

Charly N.W. Belterman

Robert A. van Hulst

Jan de Lange

Edited version of: *Microvasc Res.* 2016;105:93–102.

ABSTRACT

Hyperoxia and hyperbaric oxygen therapy can restore oxygen tensions in tissues distressed by ischemic injury and poor vascularization and is believed to also yield angiogenesis and regulate tissue perfusion. The aim of this study was to develop a model in which hyperoxia-driven microvascular changes could be quantified and to test the hypothesis that microcirculatory responses to both normobaric (NB) and hyperbaric (HB) hyperoxic maneuvers are reversible. Sublingual mucosa microcirculation vessel density, proportion of perfused vessels, vessel diameters, microvascular flow index, macrohemodynamic, and blood gas parameters were examined in male rabbits breathing sequential O₂/air mixtures of 21%, 55%, 100%, and return to 21% during NB (1.0 bar) and HB (2.5 bar) conditions. The results indicate that NB hyperoxia (55% and 100%) produced significant decreases in microvascular density and vascular diameters ($p<0.01$ and $p<0.05$, respectively) accompanied by significant increases in systolic and mean arterial blood pressure ($p<0.05$, respectively) with no changes in blood flow indices when compared to NB normoxia. HB normoxia/hyperoxia resulted in significant decreases in microvascular density ($p<0.05$), a transient rise in systolic blood pressure at 55% ($p<0.01$), and no changes in blood vessel diameter and blood flow indices when compared to NB hyperoxia. All microcirculation parameters reverted back to normal values upon return to NB normoxia. We conclude that NB/HB hyperoxia-driven changes elicit reversible physiological control of sublingual mucosa blood perfusion in the presence of steady cardiovascular function and that the absence of microvascular vasoconstriction during HB conditions suggests a beneficial mechanism associated with maintaining peak tissue perfusion states.

INTRODUCTION

It is generally acknowledged that hyperoxia and hyperbaric oxygen therapy (HBOT) can promote metabolic resuscitation,^{34,47} angiogenesis,^{18,20,42} and regulate tissue perfusion^{37,48} by restoring oxygen tensions in tissues distressed by ischemic injuries or poor vasculature. Recanalization of oxygen establishes sufficient oxygen availability necessary for sustaining repair and regeneration.^{39,41} However, research-based evidence in support of the beneficial effects associated with hyperoxia and hyperbaric oxygen (HBO) have been controversial. For example, breathing high oxygen concentrations has been associated with adverse events such as elevated reactive oxygen species (ROS),^{8,46} altered cellular metabolic^{25,37,38} and rheological properties,^{1,50} activation of coagulation,^{27,30,32,35} endothelial dysfunction⁷ and vasoconstriction.^{37,48} While it is plausible that mutual advantages and disadvantages associated with hyperoxia may yield ultimately beneficial therapeutic effects, the net result depends on what the treatment strategy demands for achieving a desired therapeutic outcome.

Intrabarochamber measurements (HBO_m) of microhemodynamic responses in oral tissues are very limited since data acquisitions involving oxygen rich environments and electrical equipment remain a safety and technical challenge. Most studies report data obtained before and after HBOT and few directly from inside the HB tank. To our knowledge laser Doppler flowmetry (LDF),^{36,44} near-infrared spectroscopy (NIRS),²⁶ and video capillaroscopy (VC)⁵⁰ have been used inside HBO environments to investigate peripheral cutaneous microcirculation from the posterior region of the medial malleolus (foot), the thenar eminence (thumb), and the nailfold microcirculation respectively. However, the extent of measuring functional vascular changes in specified tissue compartments such as the subepithelial microcirculation of the oral mucosa remains nihil since LDF and NIRS are unable to produce information based on anatomic inspection. VC on the other hand can provide anatomic based information; however, its size and cumbersome setup have hindered its introduction for applications intraorally. In view of this, the evolution and commercialization of technology incorporating optics and spectroscopy into compact handheld instruments today enables the application of sidestream dark-field video imaging (SDFI) for studying the microcirculation in oral tissues. Recently, the influence of HBOT on keratinized oral mucosal flap vascularization was investigated with SDFI for



the first time¹⁸ and demonstrated a robust increase in microvascular density prospectively.

The aims of this study were to develop a model in which the feasibility of performing HBO_m with an optical spectroscopic-based microvascular imaging instrument could be examined and to test the hypothesis that hyperoxia-driven microvascular blood perfusion response measured in the sublingual region elicits reversible perfusional changes associated with ambient normobaric (NB) and HB hyperoxic maneuvers.

METHODS

The study guidelines and protocols for this investigation were reviewed and approved by the institutional Animal Experimentation Committee of the Academic Medical Center of the University of Amsterdam. Animal care and use was performed in accordance with the EU Directive 2010/63/EU (22 September 2010) and the Dutch Act on Laboratory Animal Experiments.

Animals

Eight male specific-pathogen free New Zealand White rabbits (*Oryctolagus cuniculus*) (Charles River Laboratories France, L'Arbresle Cedex, France) with a mean body weight of 3.4 ± 0.3 kg were used in this study. All animals were individually housed in large conventional cages (R-SUITE Enriched Rabbit Housing, Techniplast S.p.A., Buguggiate (Varese), Italy) in a light-controlled room (12 hours light/dark cycle) kept at $22 \pm 2^\circ\text{C}$ with a relative humidity of $55 \pm 15\%$ and were given 2 weeks to acclimatize to their new environment with access to a standard food pellet diet (LK-04, AB Diets, Woerden, The Netherlands) and water (acidified to pH 2.7) for consumption *ad libitum*. All investigations were conducted in the Academic Medical Center of the University of Amsterdam and at the same time of day (from 16:30 to 19:45). Each subject underwent induction and partial instrumentation in the laboratory animal facility before transport to a 98-m³ multiplace HB chamber in the Department of Hyperbaric Medicine for final instrumentation and the investigational procedures.



Anesthesia and instrumentation

Sedation and anesthesia was induced subcutaneously (sc) with a mixture of ketamine (Nimatek, Eurovet Animal Health BV, Bladel, The Netherlands; 15 mg·kg⁻¹) and dexmedetomidine (Dexdomitor, Pfizer Animal Health BV, Capelle aan den IJssel, The Netherlands; 0.2 mg·kg⁻¹) for orotracheal intubation and cannulation with indwelling arterial and venous catheters for blood sampling, monitoring basic hemodynamic parameters, and maintenance anesthesia according to our standardized anesthesia protocol. Prior to endotracheal intubation, an analgesic injection of buprenorphine (Temgesic®, Schering-Plough BV, Utrecht, The Netherlands; 0.03 mg·kg⁻¹ sc) was administered. Within one minute after full anesthesia (paw-pinch test) endotracheal intubation was performed blindly using a cuffed endotracheal tube (Mallinckrodt™ Hi-Contour Oral/Nasal Tracheal Tube 3.0 mm Ø/4.3 mm Ø_o, Covidien™, Mansfield, Massachusetts, USA). The left central auricular artery was cannulated (BD Venflon™ 20GA 1.0×32 mm, Becton Dickinson infusion Therapy, Helsingborg, Sweden) to obtain baseline whole blood count and subsequently used for serial blood gas sampling. To ascertain the general state of (hematological) health in our animal models (Hewitt et al., 1989),¹⁹ baseline whole blood count was determined prior to experimentation by an automated Sysmex XE-5000 (Sysmex Corporation, Kobe, Japan) blood cell counter from 1 mL of blood withdrawn from the central ear artery and anticoagulated in K2E 7.2 mg EDTA BD Vacutainer® 4 mL tubes (Becton, Dickinson & Co., Plymouth, United Kingdom). The left posterior auricular marginal vein and the right femoral artery were cannulated (BD Venflon™ 22GA 0.8×25 mm, Becton Dickinson infusion Therapy, Helsingborg, Sweden) for maintenance anesthesia and hemodynamic monitoring (heart rate (HR), mean arterial pressure (MAP)) respectively. Prior to transportation to the HB chamber, 40 mL (2×20 mL) of sterile 0.9% NaCl (saline) solution was administered bilaterally via sc bolus (left and right flanks) to maintain hydration without the need for using additional equipment inside the HB chamber.

Inside the HB chamber the auricular intravenous catheter was coupled to a DC-powered infusion pump (IVAC P3000, Alaris Medical Systems, Inc., San Diego, California) and set to infuse midazolam (Actavis, Hafnarfjörður, Iceland; 5.7 mg·kg⁻¹·h⁻¹). The endotracheal tube was connected to a pediatric/neonatal ventilator (Maquet Servo Ventilator 900C, Siemens-Eléma AB, Solna, Sweden) and the animals were ventilated at a tidal volume of 40 mL (1.1 L·min⁻¹), a

frequency of 30 breaths·min⁻¹, and a positive end-expiratory pressure (PEEP) of 2 mmHg at an initial baseline fraction of inspired oxygen (FiO₂) of 21%. Arterial carbon dioxide (p_aCO₂) was maintained between 35 and 40 Torr. For hemodynamic monitoring and peripheral capillary oxygen saturation (SpO₂), the right femoral artery cannula was connected to an Infinity® HemoMed™ pod (Dräger Medical Systems, Inc. Danvers, Massachusetts, USA) and a clip pulse oximeter sensor was attached to the animal's right ear. Both hemodynamic and SpO₂ data respectively were obtained from an Infinity® Delta multiparameter monitor (Dräger Medical Systems, Inc. Danvers, Massachusetts, USA) inside the NB chamber.

After infusion pump, ventilator, and hemodynamic monitoring apparatus coupling, the animals were restrained in a sternally recumbent position into a tabletop rodent mouth gag apparatus (Veterinary Instrumentation Limited, Sheffield, South Yorkshire, United Kingdom) with the jaws fixed in an open configuration; details on correct animal and apparatus adjustments have been described elsewhere.²⁹ In brief, the restrainer platform was adjusted at an inclination of 30° to reduce stress on both the neck and back muscles and to avoid excessive traction on the incisor teeth. Mandibular extension adjustments were carefully set to avoid injuring muscles and articular ligaments from excessive stretching. Since the left side of the oral commissure was used for positioning and immobilizing the endotracheal tube on the restrainer platform, the free access on the right side of the oral cavity to the sublingual mucosa was used for microcirculation assessments. All equipment used in this study was thoroughly inspected by two experienced HB chamber electrical technicians of the Royal Netherlands Navy and approved exclusively for HBO application with regard to this study specifically.

Microcirculation imaging

Continuous monitoring of the sublingual microcirculation was performed by SDFI (MicroScan Video Microscope System, MicroVision Medical, Amsterdam, The Netherlands); details on this technique have been described elsewhere.^{15,28} Briefly, the SDFI technique is incorporated into a portable handheld (347 gr) video microscopy instrument, allowing real-time noninvasive observations of tissue subsurface microcirculation. The absorption of 530-nm wavelength (green light), projected directly onto the tissue surface via stroboscopic light-emitting diodes (13 ms illumination intervals),²⁸ is absorbed by hemoglobin in red blood cells (RBCs) yielding images of well-defined dark globules (i.e. RBCs)

contrasted by a bright background. The MicroScan instrument is equipped with a 5× objective lens system (onscreen magnification approximating 380×), which in turn produce images captured by a charge-coupled device video camera with a 640×480-pixel resolution ($3\text{ }\mu\text{m}\cdot\text{pixel}^{-1}$) resulting in a 0.94 mm×0.75 mm imaged tissue segment. Prior to planning the experiments in this study, the interior components and cable connecting systems of the MicroScan instrument were carefully examined and tested by the same two experienced HB chamber electrical technicians to ascertain device safety for this investigation.

The MicroScan power supply is derived from an external DC power pack (12V/4500mAh). For this study a modified connecting system was prepared to accommodate only the MicroScan apparatus inside the HB chamber. The MicroScan and its DC power pack connecting cable system was split into two separate segments; two cables were separately assembled and equipped at each end with both a metal 6-pin (LEMO) male solder push-pull connector plug and at the other end with an Amphenol circular type 6-pin connector corresponding with the connecting panel connectors located both on the interior and exterior of the HB chamber. Outside the HB chamber, all measurements were stored on DVI tapes, recorded by a Sony DSR-11 DVCAM™ video recorder (Sony, Shinagawa-ku, Tokyo, Japan), and viewed on a 19-inch Samsung SyncMaster 932Mv LCD monitor (Samsung, Seoul, South Korea) with a 1440×900-screen resolution.

All microcirculation data acquisitions were performed with the MicroScan mounted on top of a modified micromanipulator [Fig. 1A]. Prior to advancing the imaging probe towards the ROI, excess secretions and debris (e.g. saliva and food) were gently removed using a 5 cm×5 cm non-sterile gauze moistened with 0.9% sterile NaCl kept at 38°C. Microcirculation measurements free of pressure induced artifacts, bubbles, and excess saliva were obtained after carefully advancing, positioning, and maintaining the lens of the imaging probe, covered with a sterile disposable cap (Microscan Lens, MicroVision Medical, Amsterdam, The Netherlands), with gentle contact directly on the right sublingual mucosa (base of the tongue) adjacent to the frenulum linguae [Fig. 1B]. From this point forward, with ideal focus and contrast adjustments, the probe was maintained on the same ROI for the entire duration of the two-part experimental protocol, as measurements of 2-min each were recorded sequentially at all designated time points.



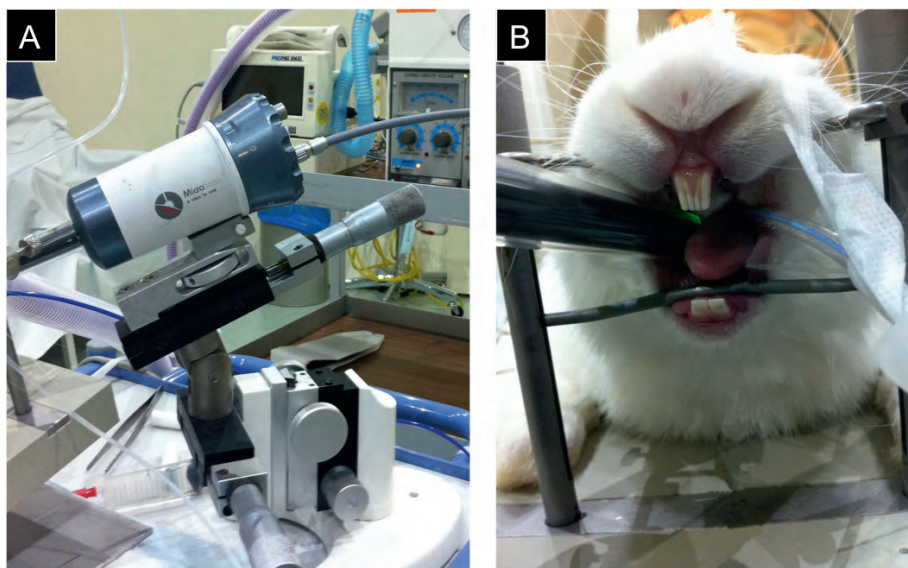


Figure 1. MicroScan mounted on top of a modified micromanipulator (A) and the setup of the MicroScan apparatus intraorally (B) targeting the right sublingual mucosa (probe the left side of the image) and the endotracheal tube oriented towards the left side of the oral cavity (on the right side of the image).

Experimental protocol

All experiments were performed at the same designated location inside the HB chamber. Since this was a two-part investigation, sequential hyperoxic experiments were conducted first during NB (1 atm [1.0 bar]) and then HB (2.5 atm [2.5 bar]) conditions. Each part of the experiment consisted of switching FiO_2 from 21% to 55%, 100%, and back to 21% once every 10 min during NB and then repeated at HB. An overview of the experimental procedures with corresponding time points is illustrated in Figure 2. Serial 0.5 mL of blood was withdrawn into heparinized (Heparin LEO®, LEO Pharma A/S, Ballerup, Denmark) 1 mL syringes (BD 1 mL Syringe Tuberculin Slip Tip, Becton, Dickinson & Co., Franklin Lakes, New Jersey, USA) for blood gas analysis by a RAPIDPoint® 500 Blood Gas System analyzer (Siemens, Mijdrecht, The Netherlands) at each inspired oxygen concentration. Upon completion of the first NB part of the protocol, a diving protocol was initiated with one investigator (DMJM, RH, or SH) inside the HB chamber to withdraw blood gas samples, reset the blood pressure probe at each level of the dive, if necessary adjust the focus of the MicroScan, and to monitor the general progress of the subjects. Each investigator entering the HB chamber was required to undergo a strict diving medical examination to

ascertain good health for participation in the second HB part of the experiments. During the second part of the investigation, blood gas samples were shuttled in- and outside the chamber through a small airlock. One of the two remaining investigators stationed outside the HB chamber (DMJM, RH, or SH) performed all microcirculation and blood gas measurements.

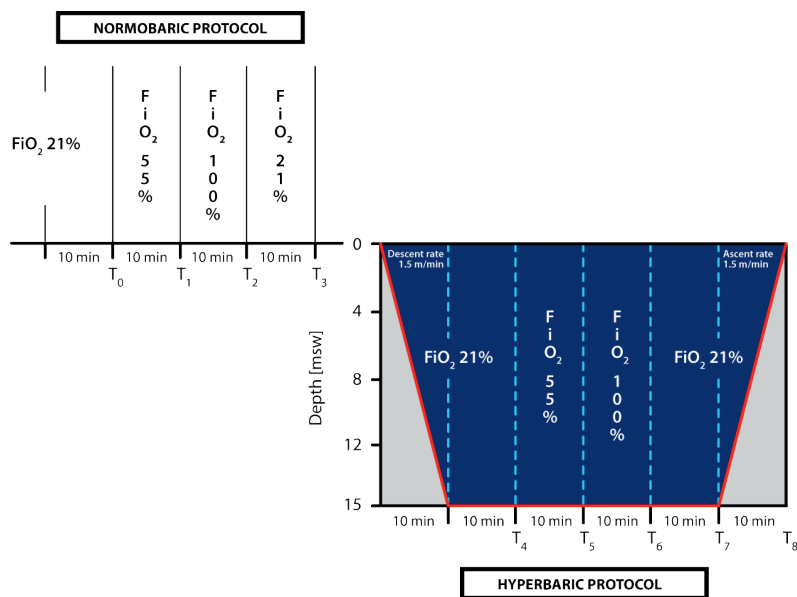


Figure 2. Overview of the experimental procedures and corresponding time points. BL baseline, FiO₂ fraction of inspired oxygen, msw meters of salt water

Microcirculation analysis

All data stored on DVI tapes were converted into AVI files for offline analysis using Adobe Premier Pro 1.5 (Adobe Systems Incorporated, San Jose, California, USA). Microcirculation video clips of 20 sec were captured from each of the 2-min recordings (9 total) corresponding with measurements for both NB and HB procedures. All video clips used for analysis conformed to the recommended standards outlined by a consensus conference based on microcirculation data acquisition and analysis (De Backer et al., 2007).¹⁰ All microcirculation data analysis was randomized and analyzed by the same experienced investigator (DMJM).

Microcirculatory analyses on vessels with diameters (\emptyset) $<25\ \mu\text{m}$ of total vessel density (TVD; mm vessel/mm²) and perfused vessel density (PVD; mm perfused vessel/mm²), proportion of perfused vessels (PPV; %),⁹ and microvascular flow index (MFI; score based on determination of the predominant flow type in four quadrants defined as either being absent (0), intermittent (1), sluggish (2), or normal (3))^{6,43} were performed on a computer with a 19-inch Samsung SyncMaster 932MV LCD monitor with a 1440×900 screen resolution using the Automated Vascular Analysis software package (AVA v3.02, MicroScan Video Microscope System, MicroVision Medical, Amsterdam, The Netherlands). Blood vessel diameter (\emptyset_{bv}) analysis was performed according to a method described elsewhere.⁴⁹ In brief, blood vessel diameter data was obtained from the skeletonization performed on the blood vessel density procedures in AVA for the TVD data. Five blood vessels ($\emptyset < 25\ \mu\text{m}$; mix of arterioles, capillaries, and venules) were selected at random from each of the four quadrants (i.e. 20 vessels total/video clip). The same 20 blood vessels and their diameters were analyzed at specific locations that were selected on each vessel segment as a landmark (e.g. bifurcation or vascular crossing) to ensure reproducibility across all measurement time points.

Statistical analysis

Based on studies correlating systemic hemodynamic variables with lingual mucosal blood flow using LDF in rabbits^{23,31} in combination with our experience using SDFI in these animal models,^{18,29} a sample size of eight was derived. Gaussian distribution of all datasets was assessed with the Shapiro-Wilk Normality Test. Each dataset was separately and accordingly analyzed using either repeated measures analysis of variance or Friedman test to detect overall time effects. Assessment of significant main effects were subsequently identified between each time point using a Fisher's Least Significant Difference (LSD) test or a Wilcoxon signed-rank test (nonparametric datasets). To adjust for inherent biological variations in each subject's microcirculation at the sublingual ROI, TVD, PVD, and \emptyset_{bv} parameters were normalized with respect to baseline and converted into percentages for ease in data presentation and statistical examination. MFI was evaluated using the Friedman test with a Dunn's multiple comparisons test for paired nonparametric repeated measurements. Differences detected with a p -value <0.05 were considered statistically significant. All data analysis was performed using IBM SPSS statistics software package (IBM® SPSS® Statistics version 23, IBM Corp. Armonk, NY, USA) and is presented accordingly as either mean \pm standard deviation (SD) or median (25th–75th percentiles).

RESULTS

Overall the experiments were uneventful and were performed and completed within the given experimental time frame. A summary of demographics with baseline hematological values and experimental procedural times are presented in Table 1. All hematological data were within normal ranges indicating a good state of health in our research subjects.

The MicroScan setup enabled continuous monitoring with sequential measurements of the same microvascular network in the sublingual mucosa across the full experimental procedure. The MicroScan instrument produced a total of 72 video clips of good quality that did not require additional contrast and focus adjustments. Minimal histogram grey scale post-acquisition tweaking (mean X-axis -0.34 ± 0.20 , mean Y-axis 2.50 ± 0.28) was performed for each subject’s dataset to reduce investigator interactions with the vascular analysis software by facilitating maximum vessel recognition. For each experiment dataset the same histogram grey scale setting was maintained and used across all time points.

Table 1. Summary of basic demographic, hematology, and investigational procedure times from 8 SPF NZW rabbits. All datasets are presented as mean±SD. Corresponding normal hematological reference ranges from healthy animals from literature^{14,19†} are provided for comparison.

Demographics:				
Age	[weeks]	16	±	1
Weight	[kg]	3.4	±	0.3
Hematology:		Normal ranges:		
RBC	[×10 ¹² /L]	5.7	±	0.6 (3.7-7.5) [†]
Hb	[mmol/L]	7.5	±	0.9 (6.2-9.3) [†]
PCV (Hct)	[L/L]	0.38	±	0.04 (0.27-0.48) [†]
MCV	[fL]	67.1	±	2.7 (58.0-79.6) [†]
WBC	[×10 ⁹ /L]	7.1	±	0.8 (5.0-16.5) [†]
PLT	[×10 ⁹ /L]	242	±	45 (112-795) [†]
Procedural times:				
Induction & instrumentation	[min]	20	±	5
Normobaric protocol	[min]	40	±	0
Hyperbaric protocol	[min]	40	±	0
Total experimental time	[min]	120	±	5

Hb hemoglobin, Hct hematocrit, MCV mean cell volume, NZW New Zealand White, PCV packed cell volume, PLT platelet count, RBC red blood cell count, WBC white blood cell count



Normobaric hyperoxia

A summary of NB hyperoxia basic hemodynamic and blood gas parameters is presented in the first part of Tables 2 and 3 respectively. A statistically significant increase in systolic blood pressure was observed at FiO_2 55% (T1) and 100% (T2) when compared to baseline (T0) ($p=0.009$ and $p=0.040$ respectively). MAP was stable throughout the experimental procedures except during the first hyperoxic maneuver, when the highest statistically significant rise in MAP was observed during FiO_2 55% (T1) ($p=0.023$ vs. T0). No other statistically significant differences were observed for the remaining hemodynamic parameters. There were no statistically significant changes in arterial pH levels. Assessments of $p_a\text{O}_2$ and $s\text{O}_2$ revealed significant elevations in both parameters during FiO_2 55% (T1) and 100% (T2) ($p=0.018$ respectively), these parameters normalized again after returning to normoxia (T3).

Microcirculation data coinciding with NB hyperoxic time points is presented in the first part of Table 4. Comparative analysis of baseline (T0) TVD and PVD revealed a significant mean 16% decrease in sublingual microvascular density for both FiO_2 55% (T1) and 100% (T2) ($p=0.005$ and $p=0.003$ respectively). A sample of an SDFI-derived sequence of vessel density changes during the NB experiments is illustrated in Figure 3A. A statistically significant increase in vasoconstriction (10%) compared to baseline (T0) was observed for \emptyset_{bv} during FiO_2 55% (T1) and 100% (T2) ($p=0.009$ and $p=0.047$ respectively). Further visual inspection of microhemodynamics in the SDFI footage during hyperoxia FiO_2 55% (T1) and 100% (T2) revealed the presence of scattered circulating microthrombi in small arterioles and venules and crawling leukocytes in larger venules in the microcirculation. No significant differences were observed for PPV or MFI.

Table 2. Summary of systemic hemodynamics.
All parameters are presented as mean \pm SD.

		NB											
		T0: BL (FiO_2 : 21%)			T1 (FiO_2 : 55%)			T2 (FiO_2 : 100%)			T3 (FiO_2 : 21%)		
HR	[bpm]	172	\pm	47	150	\pm	22	146	\pm	23	153	\pm	21
Systole	[mmHg]	67	\pm	13	76	\pm	11**	73	\pm	11*	63	\pm	6
MAP	[mmHg]	64	\pm	15	71	\pm	11*	64	\pm	11	54	\pm	5
Diastole	[mmHg]	62	\pm	16	65	\pm	14	59	\pm	11	51	\pm	7
SpO_2	[%]	94	\pm	4	95	\pm	4	96	\pm	3	93	\pm	0

BL baseline, bpm beats per minute, HR heart rate, HB hyperbaric, MAP mean arterial pressure, NB normobaric, SpO_2 peripheral capillary oxygen saturation

** $p<0.01$ vs. T0, RM ANOVA

* $p<0.05$ vs. T0, RM ANOVA

Hyperbaric hyperoxia

HB hyperoxia basic hemodynamic and blood gas parameters are summarized in the second part of Tables 2 and 3 respectively. A statistically significant increase in systolic blood pressure was observed at FiO_2 55% (T5) when compared to baseline ($p=0.009$), no other significant difference in systolic pressure was found for other HB time points. No other statistically significant differences were observed for the remaining hemodynamics parameters. Arterial pH remained within normal reference ranges across all time points. Interestingly although within normal range, a statistically significant decrease in arterial pH was observed at the end of the experimental protocol after ascending back to 1 atm (1.0 bar) (T8) from 2.5 atm (2.5 bar) ($p=0.028$), indicating mild acidosis. P_aO_2 and sO_2 revealed statistically significant elevations in both parameters across all HB time points (FiO_2 21%, 55%, 100%, and 21%, $p=0.018$ respectively), these normalized again following return to normoxia at 1 atm (1 bar) (T8). Total hemoglobin (tHb) remained within normal ranges across all time points despite a statistically significant increase at the end of the experimental protocol after returning back to 1 atm (1.0 bar) and normoxia (T8) ($p=0.018$ vs. T0).

The MicroScan instrument was stable under HB pressure. A summary of all microcirculation parameters coinciding with HB hyperoxic time points is presented in the second part of Table 4. Comparative analysis of TVD and PVD with respect to baseline (T0) revealed a significant mean 18% decrease for all HB time points (FiO_2 21% (T4), $p=0.017$; 55% (T5), $p=0.004$; 100% (T6), $p=0.002$; and 21% (T7), $p=0.007$). A sequence of SDFI frames illustrating changes in the microcirculation during the HB experiments is presented in Figure 3B. Return to NB normoxia at the end of the experimental procedure (T8) [Fig. 3C] fully reversed the effects induced by elevated p_aO_2 by normalizing TVD and PVD back to near baseline values (4%).

HB										NB				
T4 (FiO ₂ : 21%)			T5 (FiO ₂ : 55%)			T6 (FiO ₂ : 100%)			T7 (FiO ₂ : 21%)			T8 (FiO ₂ : 21%)		
134	±	36	140	±	15	149	±	17	145	±	10	161	±	16
72	±	7	76	±	11**	76	±	7	75	±	1	73	±	9
60	±	8	64	±	7	62	±	10	61	±	2	63	±	4
53	±	7	58	±	8	57	±	7	53	±	2	58	±	2
94	±	3	97	±	1	98	±	1	98	±	1	96	±	2

Table 3. Summary of arterial blood gas results. All parameters are presented as medians (25th–75th percentiles) and were temperature-dependent analyzed at 37°C. Corresponding normal arterial blood gas reference ranges from healthy animals obtained by point-of-care blood gas analyzers from literature^{2,13} † are provided for comparison; unfortunately arterial AnGap, Cl⁻, and Lac ranges derived from point-of-care blood gas analyzers were not reported, baseline reference ranges (minimum to maximum) from our animal group are presented.

		NB			
		T0: BL (FiO ₂ : 21%)	T1 (FiO ₂ : 55%)	T2 (FiO ₂ : 100%)	T3 (FiO ₂ : 21%)
pH	[AU]	7.49 (7.45–7.50)	7.51 (7.49–7.53)	7.49 (7.48–7.51)	7.49 (7.48–7.51)
p _a O ₂	[mmHg]	71 (55–84)	184 (107–196)*	452 (335–521)*	86 (75–98)
p _a CO ₂	[mmHg]	40 (33–48)	38 (32–44)	42 (37–42)	40 (38–47)
HCO ₃ ⁻	[mmol/L]	30 (27–32)	27 (26–33)	31 (27–36)	31 (28–35)
BE	[mmol/L]	5.8 (4.0–6.7)	3.9 (2.8–8.6)	6.3 (3.9–11.2)	6.5 (5.0–9.8)
tHb	[mmol/L]	7.5 (7.2–9.2)	7.6 (7.4–8.3)	8.1 (7.7–8.4)	8.2 (8.0–9.2)
sO ₂	[%]	95.5 (89.2–98.2)	99.6 (99.4–99.7)*	99.7 (99.7–99.9)*	96.7 (95.8–98.6)
Na ⁺	[mmol/L]	141 (133–142)	142 (137–146)	140 (138–143)	139 (136–141)
K ⁺	[mmol/L]	3.0 (2.7–3.2)	2.8 (2.7–3.3)	3.1 (2.8–3.3)	3.0 (2.8–3.2)
Ca ²⁺	[mmol/L]	0.85 (0.65–1.35)	0.71 (0.60–1.29)	0.73 (0.50–1.18)	0.89 (0.71–1.15)
Cl ⁻	[mmol/L]	99 (98–108)	102 (98–108)	100 (98–101)	98 (97–101)
AnGap	[mmol/L]	14 (11–15)	15 (13–15)	13 (10–13)	14 (13–15)
Glu	[mmol/L]	15.0 (8.2–16.0)	12.7 (9.3–17.4)	15.4 (11.8–18.1)	16.7 (14.0–19.9)
Lac	[mmol/L]	0.65 (0.63–0.68)	0.65 (0.58–0.68)	0.72 (0.69–0.75)	0.75 (0.75–0.84)

AnGap anion gap, BE base excess, BL baseline, FiO₂ fraction of inspired oxygen, Glu glucose, HB hyperbaric, HCO₃⁻ bicarbonate, Lac lactate, NB normobaric, paO₂ partial pressure of oxygen in arterial blood, paCO₂ partial pressure of carbon dioxide in arterial blood, sO₂ oxygen saturation, tHb total hemoglobin

*p<0.05 vs. T0, Friedman test



HB				NB	Normal range:
T4 (FiO ₂ : 21%)	T5 (FiO ₂ : 55%)	T6 (FiO ₂ : 100%)	T7 (FiO ₂ : 21%)	T8 (FiO ₂ : 21%)	
7.48 (7.44-7.52)	7.44 (7.40-7.51)	7.44 (7.42-7.46)	7.49 (7.43-7.52)	7.43 (7.41-7.46)*	(7.35-7.54) [†]
259 (241-277)*	465 (437-564)*	589 (500-679)*	296 (287-304)*	84 (81-87)	(50-101) [†]
42 (41-42)	40 (36-41)	38 (34-44)	43 (39-47)	45 (43-45)	(25-40) [†]
30 (28-34)	27 (23-29)	27 (21-30)	32 (30-35)	29 (27-31)	(18-29) [†]
5.7 (3.6-9.8)	2.5 (-2.2-5.8)	2.6 (-2.9-4.3)	7.4 (4.5-10.4)	3.5 (2.1-6.4)	(-7.0-6.5) [†]
8.5 (7.8-9.5)	7.5 (7.1-7.7)	7.6 (6.5-8.3)	8.3 (7.2-9.4)	9.2 (8.8-9.8)*	(7.8-14.3) [†]
99.8 (99.7-99.9)*	99.8 (99.7-99.8)*	99.8 (99.8-99.8)*	99.8 (99.7-99.9)*	95.9 (94.1-96.9)	(88-98) [†]
139 (135-142)	131 (128-137)	137 (136-140)	137 (137-140)	141 (139-144)	(136-145) [†]
2.8 (2.6-3.0)	2.3 (2.0-3.0)	2.7 (2.2-3.0)	2.8 (2.8-3.0)	3.3 (3.1-3.4)	(3.5-5.1) [†]
0.73 (0.42-1.03)	0.53 (0.32-0.80)	0.59 (0.52-1.01)	0.60 (0.39-0.88)	0.97 (0.91-1.03)	(1.67-1.94) [†]
99 (98-101)	99 (96-100)	100 (98-102)	98 (97-98)	102 (101-102)	(97-113)
13 (10-14)	11 (9-14)	13 (10-15)	13 (11-15)	14 (10-18)	(11-15)
15.2 (13.2-16.7)	12.6 (10.9-14.2)	13.2 (11.4-15.0)	15.9 (15.6-16.8)	14.2 (12.4-16.5)	(5.9-11.4) [†]
0.71 (0.64-0.89)	0.70 (0.69-0.72)	0.68 (0.57-0.69)	0.70 (0.66-0.70)	0.92 (0.79-1.10)	(0.63-0.68)

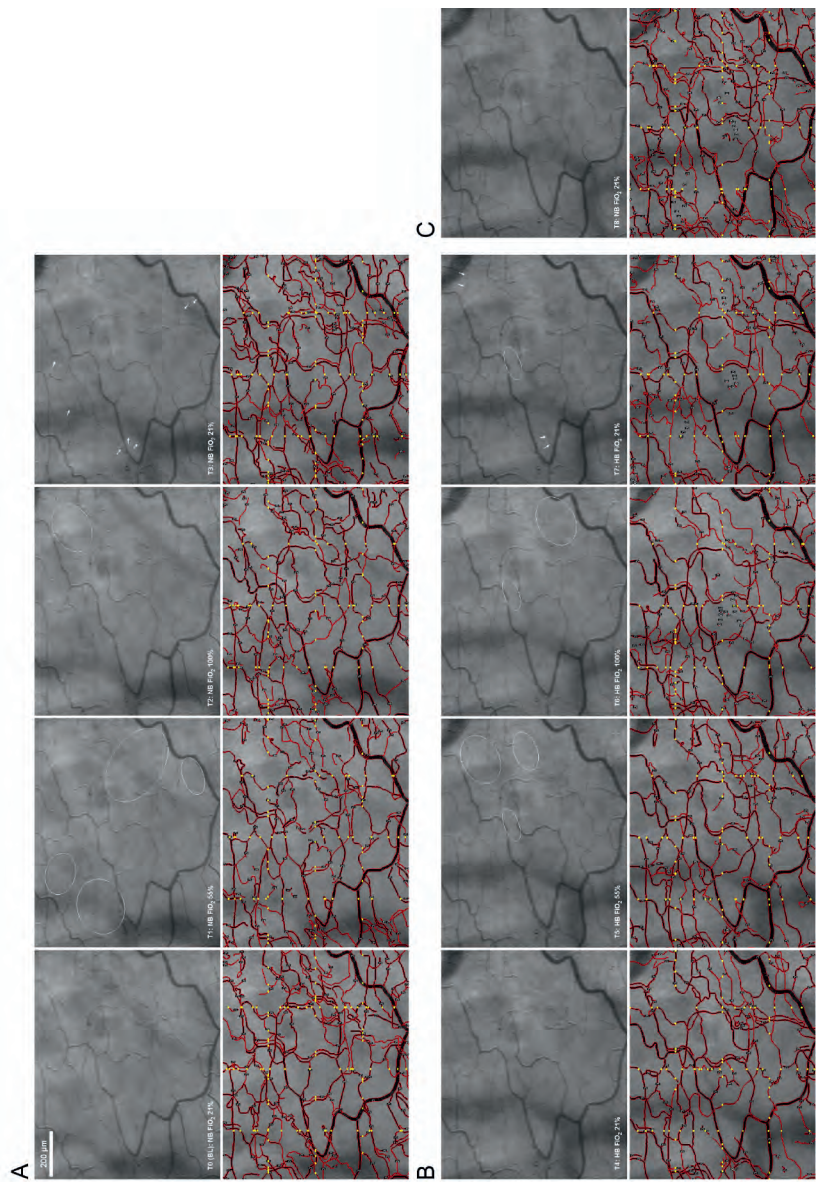


Figure 3. A sequence of 9 SDFI-derived clips with corresponding analysis (AVA v3.02) illustrating perfused vessel density changes across an entire experiment. The images demonstrate continuous reproducibility and monitoring of the same vascular network during normobaric (NB) hyperoxia (A), hyperbaric (HB) hyperoxia (B), and return to NB normoxia following hyperbaria (C). The white ovals indicate regions in the microcirculation that have been deprived of blood flow and the white arrows show vessels that appear in the vascular network that were not present before or that reappeared.

BL baseline, FI_{O₂} fraction of inspired oxygen.

Interestingly, there were no statistically significant differences observed for \emptyset_{bv} at any HB time points or return to baseline conditions. MicroScan recordings during HB conditions showed denser blood volume in the microcirculation when compared to all NB normoxic-derived images with generalized enlarged (distended) microvascular calibers [Fig. 4], no scattered microthrombi or crawling leukocytes could be observed in the microcirculation during HB time points. No significant differences were observed for PPV or MFI.

For ease in data presentation, since TVD and PVD resulted in virtually equal datasets, a graph illustrating a complete overview of all experimental time points and parameter trends between normalized PVD with p_aO_2 , MAP, and \emptyset_{bv} is presented in Figure 5.

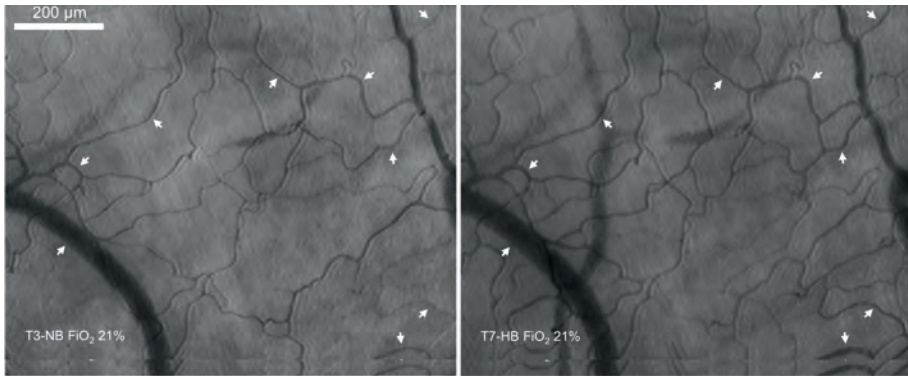


Figure 4. Sample microcirculation images of both NB and HB normoxia illustrating prominent microvascular perfusion differences consisting of denser blood volume in vessels (darker overall tone of circulating blood with no visible gaps) and generalized marginal increases in vascular calibers (white arrow heads) during HB conditions. These interesting visual features in the microcirculation indicate an adverse event associated with HB conditions suggestive of endothelial dysfunction, providing an explanation as to the benefits of enhanced blood perfusion and oxygen distribution into tissue. FiO_2 fraction of inspired oxygen.

Table 4. Summary of microcirculation data (vessels with diameters (\emptyset) $<25\ \mu\text{m}$). All parameters are presented in mean \pm SD. For blood vessel diameter change ($\Delta\emptyset_{bv}$), the negative in front of the number indicates vasodilation, all other positive $\Delta\emptyset_{bv}$ data coincide with vasoconstriction. To correct for anatomical variations between animals, datasets (TVD, PVD, and \emptyset_{bv}) were also normalized with respect to baseline and are expressed as percentages [%].

		NB											
		To: BL (FiO ₂ : 21%)				T1 (FiO ₂ : 55%)		T2 (FiO ₂ : 100%)		T3 (FiO ₂ : 21%)			
TVD	[mm/mm ²]	38	±	12	33	±	10**	31	±	8**	37	±	12
TVD	[%]	100	±	0	87	±	9**	82	±	12**	95	±	7
PVD	[mm/mm ²]	38	±	11	33	±	9**	30	±	7**	36	±	11
PVD	[%]	100	±	0	88	±	9**	80	±	11**	94	±	7
PPV	[%]	97	±	5	96	±	4	94	±	4	96	±	4
Ø _{bv}	[µm]	4.1	±	0.3	3.8	±	0.5*	3.7	±	0.6*	4.1	±	0.7
Ø _{bv}	[%]	100	±	0	91	±	5*	90	±	9*	98	±	12
ΔØ _{bv}	[µm]	0	±	0	0.35	±	0.17*	0.40	±	0.33*	0.05	±	0.48
MFI	[AU]	3	±	0	3	±	0	3	±	0	3	±	0

\emptyset_{bv} blood vessel diameter, AU arbitrary unit, BL baseline, FiO₂ fraction of inspired oxygen, HB hyperbaric, NB normobaric, MFI microvascular flow index, μm micrometer, PPV proportion of perfused vessels, PVD perfused vessels density, TVD total vessel density

** $p < 0.01$ vs. T0, RM ANOVA

* $p < 0.05$ vs. T0, RM ANOVA

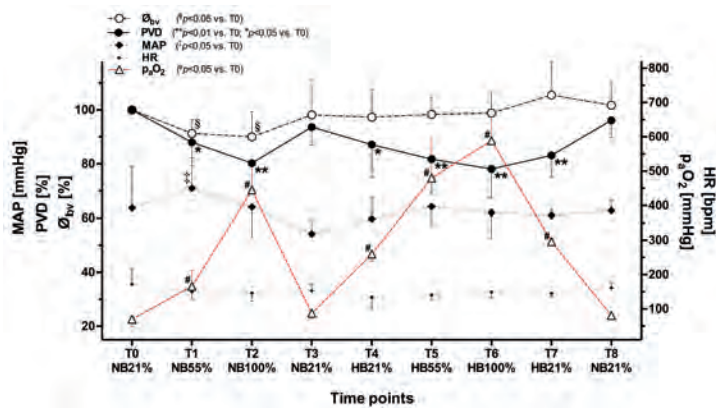


Figure 5. Multiparameter graph illustrating trends between blood vessel diameters (\emptyset_{bv}), normalized perfused vessel density (PVD), mean arterial pressure (MAP), and partial pressure of oxygen in arterial blood (p_{aO_2}).

NB normobaric, HB hyperbaric

DISCUSSION

The main research objectives were to generate a model in which HBO_m of the sublingual microcirculation in response to hyperoxia under NB and HB conditions could be performed and to measure and describe these changes in

HB										NB				
T4 (FiO ₂ : 21%)			T5 (FiO ₂ : 55%)			T6 (FiO ₂ : 100%)			T7 (FiO ₂ : 21%)			T8 (FiO ₂ : 21%)		
33	±	9*	30	±	8*	29	±	8**	32	±	9*	37	±	11
86	±	12*	80	±	13**	78	±	12**	85	±	11**	97	±	6
32	±	8*	30	±	7*	29	±	7**	31	±	8**	37	±	11
87	±	12*	82	±	13**	78	±	11**	83	±	8**	96	±	6
96	±	5	97	±	5	95	±	6	94	±	7	95	±	7
4.0	±	0.6	4.1	±	0.5	4.1	±	0.5	4.3	±	0.5	4.2	±	0.5
97	±	9	98	±	6	99	±	7	106	±	11	102	±	8
0.10	±	0.37	0.05	±	0.23	0.03	±	0.27	-0.21	±	0.45	-0.07	±	0.32
3	±	0	3	±	0	3	±	0	3	±	0	3	±	0

microcirculatory parameters. The results indicate that NB/HB hyperoxia-driven changes elicit reversible physiological control of sublingual mucosa blood perfusion in healthy subjects. The results also suggest a loss of microcirculatory vascular response since \emptyset_{bv} was unaltered during HB conditions, indicating an adaptive and potentially beneficial effect associated with maintaining peak tissue perfusion states in the presence of stable cardiovascular function. Furthermore, the use of a clinical handheld optical spectroscopic-based imaging instrument proved feasible for HBO_m and the implementation of a continuous microcirculation monitoring strategy.

Adaptation of tissue perfusion to stimuli is an important compensatory mechanism for matching metabolic demands and maintaining safe tissue physiologic biochemical equilibrium. It is well known that arterial vascular tone is increased in the presence of elevated p_aO_2 levels.^{24,37,48} Vasoconstriction is an adverse event associated with hyperoxia³⁷ as it is considered counterproductive for ameliorating poor blood perfusion in tissue distressed by hypoxia.²¹ In the present model NB hyperoxia elicited dose-dependent vasoconstriction with rising p_aO_2 levels as indicated by reduced \emptyset_{bv} . Our observations on decreased vessel calibers and capillary density in the presence of elevated p_aO_2 corroborate findings reported in other animal models.^{44,48} Paralleled with altered sublingual perfusion, basic hemodynamics revealed a trend towards decreased HR (though not significant) with a transient rise in systolic blood pressure during NB hyperoxia. Transiently elevated systolic pressures have been recorded previously in studies based on other animal models,⁵ similarly observations

regarding elevated systolic pressure trends have also been reported during NB hyperoxia in healthy human volunteers.¹⁶ Vasoconstriction and reduced microvascular densities mobilize microcirculatory blood volume into systemic circulation and can explain the transient rise in systolic pressures. Although difficult to compare due to different measurement and analytical approaches, decreased PVD outcomes derived from sublingual mucosa using SDFI have also been reported in healthy human volunteers exposed to NB hyperoxia.³³

Observations on the presence of scattered circulating microthrombi in the microcirculation during NB hyperoxia corroborate findings on coagulation and platelet events^{27,30,35} by others. Coagulation during hyperoxia may represent a host defense mechanism for antagonizing oxygen toxicity by limiting the dissemination of excessive oxygen in circulating blood. Although no systematic analysis of microthrombi and white blood cells in the microcirculation were systematically analyzed in this report, TVD and PVD rarefaction in response to NB hyperoxia may have been attributed to a combination of factors including vasoconstriction, activation of coagulation,²⁷ and crawling leukocytes.²² The mechanisms underlying the effects of hyperoxia on regulating microvascular perfusion remain largely elusive and may be potentially different for each type of anatomical compartment or tissue. Anatomic inspection of parameters conveying both oxygen diffusion- (vascular density) and convection-based (blood flow and vessel diameter characteristics) data provide direct visual cues linking cellular with tissue compartmental interactions yielding potential diagnostic information on clinical relevance and therapeutic efficacy of oxygenation.

Previous HBO studies directed at peripheral vascular effects have reported vasoconstriction as a commonly occurring phenomenon from measurements obtained nonspecifically across whole cutaneous tissue >1 mm depth using LDF.^{36,44} In this regard subsurface microvascular regulation confined to the first 500 μm cannot be separately investigated by LDF to determine the precise nature of subepithelial microvascular perfusion dynamics. HBO_m were performed on human nailfold microcirculation using VC and revealed that blood perfusion remained continuous with escalating RBC flow velocities as barometric pressure increased from 1ATA to 3ATA in the presence of transient decreases in HR.⁵⁰ Our sublingual MFI dataset is in line with these observations as continuous blood perfusion was recorded at all HB hyperoxia time points, despite the different anatomical locations. Both cutaneous nailfold tissue and the sublingual oral mucosa share common embryonic origins and histology

demonstrating translational similarities.^{3,51} In our model no microvascular vasoconstriction was observed during HB hyperoxia, this finding was surprising and controversial; we can only hypothesize that the absence of vasoconstriction may have been due to discordance in vascular regulatory signals and/or hemodynamic shear stresses in relation to the observed denser blood volume. Furthermore regarding microthrombi, recent investigations indicate engaging of platelet activation via thrombin and arachidonic acid pathways in patients³⁰ subjected to similar hyperbaric conditions as presented in this report. It is important to consider that the unseen microthrombi and activated leukocytes in the microcirculation may have been due to the overshadowing effects of vasodilation and dense blood volume described in the microcirculation during HB hyperoxia. For example, recall that the SDFI relies on hemoglobin in RBCs absorbing green light, this poses a technical challenge and makes discerning microthrombi from free RBCs in dense blood volume difficult and does not exclude their presence in the microcirculation under HB conditions. Under influence of HBO conditions the absence of vasoconstriction may be an advantageous mechanism enabling maximum tissue blood perfusion despite the contemplated presence of activated immune cells and/or circulating microthrombi; this is supported by the \emptyset_{bv} that remained near baseline values during the first three HB time points (T4, T5, and T6) and the small increase in vasodilation (though not significant) that was observed during HB normoxia (T7) and NB normoxia at the end of the experiments (T8).

Several considerations need to be addressed based on the present model. First, in pilot experiments we found that 10 min was sufficient time to enable transition towards oxygen acclimatization from normoxia to hyperoxia and back to normoxia (data not published). Second, the sequence of the experiments presented in the protocol was not randomized and the duration of anesthesia may have influenced the HB hyperoxia segment of the investigation. Third, the measured calcium levels were below the normal reference range. Vascular smooth muscle cell contractility is regulated by intracellular calcium concentrations that in turn set vascular tone and blood pressure. Interestingly though despite being low already at baseline, circulating calcium levels decreased (though not significant) during hyperoxia under both NB and HB conditions; these minute oscillations seem to indicate that calcium consumption may have been present during hyperoxia. We cannot explain why no direct vasoconstriction was measured during HB hyperoxia. We can only speculate that



the complex interactions associated with several factor (including anesthesia protocol) may have superseded the magnitude of the vasoconstrictive response opposing the expected observable effect during HB hyperoxia. Furthermore, it is difficult to explain why the measured calcium levels were low in comparison to the reference values; two possible explanations are that the diet from domesticated animals may have been more varied and different compared to the standardized diet associated with controlled experiments and there may be calibration discrepancies between different blood gas instruments used by other studies. Fourth, hyperglycemia is commonly observed when anesthetic and sedative agents such as dexmedetomidine and/or midazolam^{11,52} are used; this is true for both human and animal models and was also measured across all time points. Vasoconstriction may not have been directly attributed to hyperglycemia during NB hyperoxia as no vasoconstriction response was observed despite decreased TCD/PVD during HB hyperoxia. Interestingly in vitro research on glucose incubated rabbit aortic rings showed that raised glucose levels contributed directly to endothelium-derived increased synthesis of vasoconstrictor prostanoids;⁴⁵ however this finding may not directly apply to microcirculatory vascular responses. Although difficult to explain based on our observations and the available literature, one may speculate that the effects of HBO on activation of leukocytes, microthrombi, hematology, and altered hemorheological properties may have contributed to the decreases in TVD/PVD during the HB segment of our experiments. Rabbits have an unpredictable tendency of displaying oscillations in hematological values, which is why it may be possible that some hematological components may have contributed towards denser blood volume and failed vasoconstriction registrations in the microcirculation during hyperbaria. Increases in RBC deformability and mean cell volume under HBO conditions have been reported.¹ From the present animal model it is difficult to pin an exact explanation on a vasoregulatory mechanism that would equally satisfy both NB and HB hyperoxic scenarios. Given the complex interplay of multiple factors, it appears that final blood vessel caliber settings may be the result of many influences. Furthermore, the hemodynamic effects associated with NB/HB hyperoxia observed in the present model are in line with reviewed reports on HR and blood pressure.⁴⁰ Interestingly the levels of p_aO_2 during HB hyperoxia did not reach >600 mmHg, it is possible that the effects of hyperoxia may have induced pulmonary vascular paralysis¹⁷ and as a consequence resulted in lowered tensions in blood gas values.

The MicroScan has a long history of application in the oral compartment, and in particular the sublingual region since non-keratinized epithelium is thin and facilitates observations of branching microvasculature networks that regulate nutritive blood perfusion to the mucosa. Serving as a clinical model for investigating central microhemodynamics and cardiovascular system, the sublingual area is an easily accessible ROI in which normothermic conditions are isolated from environmental stimuli. Clinical literature on sublingual microcirculation describes research designs that have solely been based on intermittent measurements on different sublingual sites resulting in irreproducible data as measurements of different branched microvascular networks make it very difficult to draw sound scientific conclusions on interventional courses. It is difficult to extrapolate the data reported in this study with other experimental and clinical researches using the MicroScan due to large variations in research methodology and limited investigations designed around a continuous monitoring scenario capturing the dynamics of one and same vascular network. For example, recently Orbegozo Cortés et al.³³, using SDFI, reported similar microcirculatory observations during NB hyperoxia in a cohort of healthy volunteers, though their intermittent measurements and analytical method differ from our approach, they report approximately 36% reduction in PVD versus our continuous measurement approach with 16% reduction in PVD. Since our investigation consisted of two separate experimental procedures it is interesting to consider the reproducibility achieved in PVD magnitudes. To date only four studies have reported data on continuous-based monitoring in one and the same ROI to intercept both the onset of tissue perfusion changes and the clinical relevance of these observations.^{4,12,29,49} Continuous monitoring with sequential measurements provide strong evidence of changes in microcirculation parameters from specific tissue microvascular networks that could translate in the near future to identify a host's state of health and their ability to elicit a physiological response associated with oxygen and/or other interventional strategies. Continuous measurement approaches favor reproducibility in data acquisitions, however careful experimental design and planning is required to obtain viable data for translational interpretations linking patient response with predicting and/or achieving a desired therapeutic outcome. Ultimately the aim of oxygen therapy is to maximize oxygen supplementation to sustain tissue aerobic metabolism. To our knowledge no investigation has as yet advanced knowledge towards sublingual microcirculatory assessments during HBO conditions.



Administering supplementary oxygen in the form of either NB hyperoxia or HBOT is used with an intention to treat conditions in which hypoxia, infection, and/or poor tissue vasculature are central to an underlying pathology. Despite mechanical and pharmacological strategies for stabilizing metabolism and resetting tissue regulatory mechanisms in treatment-refractory pathologies, oxygen therapy is not without consequences and should be administered with caution. Under- or over-treating with oxygen is risky particularly because no consensus exists indicating the exact adequate clinical levels for achieving medically beneficial results. Nonetheless, supplementary oxygen is routinely administered in patients with adequate oxygen saturation levels with the belief that it will improve oxygen delivery in patients with distressed tissues afflicted by ischemic insults. In view of the clinical relevance of the present research model, bedside microvascular perfusion assessments have identified the oral microcirculation in recent years as an important prognostic ROI for clinical and translational monitoring of both disease pathophysiology and the course of therapeutic response.

Conclusions

We report for the first time the application of SDFI inside a multiplace HB chamber for continuous monitoring and measurement of sublingual mucosa microcirculation. The present research model demonstrated the feasibility of performing intrabarochamber microcirculation data acquisitions simultaneously for local and systemically derived parameters under influence of changing barometric and hyperoxic conditions. Within the scope of the experiments presented in this report, the effects of NB and HB hyperoxia on microcirculation parameters in healthy subjects indicate reversibility in microvascular perfusion in the presence of steady cardiovascular function. To assess whether these observations hold true for other tissues and/or other pathophysiological conditions further investigation is warranted.

Acknowledgments

The authors thank the staff of the Department of Hyperbaric Medicine for their kind assistance during the late hours operating the hyperbaric tank for these investigations. *Important note:* The investigators of this study do not claim, nor do the results of this study suggest, that it is safe to use a MicroScan (Sidestream Dark-Field Video Microscopy system) in pressurized oxygen

rich environments such as hyperbaric chambers. The commercially available MicroScan device was not designed nor was it built for use inside pressurized oxygenated conditions. The MicroScan instrument used in this study was both electrically and mechanically tested by trained professionals and proper safety precautions were undertaken to ensure the safety of the investigators for the hyperbaric experiments described in this scientific report.

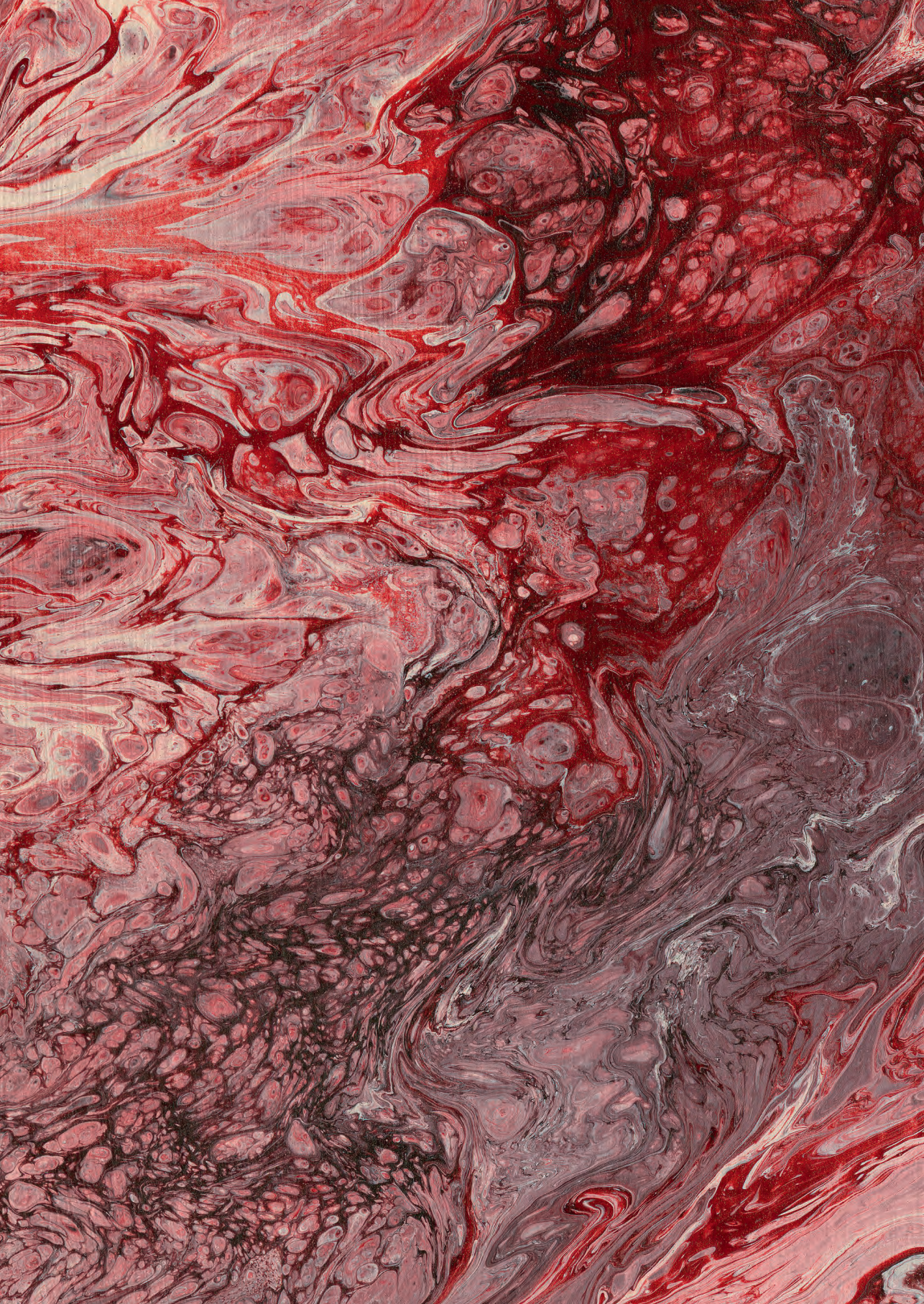


REFERENCES

1. Amin, H.M., Kaniewski, W.S., Cohen, D., Camporesi, E.M., Hakim, T.S., 1995. Effects of acute exposure to hyperbaric oxygen on the rheological and morphology of the red blood cells in the rat. *Microvasc. Res.* 50, 417–428.
2. Ardiaca, M., Bonvehí, C., Montesinos, A., 2013. Point-of-care blood gas and electrolyte analysis in rabbits. *Vet. Clin. North Am. Exot. Anim. Pract.* 16, 175–195.
3. Arnold, H.L. Jr., Odom, R.B., James, W.D., 1990. The skin: basic structure and function, in: James, W.D., Elston, D., Berger, T. (Eds.), *Andrew's Disease of the Skin*. Elsevier, San Francisco, pp. 1–13.
4. Atasever, B., Boer, C., van der Kuil, M., Lust, E., Beishuizen, A., Speekenbrink, R., Seyffert, J., de Mol, B., Ince, C., 2011. Quantitative imaging of microcirculatory response during nitroglycerin-induced hypotension. *J. Cardiothorac. Vasc. Anesth.* 25, 140–144.
5. Bergø, G.W., Risberg, J., Tyssebotn, I., 1988. Effect of 5 bar oxygen on cardiac output and organ blood flow in conscious rats. *Undersea Biomed. Res.* 15, 457–470.
6. Boerma, E.C., Mathura, K.R., van der Voort, P.H., Spronk, P.E., Ince, C., 2005. Quantifying bedside-derived imaging of microcirculatory abnormalities in septic patients: a prospective validation study. *Crit. Care* 9, R601–R606.
7. Brubakk, A.O., Duplancic, D., Valic, Z., Palada, I., Obad, A., Bakovic, D., Wisloff, U., Dujic, Z., 2005. A single air dive reduces arterial endothelial function in man. *J. Physiol.* 566, 901–906.
8. Brueckl, C., Kaestle, S., Kerem, A., Habazettl, H., Krombach, F., Kuppe, H., Kuebler, W.M., 2006. Hyperoxia-induced reactive oxygen species formation in pulmonary capillary endothelial cells in situ. *Am. J. Respir. Cell Mol. Biol.* 34, 453–463.
9. De Backer, D., Creteur, J., Preiser, J.C., Dubois, M.J., Vincent, J.L., 2002. Microvascular blood flow is altered in patients with sepsis. *Am. J. Respir. Care Med.* 166, 98–104.
10. De Backer, D., Hollenberg, S., Boerma, C., Goedhart, P., Büchele, G., Ospina-Tascon, G., Dobbe, I., Ince, C., 2007. How to evaluate the microcirculation: report of a round table conference. *Crit. Care* 11, R101.
11. Desborough, J.P., Hall, G.M., Hart, G.R., Burrin, J.M., 1991. Midazolam modifies pancreatic and anterior pituitary hormone secretion during upper abdominal surgery. *Br. J. Anaesth.* 67, 390–396.
12. Dirkes, M.C., Milstein, D.M., Heger, M., van Gulik, T.M., 2015. Absence of hydrogen sulfide-induced hypometabolism in pigs: a mechanistic explanation in relation to small nonhibernating mammals. *Eur. Surg. Res.* 54, 178–191.
13. Eatwell, K., Mancinelli, E., Hedley, J., Benato, L., Shaw, D.J., Self, I., Meredith, A., 2013. Use of arterial blood gas analysis as a superior method for evaluating respiratory function in pet rabbits (*Oryctolagus cuniculus*). *Vet. Rec.* 173, 166.
14. Gillett, C.S., 1994. Selected drug dosages and clinical references data. In: Manning, P.J., Ringler, D.H., Newcomer, C.E., (Eds.), *The Biology of the Laboratory Rabbit*, 2nd ed., San Diego: Academic Press, 467–472.
15. Goedhart, P.T., Khalilzadeh, M., Bezemer, R., Merza, J., Ince, C., 2007. Sidestream dark field (SDF) imaging: a novel stroboscopic LED ring-based imaging modality for clinical assessment of the microcirculation. *Opt. Express* 15, 15101–15114.
16. Graff, B., Szyndler, A., Czechowicz, K., Kucharska, W., Graff, G., Boutouyrie, P., Laurent, S., Narkiewicz, K., 2013. Relationship between heart rate variability, blood pressure and arterial wall properties during air and oxygen breathing in healthy subjects. *Auton. Neurosci.* 178, 60–66.
17. Gurtner, G.H., Michael, J.R., Farrukh, I.S., Sciuto, A.M., Adkinson, N.F., 1985. Mechanism of hyperoxia-induced pulmonary vascular paralysis: effect of antioxidant pretreatment. *J. Appl. Physiol.* 59, 953–958.
18. Helmers, R., Milstien, D.M., van Hulst, R.A., de Lange, J., 2014. Hyperbaric oxygen therapy accelerates vascularization in keratinized oral mucosal surgical flaps. *Head. Neck.* 36, 1241–1247.
19. Hewitt, C.D., Innes, D.J., Savory, J., Wills, M.R., 1989. Normal biochemical and hematological values in New Zealand white rabbits. *Clin. Chem.* 35, 1777–1779.
20. Hopf, H.W., Gibson, J.J., Angeles, A.P., Constant, J.S., Feng, J.J., Rollins, M.D., Zamirul Hussain, M., Hunt, T.K., 2005. Hyperoxia and angiogenesis. *Wound Rep. Reg.* 13, 558–564.
21. Jenkinson, S.G., 1993. Oxygen toxicity. *New Horiz.* 1, 504–511.
22. Kamler, M., Wendt, D., Pizanis, N., Milekhin, V., Schade, U., Jakob, H., 2004. Deleterious effects of oxygen during extracorporeal circulation for the microcirculation in vivo. *Eur. J. Cardiothorac. Surg.* 26, 564–570.
23. Kemmochi, M., Ichinohe, T., Kaneko, Y., 2009. Remifentanyl decreases mandibular bone marrow blood flow during propofol or sevoflurane anesthesia in rabbits. *J. Oral Maxillofac. Surg.* 67, 1245–1250.
24. Lindbom, L., Arfors, K.E., 1985. Mechanisms and site of control for variation in the number of perfused capillaries in skeletal muscle. *Int. J. Microcirc. Clin. Exp.* 4, 19–30.
25. Lodato, R.F., 1989. Decreased O₂ consumption and cardiac output during normobaric hyperoxia in conscious dogs. *J. Appl. Physiol.* (1985) 67, 1551–1559.

26. Larsson, A., Uusijärvi, J., Eksborg, S., Lindholm, P., 2010. Tissue oxygenation measured with near-infrared spectroscopy during normobaric and hyperbaric oxygen breathing in healthy subjects. *Eur. J. Appl. Physiol.* 109, 757–761.
27. Mirrakhimov, M.M., Prizhivoit G.N., Chotoev, Zh.A., Rachkov, A.G., 1977. Mechanism of the hypercoagulation effect of hyperoxia. *Bull. Exp. Biol. Med.* 84, 421–423.
28. Milstein, D.M., Bezemer, R., Ince, C., 2012. Sidestream Dark-Field (SDF) Video Microscopy for Clinical Imaging of the Microcirculation. In: Leahy MJ editor. *Microcirculation Imaging*. Weinheim, Germany: Wiley-VCH Verlag GmbH & Co. KGaA, 37–52.
29. Milstein, D.M., Bezemer, R., Lindeboom, J.A., Ince, C., 2009. The acute effects of CMF-based chemotherapy on maxillary periodontal microcirculation. *Cancer Chemother. Pharmacol.* 64, 1047–1052.
30. Monaca, E., Strelow, H., Jüttner, T., Hoffmann, T., Potempa, T., Windold, J., Winterhalter, M., 2014. Assessment of hemostaseologic alterations induced by hyperbaric oxygen therapy using point-of-care analyzers. *Undersea Hyperb. Med.* 41, 17–26.
31. Nishizawa, S., Ichinohe, T., Kaneko, Y., 2012. Tissue blood flow reductions induced by remifentanyl in rabbits and the effect of naloxone and phentolamine on these changes. *J. Oral Maxillofac. Surg.* 70, 797–802.
32. Olszanski, R., Radziwon, P., Piszcz, J., Jarzemowski, J., Gosk, P., Bujno, M., Schenk, J.F., 2010. Activation of platelets and fibrinolysis induced by saturated air dives. *Aviat. Space Environ. Med.* 81, 585–588.
33. Orbegozo Cortés, D., Puflea, F., Donadello, K., Taccone, F.S., Gottin, L., Creteur, J., Vincent, J.L., De Backer, D., 2015. Normobaric hyperoxia alters the microcirculation in healthy volunteers. *Microvasc. Res.* 98, 23–28.
34. Pace, N., Strajman, E., Walker, E.L., 1950. Acceleration of carbon monoxide elimination in man by high pressure oxygen. *Science* 111, 652–654.
35. Pálos, L.A., Agadjanjan, N.A., 1978. Disseminated intravascular coagulation development in hyperbaric oxygen. *Aviat. Space Environ. Med.* 49, 722–723.
36. Ratzenhofer-Komenda, B., Kovac, H., Smolle-Jüttner, F.M., Friehs, G.B., Schwarz, G., 1998. Quantification of the dermal vascular response to hyperbaric oxygen with laser-Doppler flowmetry. *Undersea Hyper. Med.* 25, 223–227.
37. Reinhart, K., Bloos, F., König, F., Bredle, D., Hannemann, L., 1991. Reversible decrease of oxygen consumption by hyperoxia. *Chest* 99, 690–694.
38. Robin, E.D., 1977. Dysoxia: Abnormal tissue oxygen utilization. *Arch. Intern. Med.* 137, 905–910.
39. Rodriguez, P.G., Felix, F.N., Woodley, D.T., Shim, E.K., 2008. The role of oxygen in wound healing: A review of the literature. *Dermatol. Surg.* 34, 1159–1169.
40. Rogatsky, G.G., Shifrin, E.G., Mayevsky, A., 1999. Physiologic and biochemical monitoring during hyperbaric oxygenation: a review. *Undersea Hyperb. Med.* 26, 111–122.
41. Sheikh, A.Y., Rollins, M.D., Hopf, H.W., Hunt, T.K., 2005. Hyperoxia improves microvascular perfusion in a murine wound model. *Wound Rep. Reg.* 13, 303–308.
42. Shweiki, D., Itin, A., Soffer, D., Keshet, E., 1992. Vascular endothelial growth factor induced by hypoxia may mediate hypoxia-initiated angiogenesis. *Nature* 359, 843–845.
43. Spronk, P.E., Ince, C., Gardien, M.J., Mathura, K.R., Oudemans-van Straaten, H.M., Zandstra, D.F., 2002. Nitroglycerin in septic shock after intravascular volume resuscitation. *Lancet* 360, 1395–1396.
44. Stirban, A., Lentrodt, S., Nandrea, S., Pop, A., Tschoepe, D., Scherbaum, W.A., 2009. Functional changes in microcirculation during hyperbaric and normobaric oxygen therapy. *Undersea Hyper. Med.* 36, 381–390.
45. Tesfamariam, B., Brown, M.L., Deykin, D., Cohen, R.A., 1990. Elevated glucose promotes generation of endothelium-derived vasoconstrictor prostanoids in rabbit aorta. *J. Clin. Invest.* 85, 929–932.
46. Thom, S.R., 2009. Oxidative stress is fundamental to hyperbaric oxygen therapy. *J. Appl. Physiol.* 106, 988–995.
47. Thom, S.R., Elbuku, M.E., 1991. Oxygen-dependent antagonism of lipid peroxidation. *Free Rad. Biol. Med.* 10, 413–426.
48. Tsai, A.G., Cabrales, P., Winslow, R.M., Intaglietta, M., 2003. Microvascular oxygen distribution in awake window chamber model during hyperoxia. *Am. J. Physiol. Heart Circ. Physiol.* 285, H1537–H1545.
49. Tytgat, S.H., van der Zee, D.C., Ince, C., Milstein, D.M., 2013. Carbon dioxide gas pneumoperitoneum induces minimal microcirculatory changes in neonates during laparoscopic pyloromyotomy. *Surg. Endosc.* 27, 3465–3473.
50. Van der Kleij, A.J., Vink, H., Henny, C.P., Bakker, D.J., Spaan, J.A., 1994. Red blood cell velocity in nailfold capillaries during hyperbaric oxygenation. *Adv. Exp. Med. Biol.* 345, 175–180.
51. Winning, T.A., Townsend, G.C., 2000. Oral mucosal embryology and histology. *Clin. Dermatol.* 18, 499–511.
52. Zuurbier, C.J., Koeman, A., Houten, S.M., Hollman, M.W., Florijn, W.J., 2014. Optimizing anesthetic regimen for surgery in mice through minimization of hemodynamic, metabolic, and inflammatory perturbations. *Exp. Biol. Med.* (Maywood) 239, 737–746.





CHAPTER 3

Hyperbaric oxygen therapy accelerates vascularization in keratinized oral mucosal surgical flaps

Renée Helmers
Dan M.J. Milstein
Robert A. van Hulst
Jan de Lange

Edited version of: Head Neck. 2014;36:1241-1247.

ABSTRACT

Background: Hyperbaric oxygen therapy (HBOT) is thought to promote vascular regeneration in wounds. The aim of this study was to investigate the role of HBOT in advancing vascular regeneration in healing oral mucosal surgical flaps.

Materials and methods: A palatine partial-thickness mucosal flap was raised in 10 male specific-pathogen free New Zealand White rabbits. Randomized into two groups of 5 animals each (control and HBOT), functional capillary density was measured preoperatively (baseline), immediately postoperatively until day 21 using sidestream dark-field video microscopy. Ten HBOT sessions were administered over the course of 2 weeks at 2.5 atmospheres (2.5 bar O₂/90 min).

Results: Repeated measures ANOVA was used to compare the HBOT and control group on the sequential functional capillary density measurements. A significant interaction effect was present between time and group, $F(8, 64) = 9.60$, $p < 0.0001$, resulting from a significant increase in microcirculation in the HBOT group relative to the control group on days 7, 9, and 11.

Conclusion: Our results suggest that HBOT is capable of advancing wound vascular regeneration in healing keratinized oral mucosal flaps.

INTRODUCTION

Chronic wounds are common and persistent health problems with significant economic burden and impact on patient quality of life.¹² Most chronic wounds emerge as a consequence of arterial, venous and microvascular diseases, linked to diabetes, sustained pressure (decubitus), and therapeutic irradiation for malignant tumors. Poor blood supply and low oxygen tension (pO_2) due to decreased vascularity produce chronic hypoxia, a condition that is clinically difficult to control and may compel a wound to succumb to infection, which in turn could result in tissue necrosis and sepsis.^{18,21,24,25} Hyperbaric oxygen (HBO) is thought to promote angiogenesis by restoring oxygen tensions in the injured tissues and thereby establish proper oxygen delivery necessary for repair and regeneration.^{8,19,22} Although HBO is used as an adjunct to conventional medical treatments for management of chronic wounds, the validity of hyperbaric oxygen therapy (HBOT) for clinical use remains controversial. One of the indications for HBOT is for the treatment of osteoradionecrosis (ORN) of the jaw in head and neck oncology patients who undergo postirradiation tooth extractions. Evidence-based studies show that the incidence of ORN is 2-18% in patients who receive tooth extractions after radiotherapy.¹⁷ Interestingly, despite improving a variety of conditions that otherwise fail with conventional therapeutic approaches, the mechanisms of action associated with the benefits obtained using HBOT in preventing and/or treating ORN remain largely unknown.⁶

Research directed at evaluating wound healing responses to HBOT have generated numerous studies that investigated tissue vitality by assessing wound blood perfusion status using laser Doppler flowmetry (LDF), laser Doppler imaging (LDI), and intravital microscopy (IVM).^{11,20,22,28,29} Interestingly, even with many studies using well recognized and accepted diagnostic instruments, most techniques are only able to quantify a particular parameter (e.g. circulatory flux or blood flow) and are unable to provide information on vascular morphology and angioarchitecture. To this end, we used sidestream dark-field (SDF) imaging, a commercially available handheld video microscopy system that enabled direct noninvasive observations and quantifications of tissue subsurface microcirculation.¹⁰ Embodied into a portable handheld device, SDF imaging provides a way of quantifying functional anatomic changes *in vivo* without the use of contrast enhancement agents and destructive



tissue preparations for targeted tissue investigations under different (patho-) physiological conditions.²⁷ SDF imaging has been used in various medical fields for investigations into tissue perfusion abnormalities in critically ill patients associated with sepsis, septic shock and cardiac surgery.^{2,3} Recently, SDF imaging has been used for investigating the dynamics of wound vascular regeneration under both normal and pharmacological conditions.^{14,15}

The purpose of this study was to investigate the role of HBOT in promoting vascular regeneration in healing oral mucosal surgical flaps. Functional capillary density (FCD), a diffusion-related parameter derived from direct anatomical examination of blood perfused capillaries, was used to objectively quantify the temporal course of mucosal flap vascularization under normal and HBOT conditions using SDF imaging.

MATERIALS AND METHODS

The protocols and study guidelines for this investigation were reviewed and approved by the institutional Animal Experimentation Committee of the Academic Medical Center of the University of Amsterdam. Animal care and use was performed in accordance with the guidelines of the Dutch Committee of Animal Experiments.

Animals

Ten male specific-pathogen free New Zealand White rabbits (Charles River Laboratories France, L'Arbresle Cedex, France) with a mean body weight of 3.3 ± 0.1 kg were randomly allocated into two groups of 5: control and HBOT. Before initiating the study, all animals were permitted 1 week to adapt to their new environments and were housed individually in large conventional cages in a light-controlled room (12 hours light: 12 hours dark) kept at $22 \pm 1^\circ\text{C}$ with a relative humidity of $55 \pm 10\%$ and received standard food pellets and water for consumption *ad libitum*. Animals designated to receive HBOT were trained simultaneously during their 1-week acclimatization to get accustomed to their individual HBOT compartment. Animals were accommodated in their own compartment daily for 90 minutes at the same time of day.

All animals received a mixture of ketamine (Nimatek, Eurovet Animal Health BV, Bladel, The Netherlands; 15 mg/kg) and dexmedetomidine (Dexdomitor, Pfizer Animal Health BV, Capelle aan den IJssel, The Netherlands;

0.2 mg/kg), injected subcutaneously, to achieve sedation and anesthesia for blood sampling, wound preparation, and microcirculation measurements. After induction of anesthesia, baseline and consecutive whole blood counts were determined from 1 mL of blood obtained at each time point from the central auricular artery. After performing baseline and serial microvascular imaging on the designated wound flap region of interest (ROI), anesthesia was antagonized with atipamezole (Antisedan®, Pfizer Animal Health BV, Capelle aan den IJssel, The Netherlands; 1 mg/kg SC). All animals were subjected to the same experimental procedures; weighing, anesthesia, blood sampling, baseline capillary density measurements, surgical preparation of palatine flap wound (only on the first day), immediate postoperative and prospective flap FCD assessments followed by reversal of anesthesia, and exposed in two separate groups for two weeks to either normobaric/normoxic conditions (control) or HBOT.

Surgical wound preparation

After performing preoperative (baseline) capillary density measurements, a split-thickness flap in the anterior hard palatine mucosa was raised in all animals; details describing the wound model and surgical procedure have been described elsewhere.¹⁴ Briefly, just posterior to the maxillary auxiliary incisors or “peg teeth”, a partial-thickness mucosal flap was prepared by creating a transverse incision, 1 mm thick, along the length of the caudal side of the fourth plial ridge with two lateral releasing incisions. The mucosal flap was raised, suspended for 30 min, rinsed intermittently with warm $37\pm1^{\circ}\text{C}$ sterile 0.9% NaCl (saline) solution, repositioned, and subsequently closed primarily with 6-0 Ethilon monofilament non-resorbable sutures (Ethicon, Johnson & Johnson, Langhorne, Pennsylvania, USA) placed 1 mm medially from the left and the right flap corners. One week after wound preparation the sutures were removed. The same investigator (RH) performed all surgical procedures.

Hyperbaric oxygen therapy protocol

For two consecutive weeks, during weekdays (i.e. 10 days total) after the last clinical HBOT session in the evenings, the animals designated to receive a medical grade protocol for HBOT were transported to the Department of Hyperbaric Medicine. A specially designed stainless steel transport pushcart-container built with adjustable compartments to accommodate at least 6 rabbit-sized animals was constructed. Equipped with both oxygen in- and



outflow nozzle connections to evenly dissipate oxygen in the entire pushcart-container, each of the 6 individual compartments could effectively contain 100% oxygen and were completely isolated once the installation of a 1 cm-thick poly(methyl methacrylate) (PMMA) or acrylic glass cover was lowered and fitted on the top of the entire pushcart-container. A photograph of the transport pushcart-container, compartment oxygenations test using a compact air oxygen-measuring device (GOX 100, Geisinger Electronic GmbH, Regenstauf, Germany), and use of the pushcart-container during a running experiment is illustrated in Figure 1.

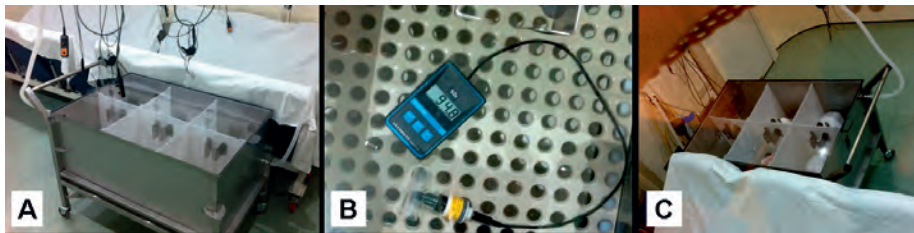


Figure 1. A custom-built transport pushcart-container with its oxygen inflow and outflow tube connections stationed in the hyperbaric tank (Panel A). To test if each compartment was able to properly contain 100% oxygen, a compact air oxygen measuring instrument was used (Panel B); the oxygen meter registered 94.8% oxygen in the posterior compartments (i.e. most distal from oxygen inflow source) after 10 minutes of switching on the oxygen inflow. A photograph illustrating an actual experimental procedure during HBOT is presented in Panel C.

Preparation for the HBOT experimental procedure was initiated everyday at 11:00 in the morning by withdrawing of food and drink from each animal at their normal housing establishment until the start of the HBOT protocol onsite. This was intended to produce an urge to drink as a response from mild dehydration in order to stimulate deglutition for equalization of pressure in all animals during the pressurization phase of the diving protocol. Control animals were treated according to the same procedures, but did not undergo HBOT. Upon arrival at the hyperbaric tank site, the pushcart-container was rolled carefully into the tank and positioned directly under a ceiling-rack from which oxygen supply was obtained.

Fifteen minutes prior to commencing the hyperbaric diving protocol, solid food and drinking gel was provided to each animal and saturation of 100% oxygen in all compartments was initiated. An investigator was present in the hyperbaric tank during every experiment to monitor the animals during the HBOT procedure. Three in-tank investigators (RH, DMJM, and SH) were required

to conform to a diving medical examination and credited with good health and physical condition in order to participate in the hyperbaric tank experiments. A diagram summarizing the HBOT protocol is illustrated in Figure 2.

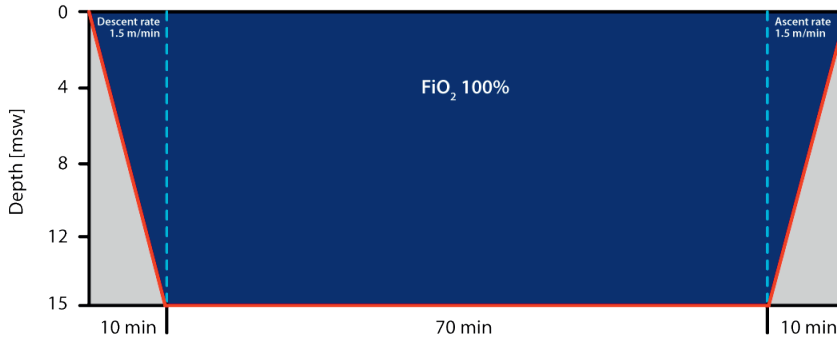


Figure 2. Hyperbaric tank dive plan illustrating the HBOT protocol.

FiO_2 : fraction of inspired oxygen, msw: meters of salt water

Microvascular imaging

Palatine microcirculatory measurements of FCD were obtained using SDF imaging (MicroScan Video Microscope System, MicroVision Medical, Amsterdam, The Netherlands); details about the technique have been described elsewhere.^{7,16} Briefly, the SDF technique is built into a commercially available handheld video microscopy instrument that operates by epilluminating the surface of the ROI with six concentrically arranged light-emitting diodes (LEDs) placed around the exterior tip of the imaging probe light guide. The LEDs emit green light at a 530 nm wavelength, which is scattered into the tissue and absorbed by hemoglobin in the circulating erythrocytes. The absorbed light, reflected by the erythrocytes, produces clear images of dark intraluminal circulating globules contrasted by a light background. All microcirculation imaging was recorded using a 5x objective lens system (equal to 380x onscreen magnification), which was captured by a CCD video camera with a 720x576 pixel resolution, producing a 1.0x0.75 mm² imaged tissue segment. All measurements were recorded for 2 minutes, stored on DVI tapes on a Sony DSR-11 DVCAM™ recorder (Sony, Shinagawa-ku, Tokyo, Japan), and viewed on a 19-inch Samsung SyncMaster 932Mv LCD monitor (Samsung, Seoul, South Korea) with a 1440x900-screen resolution.

SDF measurements

All microcirculatory measurements were performed by the same investigator (RH) in the same room kept at a constant temperature of $22\pm 1^\circ\text{C}$; data was obtained from all animals preoperatively (baseline), directly postoperatively and on days 2, 4, 7, 9, 11, 14, and 21. As the HBOT lasted until day 11, the last SDF measurement was carried out 10 days after the final tank session. After anesthetizing and withdrawing 1 mL of blood, the animals were placed on their back and a short (1 cm) cotton dental roll was wedged between the right first and second mandible and maxillary premolars to keep the jaws in an open configuration on an operating table. Using a small piece of sterile gauze, the tongue was rolled towards the back of the oral cavity to create free access to the palatine wound flap for positioning of the SDF imaging probe. The ROI was subsequently moistened with a drop of warm (37°C) sterile 0.9% NaCl (saline) solution to enable proper contact between the probe lens and the mucosal surface.

FCD measurements were performed by gently positioning the lens of the imaging probe, covered with a sterile disposable cap (MicroScan Lens, MicroVision Medical, Amsterdam, The Netherlands), perpendicularly over the palatine mucosal surface on the area between the 2 sutures. Without applying pressure and gently gliding the imaging probe at a 1 mm distance from the edge of the flap posterior border, a 2-min video recording of 5 adjacent sites in the length of the wound surface was obtained. A minimum of 10 seconds of stable image acquisition, with proper brightness and contrast adjustments, was recorded at each time point. To ensure no pressure artifacts were present during image acquisition, the SDF probe objective was briefly withdrawn and then advanced between image recordings on each of the 5 adjacent sites in the ROI.

Vessel enumeration

All microcirculatory data stored on DVI tapes were digitalized into AVI files for offline analysis with Adobe Premier Pro 1.5 (Adobe Systems Incorporated, San Jose, California, USA); image analysis was performed by isolating one image frame per adjacent site from each 2-min recording from all time points (45 in total). The selection criteria for isolation of individual image frames for analysis was based on image resolution, clarity, and elimination of pressure induced artifacts as described previously in a consensus meeting on evaluating microcirculation data for analysis.¹ All microcirculation data were analyzed at random by the same investigator (RH).

Assessment of FCD was performed by counting the total number of capillary loops per visual field (area of 0.75 mm²) on a 19-inch Samsung SyncMaster 932Mv LCD monitor (Samsung, Seoul, South Korea) with a 1440x900-screen resolution. The mean FCD obtained from the 5 isolated image frames, expressed as the number of capillaries per millimeter squared (cpl/mm²), was used to quantify the course of vascular regeneration at each time point. By calculating the mean from the 5 sampled video frames we averaged FCD to represent the overall wound area.

Statistical analysis

Sample size was based on a previously reported intraoral wound healing model with repeated (functional) capillary density measurements.¹⁴ Normal distribution of all microcirculation and supportive data was confirmed with the D'Agostino and Pearson omnibus normality test. All parameters (FCD, body weight, and whole blood counts) were analyzed separately. Repeated measures two-way analysis of variance (ANOVA) was used to detect overall time effects and time by group effects. Significant main effects were subsequently analyzed using paired-samples t-test (within group over time) and independent-samples t-tests (between groups) with Bonferroni correction. To adjust for innate microcirculatory biological variations, all microvascular measurements were standardized for ease in data interpretation; mean FCD measurements were normalized with respect to baseline and converted into percentages. A *p*-value less than 0.05 was considered statistically significant; all data are presented in mean ± SD. Data analyses was performed with GraphPad Prism version 5.0 for Windows (GraphPad Software Inc., La Jolla, California, USA).

RESULTS

In both study groups, postoperative flap recovery was uneventful with no signs of wound dehiscence or infection. The wound model and experimental procedures were well tolerated by all subjects and health did not decline at the cost of malnutrition or dehydration as indicated by the significant increase in body weight by day 21 (*p*<0.05 vs. baseline; paired-samples t-test) in both groups. There were no significant differences in body weight between the two groups and no significant differences in whole blood counts were detected within or between the two groups. A summary of all body weight and whole blood count data is presented in Table 1.



Table 1. Summary of body weight and whole blood counts for both animal groups at each time point. All data are presented in means \pm SD.

			BL: Day 0			Day 2			Day 4		
Mass	[kg]	CON	3.21	\pm	0.14	3.21	\pm	0.12	3.21	\pm	0.12
		HBOT	3.29	\pm	0.07	3.23	\pm	0.10	3.23	\pm	0.12
Hb	[mmol/L]	CON	7.7	\pm	0.3	7.2	\pm	0.3	7.3	\pm	0.1
		HBOT	7.8	\pm	0.1	7.7	\pm	0.3	7.6	\pm	0.2
RBC	$\times 10^{12}/L$	CON	5.77	\pm	0.33	5.28	\pm	0.20	5.34	\pm	0.11
		HBOT	5.66	\pm	0.17	5.58	\pm	0.31	5.52	\pm	0.21
WBC	$\times 10^9/L$	CON	6.32	\pm	0.77	6.92	\pm	1.18	6.62	\pm	0.65
		HBOT	7.48	\pm	1.61	7.28	\pm	0.94	7.12	\pm	1.43
PLT	$\times 10^9/L$	CON	222	\pm	40	264	\pm	37	261	\pm	20
		HBOT	248	\pm	12	286	\pm	30	306	\pm	48

BL: baseline; CON: control; HBOT: hyperbaric oxygen therapy; Hb: hemoglobin; RBC: red blood cells; WBC: white blood cells; PLT: platelets

* $p < 0.05$ vs. BL; paired samples t-test

Response to HBO procedure

The pushcart-container was designed to accommodate a flat PMMA panel or acrylic glass cover that enabled direct observation and monitoring of all (awake) animals for signs of distress or discomfort during hyperbaric procedures. Despite some ambient noise produced by the oxygen flow into the pushcart-container and pressure changes, all hyperbaric tank sessions were uneventful with no animal showing any signs of alarming behavior or pain. The animals appeared more curious than distressed and showed overall a good response to all procedures.

Table 2. Summary of normalized mucosal flap functional capillary density measurements for each time point in each animal group. All data are presented in means \pm SD.

		BL: Day 0			Postop			Day 2			Day 4		
CON	[%]	100	±	0	34	±	2*	60	±	8*	71	±	9*
HBOT	[%]	100	±	0	24	±	4*	61	±	9*	75	±	8*

BL: baseline; CON: control; HBOT: hyperbaric oxygen therapy

* $p < 0.001$ vs. BL; paired samples t-test, † $p < 0.05$ vs. BL; paired samples t-test

Day 7			Day 9			Day 11			Day 14			Day 21		
3.21	±	0.12	3.20	±	0.12	3.23	±	0.12	3.30	±	0.13	3.40	±	0.14*
3.22	±	0.19	3.24	±	0.21	3.27	±	0.21	3.33	±	0.20	3.49	±	0.25*
7.5	±	0.2	7.5	±	0.3	7.6	±	0.2	7.7	±	0.1	7.8	±	0.2
7.6	±	0.2	7.6	±	0.2	7.6	±	0.2	7.5	±	0.1	7.6	±	0.2
5.46	±	0.20	5.50	±	0.12	5.58	±	0.07	5.64	±	0.11	5.72	±	0.15
5.49	±	0.22	5.43	±	0.26	5.43	±	0.25	5.44	±	0.19	5.41	±	0.18
5.90	±	0.78	5.16	±	0.75	6.40	±	0.82	6.08	±	0.85	6.11	±	0.70
7.04	±	1.26	6.86	±	1.06	6.91	±	0.82	6.95	±	0.82	7.45	±	1.62
289	±	64	269	±	78	224	±	38	222	±	36	260	±	61
304	±	48	308	±	33	284	±	13	292	±	57	259	±	30

Wound capillary regeneration

Preoperative (baseline) mean FCD for both groups was 79 ± 4 cpl/mm² and 23 ± 6 cpl/mm² directly following wound preparation ($p < 0.0001$; unpaired t-test), no significant difference in baseline or direct postoperative measurements between the two groups was found. Microcirculation data analyses comparing normalized FCD within each group over time are presented in Table 2. In the control group, statistically significant differences in mean FCD were found between baseline and immediately postoperative, days 2, 4, 7, and 9 ($p < 0.0001$; repeated measures ANOVA). Similarly, in the HBOT group, significant differences in mean FCD were found between baseline and immediately postoperative, days 2, 4, 14, and 21 ($p < 0.0001$; repeated measures ANOVA). FCD returned to baseline values in the control and HBOT groups by day 11 and day 7 respectively. Interestingly, in the HBOT group, a significant overshoot in FCD was observed beyond baseline values on days 14 and 21 ($p < 0.05$; paired samples t-test). Figure 3 presents a series of typical SDF microcirculation image frames obtained from different time points for both groups, illustrating the progress of FCD.

Day 7			Day 9			Day 11			Day 14			Day 21		
80	±	10*	86	±	7*	93	±	7	98	±	6	103	±	3
93	±	8†	103	±	5	107	±	5	109	±	5†	109	±	7†



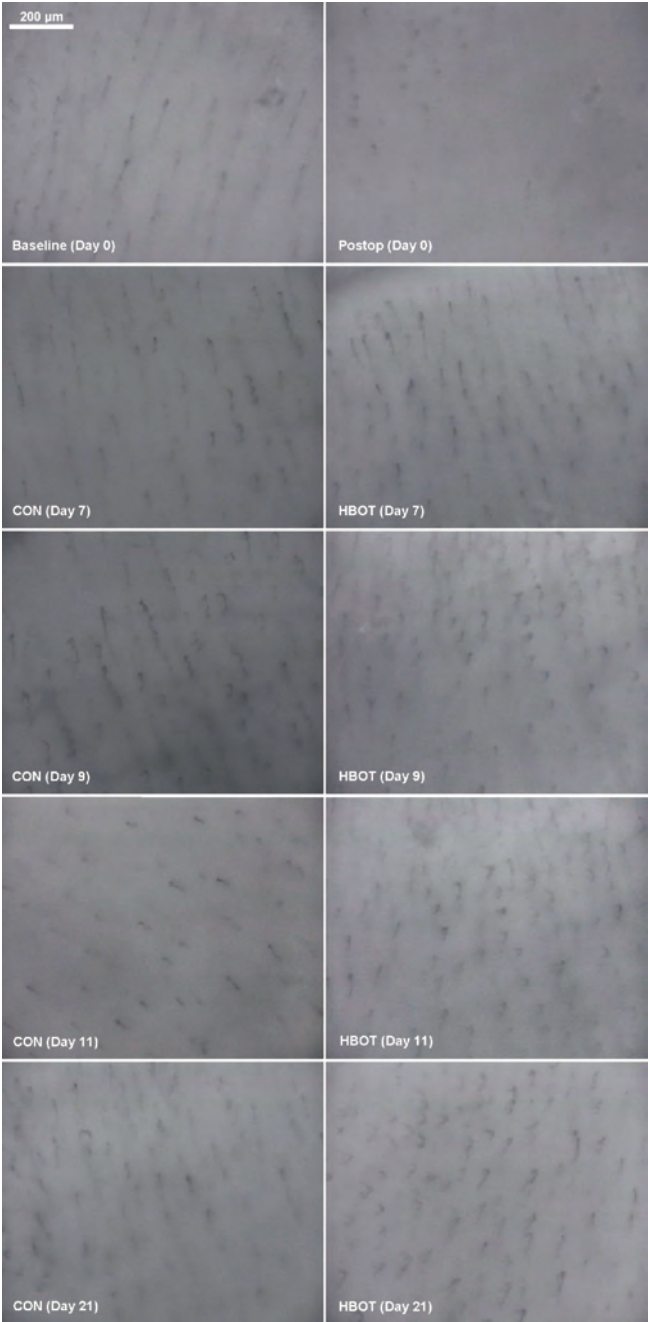


Figure 3. A series of typical SDF microcirculation image frames obtained from both groups; two frames representing baseline and postoperative measurements (day 0) are presented followed by a series of frames illustrating the progress of FCD on days 7, 9, 11, and 21 respectively.

Comparison of all normalized microvascular measurements revealed a significant interaction effect between time and group ($F(8, 64) = 9.60, p < 0.0001$) resulting from a significant increase in microcirculation in the HBOT group relative to the control group on days 7, 9 and 11 [Fig. 4].

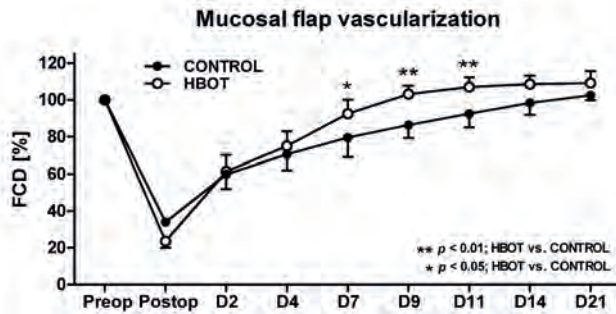


Figure 4. Comparison of normalized functional capillary density (FCD) measurements between groups (independent-samples t-test). FCD measurements were performed preoperatively (baseline), immediately postoperatively, and subsequently on postoperative days 2, 4, 7, 9, 11, 14, and 21. All data are presented as mean \pm SD.

DISCUSSION

The purpose of the present study was to investigate vascular regeneration dynamics in healing oral mucosal surgical flaps under the influence of HBOT. Our results suggest that HBOT is capable of yielding a response in wound vascular regeneration dynamics, as indicated by elevated FCD (relative to control). Equally important, our results also demonstrate that continuous microvascular measurements, used as an objective parameter to qualitatively evaluate wound status, can be utilized to quantify the progress of vascular regeneration following HBO-mediated healing in keratinized oral mucosal flaps.

Wound vascular regeneration and adequate oxygenation are essential for establishing a stable wound microenvironment to support tissue repair and restoration of anatomical function. Previous studies have confirmed a beneficial effect of HBOT on perfusion or neovascularization in chronic and non-chronic wounds.^{8,11,13,20,22,29,30} In an experimental study Hopf et al. graded neovascularization subcutaneously in mice by histological assessment after HBOT and found a greater and dose-dependent angiogenic response in a hyperbaric group compared to controls.⁸ This is supported by data of Zhao et

al. obtained from an ischemic ear model in rabbits that showed an increase in blood vessel count associated with HBO compared to ischemic controls.³⁰ In an irradiated rabbit model Marx et al. determined an eight- to ninefold increased vascular density after HBOT by histological analysis.¹³ Analogous to increasing anatomical components, Sheikh et al. reported restored tissue functionality for the first time by demonstrating elevated wound bed perfusion after HBOT on full-thickness dermal wounds in mice.²² Interestingly, Sheikh and co-workers reported a significant increase in perfusion in their HBO group on day 10, three days after the very last hyperbaric session on day 7. Although, the present study used a different wound model, our results demonstrate a similar trend in wound blood circulation restoration indicated by augmented expression in tissue vascularity between days 7, 9, and 11 in the HBOT group. In another study using LDF, it was reported that acute HBOT on ischemic rat skin flaps improves perfusion by stimulating the microcirculation.²⁹ Subsequent HBOT investigations later demonstrated elevated blood perfusion in healing tissue of a mandibular bone defect in rats and acceleration of neovascularization in impaired wound models using IVM in mice.^{11,20} However, despite positive results using HBOT to improve tissue vascularization and microperfusion, contradicting results associated with HBO still persist. One example of such contradictory results was reported in a study using LDI, in which no significant improvement in blood flow patterns between HBO group and controls was found.²⁸ However, there is very little experimental evidence regarding wound microperfusion restoration after injuries. Although previous dermal perfusion studies were performed using LDI and LDF, observations of microcirculatory angioarchitecture and hemodynamics has as yet not been observed in vivo after HBOT. Moreover, laser Doppler techniques though useful in detecting the absence or presence of blood flow, the data obtained using LDF or LDI cannot be attributed to specific microvascular networks nor can they reveal angioarchitecture or angiomorphology.

As HBO increases the amount of oxygen dissolved in blood plasma (pO_2), higher oxygen tensions can be obtained in injured tissues and in ischemic wounds.²⁶ When a higher pO_2 is measured in tissue adjacent to an ischemic wound, an accelerated wound healing was observed.^{4,23} In vitro HBO experiments have been shown to accelerate enzymatic processes that among others improve cellular response and proliferation.²⁴ New fibroblasts in a wound require sufficient oxygen for sequential synthesis and maturation of collagen to support blood vessel proliferation.^{9,18}

Differences in diving times, depth, and frequency of HBOT make it difficult to compare studies, since a higher dose of oxygen and tissue pO_2 determines the degree of angiogenic potency and wound healing.^{4,8,23} Determining wound oximetry might give a good prediction for wound healing.^{4,23} With this in mind, it would be advantageous to combine wound oximetry with SDF-measurements in the future. Higher oxygen tension in wounds might be correlated with a particular percentage in FCD expression, this might aid in predicting in which wounds HBOT is most beneficial, creating a clear indication for HBO treatment. It is interesting to point out that stress may have a negative influence in animal wounds by diverting oxygen supply from a wound region to accommodate other physiological needs.⁵ Following the findings of Gajendrareddy et al., best efforts were practiced in order to decrease stress to a very minimum to provide the best possible environment for our animal groups. Transportation to the hyperbaric tank, oxygen gas inflow, and other miscellaneous noises were kept at an absolute minimum to evade anxiety in the animals; no alarming behavior or distress was observed in any of the animals.

In routine practice, patients who are at risk of developing ORN are treated preventively, both pre- and postoperatively with HBOT. However, despite these preventive practices, no direct evidence-based consensus currently exists that specifies in which patients HBOT is truly indicated; such a consensus could strategically alleviate patients from being subjected to expensive and lengthy therapeutic sessions that are unsubstantiated by a lack of both consistent and convincing data that clearly defines predictable outcomes. Our results indicate that vascular regeneration can be accelerated by HBO; however, care should be taken when trying to extrapolate data from the present study to other anatomical tissues. Although keratinized epithelial tissues such as in the oral mucosa and the skin share similar histological constructions and follow similar wound healing patterns, both tissues may respond differently to HBOT regimens.

In conclusion, the present study introduces for the first time quantification of postoperative microcirculatory regeneration with SDF imaging in keratinized oral mucosal surgical flaps treated with HBOT. Our results, characterized by a rise in FCD, appears to share a similar trend with findings from other experimental studies reporting an improvement in wound blood perfusion in response to HBOT. While it may be true that elevating tissue pO_2 in ischemic wounds with poor vascularity provides the necessary oxygenation for angiogenesis and cellular proliferation, it is important to emphasize consistency in selecting



wound model and a consensus in HBO regimens in order to measure and properly compare the evolution of angiogenesis in wounds treated by hyperoxia across different clinical and experimental scenarios.

ACKNOWLEDGEMENTS

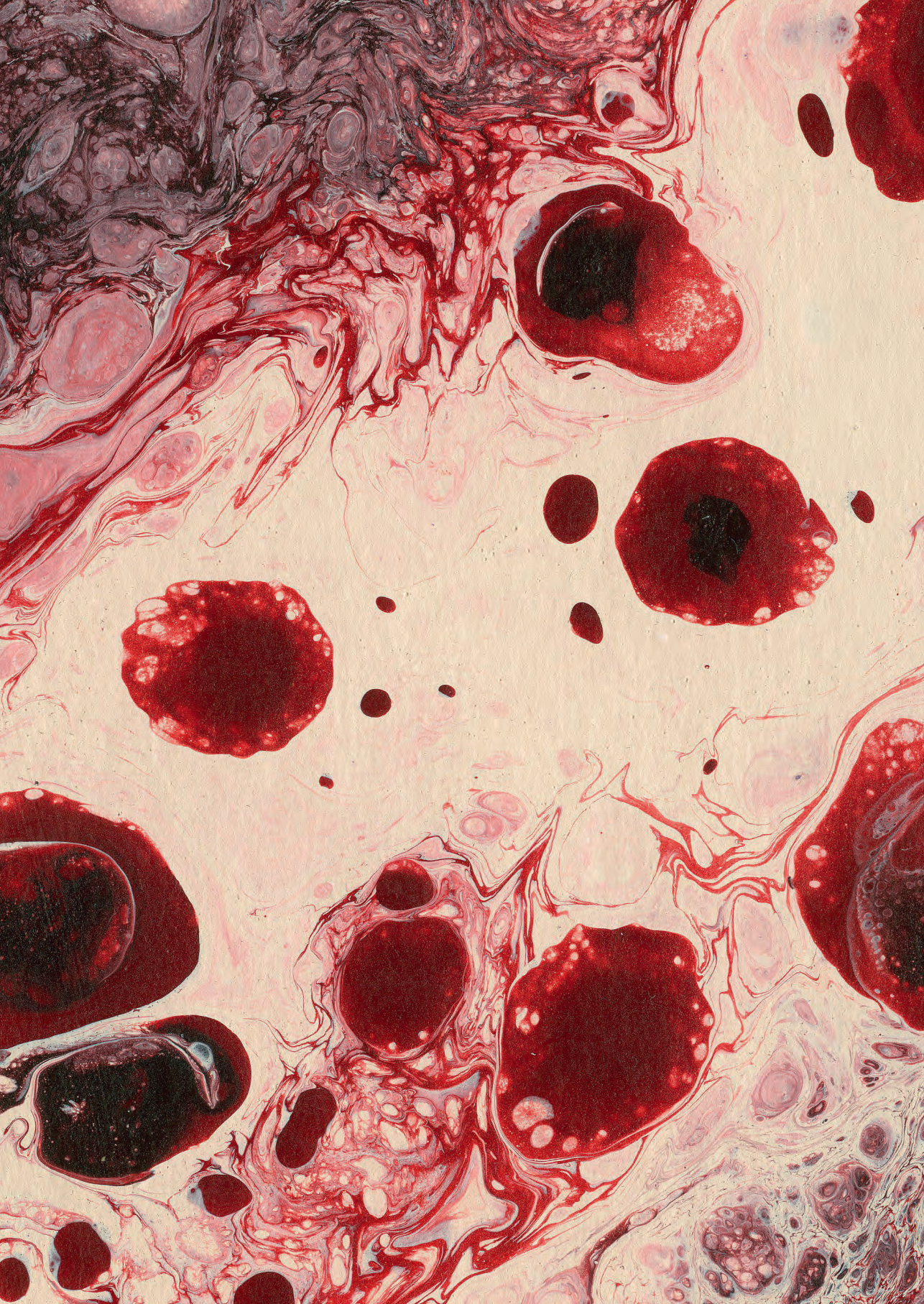
We would like to acknowledge and thank the staff of the Department of Hyperbaric Medicine of the Academic Medical Center for their kind support for this investigation. We acknowledge Sanne Hackmann and Alwin W. Blankestijn from the Animal Research Institute Academic Medical Center (ARIA) for their excellent biotechnical support.

REFERENCES

1. De Backer D, Hollenberg S, Boerma C et al. How to evaluate the microcirculation: report of a round table conference. *Crit Care* 2007; 11:R101.
2. Elbers PWG, Ince C. Bench-to-bedside review: Mechanisms of critical illness – classifying microcirculatory flow abnormalities in distributive shock. *Crit Care* 2006; 10:221.
3. Elbers PWG, Ozdemir A, van Iterson M, van Dongen EPA, Ince C. Microcirculatory imaging in cardiac anesthesia: Ketanserin reduces blood pressure but not perfused capillary density. *J Cardiothorac Vasc Anesth* 2009; 23:95–101.
4. Fife CE, Buyukcakil C, Otto GH et al. The predictive value of transcutaneous oxygen tension measurement in diabetic lower extremity ulcers treated with hyperbaric oxygen therapy: a retrospective analysis of 1144 patients. *Wound Rep Reg* 2002; 10:198–207.
5. Gajendrareddy PK, Sen CK, Horan MP, Marucha PT. Hyperbaric oxygen therapy ameliorates stress-impaired dermal wound healing. *Brain Behav Immun* 2005; 19:217–222.
6. Gill AL, Bell CN. Hyperbaric oxygen: its uses, mechanisms of action and outcomes. *QJM* 2004; 97:385–395.
7. Goedhart PT, Khalilzade M, Bezemer R, Merza J, Ince C. Sidestream dark field (SDF) imaging: a novel stroboscopic LED ring-based imaging modality for clinical assessment of the microcirculation. *Opt Express* 2007; 15:15101–15114.
8. Hopf HW, Gibson JJ, Angeles AP et al. Hyperoxia and angiogenesis. *Wound Rep Reg* 2005; 13:558–564.
9. Hunt TK. The physiology of wound healing. *Ann Emerg Med* 1988; 17:1265–1273.
10. Ince C. The microcirculation is the motor of sepsis. *Crit Care* 2005; 9(Suppl. 4):S13–19.
11. Klemetti E, Rico-Vargas S, Mojon P. Short duration of hyperbaric oxygen treatment effects blood flow in rats: pilot observations. *Lab Anim* 2005; 39:116–121.
12. Kranke P, Bennett MH, Martyn-St James M, Schnabel A, Debus SE. Hyperbaric oxygen therapy for chronic wounds. *Cochrane Database Syst Rev* 2012; 18:4:CD004123.
13. Marx RE, Ehler WJ, Tayapongsak P, Pierce LW. Relationship of oxygen dose to angiogenesis induction in irradiated tissue. *Am J Surg* 1990; 160:519–524.
14. Milstein DM, Lindeboom JA, Ince C. Intravital sidestream dark-field (SDF) imaging is used in a rabbit model for continuous noninvasive monitoring and quantification of mucosal capillary regeneration during wound healing in the oral cavity: a pilot study. *Arch Oral Biol* 2010; 55:343–349.
15. Milstein DM, Lindeboom JA, Ince C. The influence of zoledronic acid and cyclophosphamide on microcirculation regeneration in healing oral mucosal flaps. *Arch Oral Biol* 2011; 56:599–606.
16. Milstein DMJ, Bezemer R, Ince C. Sidestream Dark-Field (SDF) Video Microscopy for Clinical Imaging of the Microcirculation. In: Leahy MJ editor. *Microcirculation Imaging*. Weinheim, Germany: Wiley-VCH Verlag GmbH & Co. KGaA; 2012. pp 37–52.
17. Nabil S, Samman N. Incidence and prevention of osteoradionecrosis after dental extraction in irradiated patients: a systematic review. *Int J Oral Maxillofac Surg* 2011; 40:229–243.
18. Niinikoski JHA. Clinical hyperbaric oxygen therapy, wound perfusion, and transcutaneous oximetry. *World J Surg* 2004; 28:307–311.
19. Rodriguez PG, Felix FN, Woodley DT, Shim EK. The role of oxygen in wound healing: A review of the literature. *Dermatol Surg* 2008; 34:1159–1169.
20. Sander AL, Henrich D, Muth CM, Marzi I, Barker JH, Frank JM. In vivo effect of hyperbaric oxygen on wound angiogenesis and epithelialization. *Wound Repair Regen* 2009; 17:179–184.
21. Schreml S, Squeimies RM, Prantl L, Karrer S, Landthaler M, Babilas P. Oxygen in acute and chronic wound healing. *Br J of Dermatol* 2010; 163:257–268.
22. Sheikh AY, Rollins MD, Hopf HW, Hunt TK. Hyperoxia improves microvascular perfusion in a murine wound model. *Wound Rep Reg* 2005; 13:303–308.
23. Smith BM, Desvigne LD, Slade JB, Dooley JW, Warren DC. Transcutaneous oxygen measurements predict healing of leg wounds with hyperbaric therapy. *Wound Repair Regen* 1996; 4:224–229.



24. Tandara AA, Mustoe TA. Oxygen in wound healing – more than a nutrient. *World J Surg* 2004; 28:294–300.
25. Thackham JA, McElwain S, Long RJ. The use of hyperbaric oxygen therapy to treat chronic wounds: A review. *Wound Rep Reg* 2008; 16:321–330.
26. Tibbles PM, Edelsberg JS. Hyperbaric-oxygen therapy. *N Engl J Med* 1996; 334:1642–1648.
27. Treu CM, Lupi O, Bottino DA, Bouskela E. Sidestream dark field imaging: the evolution of real-time visualization of cutaneous microcirculation and its potential application in dermatology. *Arch Dermatol Res* 2011; 303:69–78.
28. Uhl E, Sirsjo A, Haapaniemi T, Nilsson G, Nylander G. Hyperbaric oxygen improves wound healing in normal and ischemic skin tissue. *Plast Reconstr Surg* 1994; 4:835–841.
29. Zamboni WA, Roth AC, Russell RC, Smooth EC. The effect of hyperbaric oxygen on reperfusion of ischemic axial skin flaps: a laser Doppler analysis. *Ann Plast Surg* 1992; 28:339–341.
30. Zhao LL, Davidson JD, Wee SC, Roth SI, Mustoe TA. Effect of hyperbaric oxygen and growth factors on rabbit ear ischemic ulcers. *Arch Surg* 1994; 129(10):1043–1049.





CHAPTER 4

Outcome of a rabbit model for late irradiation effects in mandibular oral mucosa and bone: a pilot study

R. Helmers

D.M.J. Milstein

N.F. Straat

H.M. Rodermond

N.A.P. Franken

C.D. Savci-Heijink

H.H. de Boer

J. de Lange

Edited version of: J Clin Transl Res. 2020;6:225–235.

ABSTRACT

Background: Late side effects of radiotherapy (RT) in the treatment for head and neck malignancies involve an inadequate healing response of the distressed tissue due to RT induced hypovascularity. The aim of this study was to develop a pilot model in which vascular alterations associated with late irradiation (IR) injury could be measured in rabbit oral mucosa and mandibular bone.

Materials and methods: Eight male New Zealand White rabbits were divided over 4 treatment groups. Group I-III received 4 fractions of RT (5.6 Gy, 6.5 Gy and 8 Gy respectively) and group IV received 1 fraction of 30 Gy. Oral microcirculatory measurements were performed at baseline (before RT) and once a week during 11 consecutive weeks after RT assessing perfusion parameters, i.e. total vessel density (TVD), perfused vessel density (PVD), proportion of perfused vessels (PPV) and microvascular flow index (MFI). Post-mortem histopathology specimens were analyzed.

Results: 5 weeks after RT, TVD and PVD in all groups showed a decrease of >10% compared to baseline, a significant difference was observed for groups I, II and IV ($p < 0.05$). At T11 no lasting effect of decreased vessel density was observed. PPV and MFI remained unaltered at all time points. Group IV showed a marked difference in scattered telangiectasia-like microangiopathies, histological necrosis and loss of vasculature.

Conclusion: No significant lasting effect in mucosal microcirculation density due to IR damage was detected. Observed changes in microcirculation vasculature and histology may align preliminary tissue transition towards clinical pathology in a very early state associated with late IR injury in the oral compartment.

INTRODUCTION

Radiotherapy (RT) has an essential role in the treatment of head and neck (HN) cancer patients. Irradiation (IR) of HN malignancies concomitantly elicits acute and late injuries to healthy tissues resulting in clinical side effects such as oral mucositis, dry mouth, ulceration and osteoradionecrosis.^{11,35} Acute side effects of RT usually heal by the end of treatment, whereas possible late effects due to reduced vascularity and fibrosis tend to occur after a period of several months to years after treatment.^{4,31,33} RT induced hypovascularity could progress in a hypocellular and hypoxic tissue state in which the distressed tissue is unable to establish an adequate healing response to injury and eventually succumbs to tissue breakdown and osteoradionecrosis (ORN).²⁰ ORN in HN has a reported incidence of 2–22%^{23,25,34} and is a potentially mutilating and complicated pathology to manage.

Experimental research fulfills an essential role in providing standardization of a model and controlled environments for studying pathophysiology and interventional responses associated with HN IR injury. In clinical studies standardization in design is difficult to achieve as tumor location and radiation dose varies between patients. Late IR tissue histopathology involving human jawbone presents as a progressive state of hypovascularity and fibrosis.^{6,19} Experimental studies that aimed to create a late IR tissue injury model in the HN region were previously conducted. Distraction osteogenesis on rabbit irradiated mandibles showed general reduction in vascularity, osteoblastic activity and bone regeneration compared to non-IR controls.^{7,17,24,38} Increased fibrosis and decreased vascularity in the soft tissues surrounding the irradiated mandible was observed after 5 fractions of 15 Gy in a rat IR model.³¹ In another model using mini-pigs, an increased amount of fibrosis and decreased vascular lumens in the mandible was proportionally dependent with the dose administered (25–70 Gy) 14–24 weeks after RT.²⁷ Studies directed at evaluating the effects of RT mainly investigated tissue quality at functional or subcellular level by measurements obtained using x-ray microtomography (micro-CT),^{16,38,39} microangiography,¹⁸ transmission electron microscopy³¹ and by looking at histopathology.^{6,7,16–18,24,27,29,31,38,39} A disadvantage associated with most of the techniques listed above is that they are invasive and often require tissue manipulation and/or injecting a contrast medium for data acquisition. To further advance knowledge on oral tissue microvascular integrity and



its perfusion in response to IR, the oral microcirculation was measured in vivo using a noninvasive, optical spectroscopic-based handheld imaging system, sidestream dark-field imaging (SDFI). SDFI has extensively been used at the patient bedside and experimental setting to monitor and assess pathophysiological states associated with shock (e.g. cardiogenic, hypovolemic and septic),^{2,15} interventional endpoints and therapeutic responses associated with microvascular alterations in critical care patients, wound healing and the side effects of cancer chemotherapy and RT.^{12,13,22} Decreased capillary density, irregular dilatation of blood vessels and telangiectasia were associated with late IR effects in human oral mucosa.¹³ In the present study parameters coinciding with microvascular blood flow dynamics and microvascular density were examined and compared between baseline and then after IR.

The aim of this study was to develop a pilot translational IR model in which microvascular alterations associated with late IR injury could be measured in rabbit oral mucosa and mandibular bone using SDFI and histological analysis. Microcirculatory changes in vessel density and blood flow were quantified and compared between baseline and after IR. In order to ascertain the translational accuracy of a late IR injury model, we test the hypothesis that cumulative IR dosages equal to 22.4 Gy, 26 Gy, 30 Gy and 32 Gy would result in oral mucosal and mandibular bone histological changes similar to humans.

MATERIALS AND METHODS

The institutional Animal Experimentation Committee of the Academic Medical Center of the University of Amsterdam approved the protocols and guidelines for this study (Ref. No. DFL103187). The care and use of animals were conducted in accordance with the EU Directive 2010/63/EU (22 September 2010) and the Dutch Act on Laboratory Animal Experiments.

Animals

Eight male specific-pathogen-free New Zealand White rabbits (*Oryctolagus cuniculus*) (Charles River Laboratories France, L'Arbresle Cedex, France) were randomly divided between 4 groups. Each group received a different total IR dose. Mean body weight at start of the study was 2.72 ± 0.16 kg, weighing was carried out weekly throughout the entire period of the study. Animals

were housed separately in large cages (R-SUITE Enriched Rabbit Housing, Techniplast SpA, Buguggiate (Varese), Italy) in a 24-hour light-controlled room (12 h light/dark cycle) that was maintained at a constant temperature of $22\pm1^{\circ}\text{C}$ and humidity of $55\pm10\%$. Consumption of standard food pellet diet (LK-04, AB Diets, Woerden, The Netherlands) and water (acidified to pH 2.7) was available *ad libitum*. Sedation to perform microcirculation measurements, blood sampling and administration of RT, was achieved through administration of subcutaneous injection of a mixture of ketamine (Nimatek, Eurovet Animal Health BV, Bladel, The Netherlands; $15\text{ mg}\cdot\text{kg}^{-1}$) and dexmedetomidine (Dexdomitor, Pfizer Animal Health BV, Capelle aan den IJssel, The Netherlands; $0.2\text{ mg}\cdot\text{kg}^{-1}$). To monitor general hematological health a blood sample was obtained at every measurement time point by drawing 1 mL of blood from the central ear artery, anticoagulated in K2E 7.2 mg EDTA BD Vacutainer® 4 mL tubes (Becton, Dickinson & Co., Plymouth, United Kingdom) and analyzed by an automated Sysmex XE-5000 (Sysmex Corporation, Kobe, Japan). Hereafter, microcirculation measurements and RT were performed. After all data collection and RT atipamezole (Antisedan®, Pfizer Animal Health BV, Capelle aan den IJssel, The Netherlands; $1\text{ mg}\cdot\text{kg}^{-1}\text{ sc}$) was administered to reverse anesthesia. At the end of the study the animals were sacrificed using sodium pentobarbital (Euthasol®, AST Farma BV, Oudewater, The Netherlands; $120\text{ mg}\cdot\text{kg}^{-1}\text{ iv}$) administered via the lateral ear vein. After sacrifice the mandibles with overlaying mucosa were dissected and excised for postmortem histopathological analysis. All animals were exposed to the same experimental proceedings: weighing, sedation, baseline and consecutive weekly whole blood counts, microcirculation measurements, RT, reversal of anesthesia, sacrifice and mandibular excision.

Irradiation (IR)

IR was performed using an Xstrahl X-ray generator (Xstrahl Ltd., Surrey, United Kingdom), operated at 225 kV and 15 mA and inherent filtration with 1 mm Cu, a square tube collimator with an area of $8\times8\text{ cm}^2$. After being anesthetized the fur on the right lower jaw was shaved, the right side of the mandible was marked and subsequently the animals were transported from their housing facility to the IR lab at the Department of Experimental RT. Upon arrival at the experimental RT lab each rabbit was placed in a dorsally recumbent position on a table-top under the X-ray generator. The mandible faced the focus source of



the IR with a beam to subject distance of 20 cm. A lead plate with a rectangular recess of 2x6 cm was positioned on a foam scaffold in between the IR source and the mandible. A smaller lead shield to protect the eyes, underlying intraoral tissues and maxillary region was inserted intraorally to isolate the mandible for IR. The focus was oriented to unilateral IR to the right side of the mandible and the left side was used as a non-IR control. All animals were closely monitored during the treatment procedure after which they were transported back to their housing area where reversal of anesthesia was administered with 1 mg·kg⁻¹ sc atipamezole.

IR protocol

All study animals were randomly divided into 4 groups (I, II, III and IV) of 2 animals each and each group received different total irradiation doses (i.e. 22.4 Gy, 26 Gy, 32 Gy and 30 Gy respectively). Groups I, II and III received 4 fractions (5.6 Gy, 6.5 Gy and 8 Gy respectively with a dose rate of 110 cGy/min) in 2 consecutive weeks on day 0, 3, 6 and 9. Group IV received the total dose (30 Gy with a dose rate of 110 cGy/min) in 1 fraction on day 0. All IR protocol procedures were performed by the same investigators (RH, HMR and NAPPF).

Microvascular imaging technique

The microcirculation in the oral mucosa covering the lingual aspect of the mandible was examined and measured using a commercially available SDFI instrument, also known as MicroScan (MicroScan Video Microscope System, MicroVision Medical, Amsterdam, The Netherlands). Details on SDFI are described elsewhere.^{10,21} In brief, stroboscopic emission of 530-nm wavelength (green light) via LEDs placed at the tip of the lens probe epi-illuminate the tissue and partially gets scattered and absorbed by hemoglobin in red blood cells (RBCs). The difference in absorption and scattering produces clear images of dark circulating RBCs in the vascular lumen contrasted by a light background. Videoclips were captured through a 5x objective lens system (equal to 380x onscreen magnification) on a charge-coupled device (CCD) video camera with 720x576-pixel resolution. The imaged tissue segments were 1.0x0.75 mm². DVI tapes on a Sony DSR-11 DVCAM™ recorder (Sony, Shinagawa-ku, Tokyo, Japan) were used for storage and were viewed on a 19-inch Samsung SyncMaster 932Mv LCD monitor (Samsung, Seoul, South Korea) with a 1440x900-screen resolution.

SDFI measurements

In all groups microcirculatory measurements were performed at baseline (before RT) and every week for 11 consecutive weeks. All measurements were performed by the same investigator (RH) in the same examination room, kept at a constant temperature of $22\pm1^{\circ}\text{C}$. After inducing anesthesia and blood sampling, each animal was placed in a prone position on a flat surface with a cotton dental roll wedged between the maxillary and mandibular (pre-)molars to keep the mouth open and providing space for placement of the imaging probe. Moisturizing of the mouth for good contact between mucosa and probe tip was performed by irrigation of the oral mucosa with a warm (37°C) sterile physiological saline solution (0.9% NaCl). The imaging probe was covered with a sterile disposable cap (MicroScan Lens, MicroVision Medical, Amsterdam, The Netherlands) and placed gently perpendicular on the lingual aspect of the mandibular mucosa on the diastema (gap) between the incisors and the premolars and aiming for full contact without applying any pressure thereby avoiding vascular occlusion (pressure) artifacts. Microcirculation recordings were acquired while withdrawing and advancing the lens probe from release and contacting the tissue surface in order to record segments free of pressure artifacts. A 2-min video clip was obtained of 5 adjacent sites on the IR side and the contralateral non-IR side of the inside of the mandible in each subject at each time point.

Microcirculation data analysis

The DVI tapes used for storage of the microcirculation data were converted to digital AVI files with Adobe Premier Pro 1.5 (Adobe Systems Incorporated, San Jose, California, USA) and then analyzed offline. After separating the sequentially recorded sites per time point, 1 clip of each site (4 in total) was selected based on quality judged by good image brightness/contrast, sharpness, clarity and absence of pressure artifacts in conformity with guidelines established by a round table conference based on microcirculation data acquisition and analysis consensus meeting.²⁸ Hereafter, all microcirculation data was analyzed at random by two investigators (RH, NFS) using the Automated Vascular Analysis software package (AVA v3.02, MicroScan Video Microscope System, MicroVisionMedical, Amsterdam, The Netherlands). Analysis of microcirculatory data was performed on vessels with diameters $<25\text{ }\mu\text{m}$ for total vessel density (TVD; mm vessel/ mm^2), perfused vessel density (PVD; mm perfused vessel/ mm^2), proportion of perfused vessels (PPV; %)³ and microvascular flow index



(MFI). MFI was determined by describing the type of flow in each quadrant of the clip using the following scoring system: absent (0), intermittent (1), sluggish (2) or normal (3).^{5,32}

Mandibular histopathology

Following sacrifice, the mandible of each subject was carefully dissected and fixed using 4% buffered formaldehyde. Mandibular bone cross-sections were prepared as 4 mm thick slices, which were demineralized in ethylenediaminetetraacetic acid (EDTA) and processed into standard, paraffin embedded, 8 μ m thick histological slides. All samples were (immuno-) histochemically stained with hematoxylin and eosin (H&E), Elastica van Gieson (EVG) and analyzed under a light microscope (BX50, Olympus, Tokyo, Japan) at x100 magnification. The samples were analyzed for general histological parameters for tissue integrity and reactive changes such as hemorrhage, acute and chronic inflammation, osteoblast and osteoclast activity, loss of vascular structures, fibrosis and necrosis. Current study samples were compared to the histology of 2 healthy age-matched rabbit mandibular material obtained from a tissue bank of a former study (Ref. No. DFL101932). All histological analyses were performed by the same investigator (HHdB).

Statistical analysis

As no standardized experimental IR rabbit model was available in literature, this pilot study aimed to determine which dose could induce measurable late IR damage in tissue. Since research data on the effects of late IR effects on in vivo microcirculation was not available, this study served as a basis for orientation and design. We aimed to detect an estimated difference between baseline and post-IR in TVD of approximately 8–10% in the proposed study groups. A minimum of 2 animals per group were used in order to achieve procedural endorsement. As all study groups consist of just 2 rabbits the Friedmann test, a non-parametric test with no correction for multiple comparisons, was applied to all groups to detect a statistical difference (p -value <0.05) over time compared to baseline. The data of all parameters were separately analyzed (TVD, PVD, PPV, MFI, body weight, whole blood counts) and presented in mean \pm SD. Mean TVD and PVD measurements were converted into percentages and to correct for innate biological variations datasets were normalized with respect to baseline. Data analysis was performed with Prism 8.3.1 for macOS (GraphPad Software, LLC, San Diego, California, USA).

RESULTS

All animals responded well to the IR model and the repeated microcirculation measurement protocol with no signs of distress or discomfort. Transportation of the anesthetized animals to and from the IR lab was uneventful. After returning the animals to their housing and reversing anesthesia, no signs of distress or distressed recovery was observed. At T11 groups I-III showed significant increases in body mass compared to baseline ($p<0.05$). When body mass was examined separately in each animal, a marked decrease in body mass was noted in one animal from group IV, in which weight loss started from T7 and resulted in a 16% lower body mass at T11 compared to T6. Whole blood count parameters (Hb, PLT, RBC, WBC) remained within normal reference value range^{9,14} throughout all time points. Groups I, III and IV showed a recurrent significant decrease in PLT count and group IV a significant decrease in WBC count at different time points. Whole blood count parameters and body mass are presented in Table 1.

IR-related clinical observations

In group I, II and III no remarkable clinical observations were noted. At T2 both animals in group IV showed erythema of the irradiated skin [Fig. 1A] and one subject showed signs of mucositis around the area of the lower incisors [Fig. 1B]. These observations subsided by T3. Furthermore, both animals in group IV showed no regrowth of fur at the site of IR after 5 weeks (T5) [Fig. 1C], a notable difference compared to the other groups in which all subject showed full fur regrowth by this time point (T5). At T8 general fur regrowth started to appear in group IV and was fully recovered by T11.

Mandibular mucosa microcirculation response to IR

Good image quality (i.e. brightness/contrast, sharpness, clarity and absence of pressure artifacts) was obtained with the MicroScan on the lingual aspect of the mandibular mucosa. In each animal ($n=8$), 4 clips in total were obtained per time point; a total of 384 clips were analyzed (12 time points).



Table 1. Summary of body weight and whole blood counts for all animals at each time point. All data are presented in means \pm SD.

		BL (T0)		Day 7 (T1)		Day 14 (T2)		Day 21 (T3)		Day 28 (T4)		Day 35 (T5)	
Mass	[kg]	G1	2.75 ± 0.13	2.35 ± 0.43	2.96 ± 0.37	3.09 ± 0.30	3.22 ± 0.39	3.26 ± 0.39					
		G2	2.73 ± 0.43	2.80 ± 0.25	3.02 ± 0.34	3.14 ± 0.35	3.75 ± 0.29	3.33 ± 0.45					
		G3	2.64 ± 0.14	2.87 ± 0.06	3.03 ± 0.04	3.11 ± 0.02	3.11 ± 0.02	3.19 ± 0.01					
		G4	2.77 ± 0.06	2.80 ± 0.01	2.88 ± 0.04	3.04 ± 0.07	3.19 ± 0.06	3.29 ± 0.02					
Hb	[mmol/L]	G1	8.1 ± 0.5	8.4 ± 0.4	8.0 ± 0.6	8.1 ± 0.5	8.1 ± 0.2	8.4 ± 0.5					
		G2	8.2 ± 0.5	8.2 ± 0.2	7.8 ± 0.1	8.0 ± 0.0	8.3 ± 0.1	8.4 ± 0.0					
		G3	8.0 ± 0.6	8.2 ± 0.1	7.6 ± 0.3	7.5 ± 0.1	7.6 ± 0.1	7.8 ± 0.1					
		G4	8.4 ± 0.4	8.5 ± 0.3	8.3 ± 0.4	7.9 ± 0.4	8.1 ± 0.2	8.2 ± 0.0					
Ht	[L/L]	G1	NA ± NA	0.42 ± 0.02	0.40 ± 0.03	0.40 ± 0.02	0.40 ± 0.00	0.42 ± 0.02					
		G2	NA ± NA	0.41 ± 0.01	0.39 ± 0.01	0.40 ± 0.00	0.41 ± 0.00	0.42 ± 0.00					
		G3	NA ± NA	0.41 ± 0.02	0.39 ± 0.02	0.39 ± 0.01	0.39 ± 0.01	0.40 ± 0.01					
		G4	NA ± NA	0.42 ± 0.03	0.41 ± 0.02	0.39 ± 0.02	0.41 ± 0.02	0.42 ± 0.00					
RBC	[×10 ¹² /L]	G1	6.42 ± 0.21	6.57 ± 0.16	6.25 ± 0.40	6.30 ± 0.37	6.27 ± 0.19	6.45 ± 0.35					
		G2	6.23 ± 0.27	6.31 ± 0.21	5.96 ± 0.01	6.07 ± 0.07	6.22 ± 0.01	6.35 ± 0.01					
		G3	6.43 ± 0.74	6.62 ± 0.46	6.12 ± 0.57	6.01 ± 0.24	6.00 ± 0.28	6.06 ± 0.42					
		G4	6.86 ± 0.02	6.94 ± 0.15	6.67 ± 0.17	6.44 ± 0.05	6.41 ± 0.13	6.61 ± 0.40					
WBC	[×10 ⁹ /L]	G1	7.85 ± 0.86	7.93 ± 0.07	6.42 ± 0.78	7.91 ± 0.54	6.79 ± 0.30	7.40 ± 0.16					
		G2	8.18 ± 1.57	8.71 ± 1.61	7.16 ± 0.59	6.52 ± 0.62	8.52 ± 1.43	8.12 ± 0.64					
		G3	7.92 ± 1.16	8.03 ± 0.30	6.27 ± 0.02	6.95 ± 1.07	7.76 ± 2.61	7.25 ± 2.04					
		G4	8.65 ± 0.44	7.78 ± 1.17	7.50 ± 0.59	7.43 ± 1.56	8.25 ± 1.83	7.86 ± 0.53					
PLT	[×10 ⁹ /L]	G1	260 ± 25	251 ± 34	234 ± 17	193 ± 28	137 ± 34**	155 ± 3**					
		G2	294 ± 18	356 ± 10	322 ± 28	216 ± 13	214 ± 23	225 ± 37					
		G3	192 ± 40	230 ± 34	164 ± 52	145 ± 40	174 ± 75	139 ± 37*					
		G4	386 ± 52	400 ± 64	336 ± 39	361 ± 74	322 ± 26	283 ± 51*					

BL: baseline; Hb: hemoglobin; Ht: hematocrit; RBC: red blood cells; WBC: white blood cells; PLT: platelets; NA: not available

** $p < 0.01$ vs. T0, Friedmann test

* $p < 0.05$ vs. T0, Friedmann test

Day 42 (T6)		Day 49 (T7)		Day 56 (T8)		Day 63 (T9)		Day 70 (T10)		Day 77 (T11)	
3.37	± 0.41	3.42	± 0.48	3.51	± 0.49	3.59	± 0.48	3.63	± 0.53	3.67	± 0.53
3.42	± 0.49	3.51	± 0.51	3.57	± 0.49	3.65	± 0.49	3.68	± 0.59	3.70	± 0.61
3.27	± 0.01	3.23	± 0.11	3.25	± 0.15	3.25	± 0.16	3.27	± 0.15	3.32	± 0.05
3.39	± 0.04	3.34	± 0.18	3.33	± 0.33	3.34	± 0.45	3.38	± 0.56	3.17	± 0.44
8.2	± 0.0	8.5	± 0.1	8.6	± 0.1	8.4	± 0.1	NA	± NA	8.6	± 0.4
8.4	± 0.1	8.6	± 0.1	8.7	± 0.1	8.5	± 0.1	NA	± NA	8.8	± 0.1
8.0	± 0.2	8.3	± 0.1	8.2	± 0.4	8.2	± 0.0	NA	± NA	8.4	± 0.5
8.6	± 0.1	8.7	± 0.1	9.3	± 0.5	9.0	± 0.3	9.2	± 0.3	9.2	± 0.3
0.40	± 0.01	0.42	± 0.00	0.42	± 0.01	0.44	± 0.00	NA	± NA	0.44	± 0.02
0.41	± 0.00	0.42	± 0.00	0.42	± 0.00	0.43	± 0.01	NA	± NA	0.45	± 0.00
0.39	± 0.01	0.41	± 0.01	0.41	± 0.01	0.43	± 0.01	NA	± NA	0.43	± 0.03
0.42	± 0.01	0.43	± 0.01	0.45	± 0.03	0.46	± 0.01	NA	± NA	0.47	± 0.00
6.46	± 0.14	6.61	± 0.10	6.66	± 0.04	6.54	± 0.11	6.75	± 0.13	6.64	± 0.16
6.36	± 0.03	6.46	± 0.04	6.54	± 0.08	6.40	± 0.08	6.55	± 0.20	6.67	± 0.06
6.18	± 0.41	6.43	± 0.17	6.41	± 0.04	6.44	± 0.33	6.31	± 0.49	6.52	± 0.54
6.81	± 0.28	6.83	± 0.57	7.24	± 0.85	7.11	± 0.68	7.18	± 0.41	7.28	± 0.28
7.53	± 1.27	7.63	± 0.65	7.53	± 0.50	7.21	± 0.74	NA	± NA	7.24	± 0.74
8.36	± 1.82	6.89	± 0.80	7.51	± 0.16	6.01	± 1.18	NA	± NA	8.57	± 0.06
7.02	± 0.32	7.88	± 1.34	7.32	± 2.27	8.32	± 1.15	NA	± NA	9.88	± 2.89
6.82	± 0.93	6.54	± 1.75*	8.16	± 0.39	8.41	± 0.03	NA	± NA	8.52	± 0.43
221	± 60	225	± 65	192	± 3	201	± 5	242	± 4	211	± 11
304	± 41	242	± 6	208	± 100	174	± 142	294	± 30	258	± 50
192	± 14	184	± 30	163	± 23	155	± 37	191	± 13	203	± 4
410	± 96*	255	± 144*	325	± 127	298	± 116	377	± 43	321	± 139



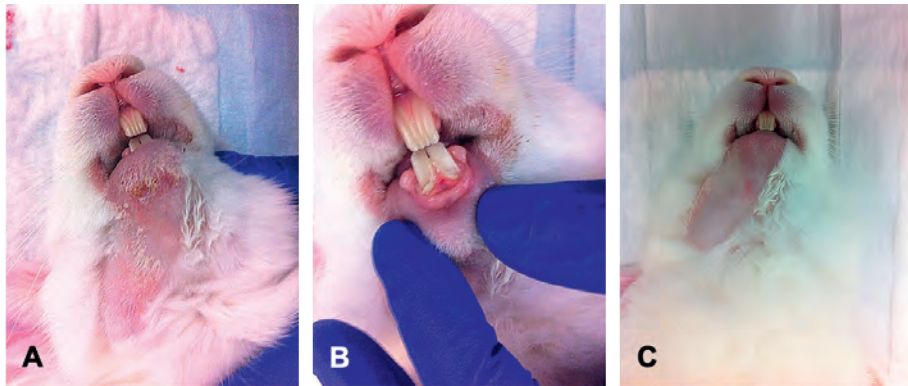


Figure 1. Photographs illustrating group IV subjects (single dose of 30 Gy) with erythema of the irradiated skin (A) and signs of mucositis around the area of the lower incisors (B) at T2 and the absence of extraoral mandibular fur (C) in the irradiated region at T5.

Table 2. Summary of microcirculation data (vessels with diameter $<100\ \mu\text{m}$). All data is presented in means \pm SD.

			BL (T0)	Day 7 (T1)	Day 14 (T2)	Day 21 (T3)	Day 28 (T4)	Day 35 (T5)
TVD	[mm/mm ²]	G1	28 \pm 5	25 \pm 1	29 \pm 1	25 \pm 2	27 \pm 2	21 \pm 1**
		G2	25 \pm 1	25 \pm 3	26 \pm 1	28 \pm 3	27 \pm 1	20 \pm 1**
		G3	27 \pm 1	31 \pm 0**	27 \pm 1	30 \pm 2	26 \pm 4	23 \pm 2
		G4	24 \pm 1	29 \pm 4	22 \pm 4*	24 \pm 0	21 \pm 1*	21 \pm 2*
TVD	[%]	G1	100 \pm 0	91 \pm 21	107 \pm 17	92 \pm 9	99 \pm 25	78 \pm 16
		G2	100 \pm 0	101 \pm 9	102 \pm 1	110 \pm 5	106 \pm 3	81 \pm 1
		G3	100 \pm 0	115 \pm 3	99 \pm 2	109 \pm 12	96 \pm 12	83 \pm 10
		G4	100 \pm 0	120 \pm 11	90 \pm 18	100 \pm 3	88 \pm 9	88 \pm 11
PVD	[mm/mm ²]	G1	28 \pm 5	25 \pm 1	29 \pm 1	25 \pm 2	27 \pm 2	21 \pm 1**
		G2	25 \pm 1	25 \pm 3	26 \pm 1	28 \pm 3	26 \pm 1	20 \pm 1**
		G3	27 \pm 1	31 \pm 0**	27 \pm 1	30 \pm 2	26 \pm 4	23 \pm 2
		G4	24 \pm 1	29 \pm 4	22 \pm 4*	24 \pm 0	21 \pm 1*	21 \pm 2*
PVD	[%]	G1	100 \pm 0	91 \pm 21	107 \pm 17	92 \pm 9	99 \pm 25	78 \pm 16
		G2	100 \pm 0	101 \pm 9	102 \pm 1	110 \pm 5	105 \pm 2	81 \pm 1
		G3	100 \pm 0	115 \pm 3	99 \pm 2	109 \pm 12	96 \pm 12	83 \pm 10
		G4	100 \pm 0	120 \pm 11	90 \pm 18	100 \pm 3	88 \pm 9	88 \pm 11
PPV	[%]	G1	100 \pm 0	100 \pm 0	100 \pm 0	100 \pm 0	100 \pm 0	100 \pm 0
		G2	100 \pm 0	100 \pm 0	100 \pm 0	100 \pm 0	100 \pm 1	100 \pm 0
		G3	100 \pm 0	100 \pm 0	100 \pm 0	100 \pm 0	100 \pm 0	100 \pm 0
		G4	100 \pm 0	100 \pm 0	100 \pm 0	100 \pm 0	100 \pm 0	100 \pm 0
MFI	[0,1,2,3]	G1	3	3	3	3	3	3
		G2	3	3	3	3	3	3
		G3	3	3	3	3	3	3
		G4	3	3	3	3	3	3

BL: baseline, MFI: microvascular flow index, PPV: proportion of perfused vessels, PVD: perfused vessel density, TVD: total vessel density

** $p < 0.01$ vs. T0, Friedmann test

* $p < 0.05$ vs. T0, Friedmann test

Table 2 presents a summary of the analyzed microvascular parameters. Baseline mean TVD and PVD for all groups was 26 ± 3 mm/mm². At T5 TVD and PVD in all groups showed a decrease of >10% compared to baseline, a significant difference was only observed for groups I, II and IV ($p < 0.05$) and return to baseline TVD and PVD was first observed at T8 in group III. Additionally, in group IV marked changes in the microcirculation presenting as multiple bud-like telangiectasia was observed at all time points with the most intense presentation at T2 in both animals [Fig. 2]. PPV and MFI remained unaltered across all time points.

Day 42 (T6)		Day 49 (T7)		Day 56 (T8)		Day 63 (T9)		Day 70 (T10)		Day 77 (T11)	
20	± 2**	21	± 0**	26	± 3	25	± 1	25	± 2	25	± 1
20	± 2**	24	± 2	24	± 0	23	± 0**	24	± 3	26	± 1
26	± 2	25	± 0	27	± 0	26	± 3	30	± 5*	28	± 2
22	± 0**	24	± 1	23	± 4*	25	± 2	26	± 4	23	± 1*
74	± 19**	78	± 15**	94	± 8	90	± 13	91	± 25	91	± 21
81	± 3	97	± 2	97	± 3	92	± 5	94	± 15	105	± 10
95	± 2	93	± 2	101	± 6	97	± 6	110	± 13	101	± 4
90	± 3	97	± 8	94	± 19	105	± 11	106	± 21	96	± 6
20	± 2**	21	± 0**	26	± 3	25	± 1	25	± 2	25	± 1
20	± 2**	24	± 2	24	± 0	23	± 0**	24	± 3	26	± 1
26	± 2	25	± 0	27	± 0	26	± 3	30	± 5*	28	± 2
22	± 0**	24	± 1	23	± 4*	25	± 2	26	± 4	23	± 1*
74	± 19**	78	± 15**	94	± 8	90	± 13	91	± 25	91	± 21
81	± 3	97	± 2	97	± 3	92	± 5	94	± 15	105	± 10
95	± 2	93	± 2	101	± 6	97	± 6	110	± 13	101	± 4
90	± 3	97	± 8	94	± 19	105	± 11	106	± 21	96	± 6
100	± 0	100	± 0	100	± 0	100	± 0	100	± 0	100	± 0
100	± 0	100	± 0	100	± 0	100	± 0	100	± 0	100	± 0
100	± 0	100	± 0	100	± 0	100	± 0	100	± 0	100	± 0
100	± 0	100	± 0	100	± 0	100	± 0	100	± 0	100	± 0
3		3		3		3		3		3	
3		3		3		3		3		3	
3		3		3		3		3		3	
3		3		3		3		3		3	



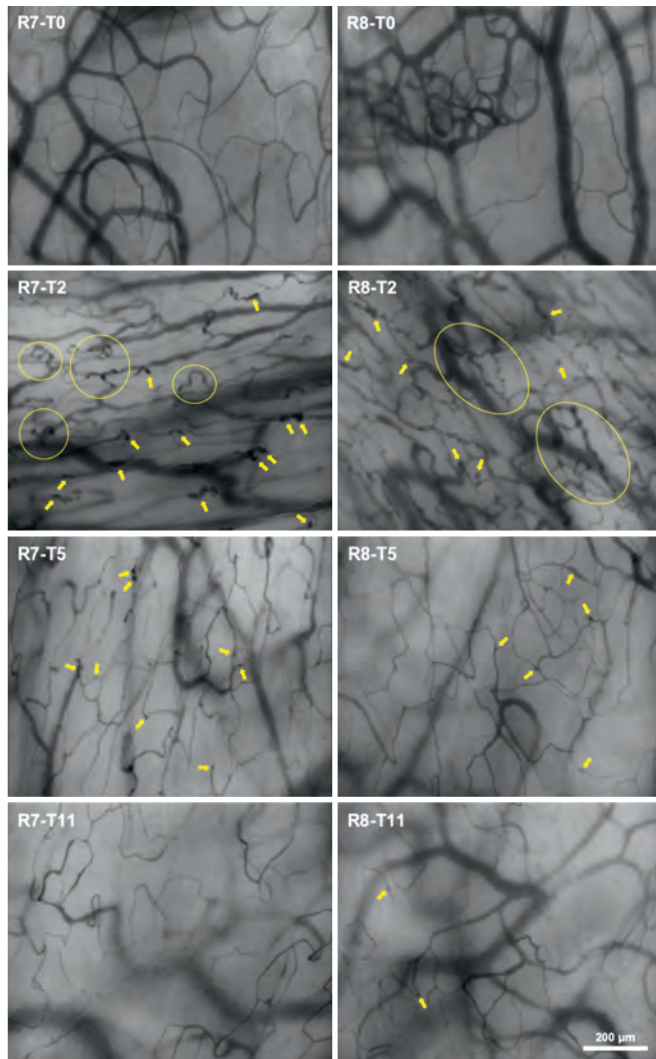


Figure 2. A series of MicroScan microcirculation image frames obtained from rabbit 7 and 8 (R7, R8; group IV) at the lingual aspect of the mandibular mucosa. Frames at baseline (T0) and 2 weeks (T2), 5 weeks (T5) and 11 weeks (T11) after irradiation (IR) are presented. Yellow arrows and encircled areas point to the microangiopathy phenomenon observed in the form of bud-like telangiectasias. Total vessel density (TVD) was reduced in T11 compared to T0 ($p<0.05$).

Mandibular bone histology

Mandibular histological specimens from groups I-IV were compared to healthy age-matched specimens. Group I did not show any deviating findings compared to healthy non-irradiated tissue. There was a gradual increase of pathological changes observed in groups II-IV. Group II showed a slight

increase of congestion of the vascular structures in bone and soft tissue with focal hemorrhage/extravasation of erythrocytes in the surrounding soft tissue. Furthermore, a slight increase in osteoblastic and osteoclastic activity was noted. The teeth showed no pathological changes except for a focal irregularity of cement which was anatomically present on the lingual site. Group III showed a marked loss of vascularity of the bone and soft tissue, with an increase of fibrotic soft tissue. The bone tissue was vital, although marked osteoblastic activation and an increase of osteoclastic bone resorption was observed [Fig. 3A]. The teeth had an avascular pulp with irregular deposits of cement at the interface between the teeth and the adjacent soft tissue on the lingual side. Group IV showed further general depletion of vascular structures and an increase of fibrosis in bone and soft tissue when compared to group III. The fibroblasts showed radiation-induced changes (i.e. enlarged, vesicular nuclei) [Fig. 3B]. The bone tissue showed small necrotic fields, although the majority of the bone tissue was vital. Some of the vital bone was devoid of an osteoblastic lining (periosteum), whilst multifocally, an increase in resorptive activity by multinucleated osteoclasts was observed. The teeth had an avascular pulp and showed partially resorbed cement on the lingual side of the teeth.

None of the groups showed thrombosis, vasculitis or reactive changes of the endothelium. Finally, no evident difference in observations between the irradiated site and the contralateral site was observed.

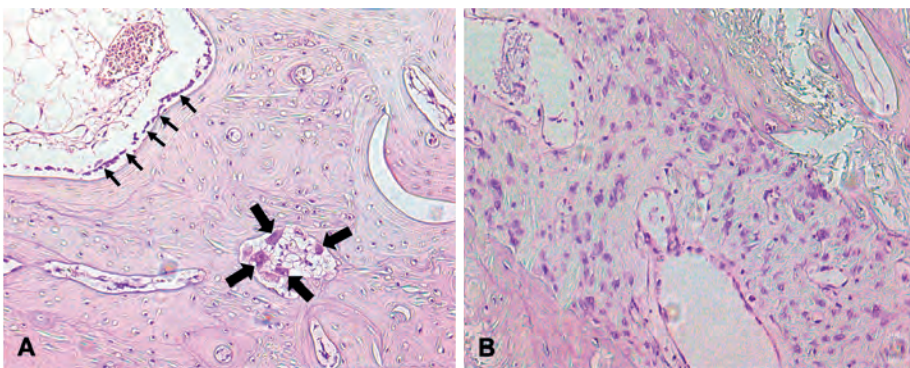


Figure 3. Micrographs of the bone histology samples stained with H&E. Panel A shows plump and enlarged osteoblasts (small arrows) and an increased number of multinucleated osteoclasts (large arrows) signaling increased bone turnover. Panel B shows enlarged atypical nuclei of the fibroblasts in the fibrous tissue, commonly associated with radiation induced changes.

DISCUSSION

The aim of the present study was to develop a pilot IR model in which the effects of late IR injury could be measured noninvasively in the oral mucosal microcirculation and in mandibular bone by histological analysis. Using the MicroScan it was possible to sequentially measure the mucosal microcirculation over an extended period of time to monitor and quantify functional and anatomic changes. Interestingly, at the end of 11 weeks the results showed that RT administered in different fractions and intensities corresponding with cumulative doses equivalent to 22.4 Gy, 26 Gy, 30 Gy and 32 Gy established no evident altered perfusion or lasting microvascular changes besides bud-like telangiectasia observed after a single dose of 30 Gy. There was a gradual IR dose-dependent increase in pathophysiological changes observed in groups II-IV that presented most prominently as reduced vascularity, fibrosis of soft tissue and bone and necrosis of teeth and bone tissue after a single dose of 30 Gy.

SDFI previously showed changes in oral microcirculation in rabbit wound vascularization studies in response to chemotherapy and hyperbaric oxygen therapy.^{12,22} Although no clear late IR effect could be detected in our microcirculation data at T11 in all groups, there was a notable recurring effect around T5 regarding clinical side effects (no regrowth of hair at side of irradiation in Group IV), reduced TVD and PVD (Group I, II and IV) and decreased PLTs (Group I, III and IV) compared to baseline. This suggests that our study may reflect microcirculation dynamics potentially associated with the onset of IR injury in a transition phase prior to late IR injury. The observation of a transient decrease in functionality of the microcirculation could be a result of leaking or thrombosed capillaries injured by IR. A decrease in PLTs associated with locoregional IR, which is supported although not valued as clinically relevant by the scarcely available literature,^{36,37} could further reduce angiogenesis and repair in compromised IR tissue as they contain platelet-derived growth factors.³⁰ Recently in an observational clinical study, late IR injury in oral mucosal microcirculation was described as showing significant rarefaction in capillary density, irregularly enlarged blood vessel diameters and telangiectasias.¹³ Interestingly, group IV showed scattered bud-like telangiectasia in the microcirculation with this appearing most prominently at T2, i.e. 2 weeks after RT. Since none of the other groups showed this type of phenomenon in the microcirculation, a higher

IR fraction dose might be necessary in order to induce comparable vascular reactions associated with RT in humans in the present animal model.

The histology of mandibular bone of groups III and IV showed increase in fibrotic interstitial tissue and loss of vascular structures in bone and soft tissue compared to the histology of healthy rabbit mandibular bone. Increased fibrosis in IR tissue was in agreement with other study reports^{6,8,18,27,39} and was described as a decrease in vessel lumen space and increase in thickness of the tunica intima.^{6,27} Group IV histologically showed small fields of bone necrosis marked by empty osteocyte lacunae 11 weeks after a single fraction of 30 Gy. Interestingly, another study reported a significant decrease in bone formation rate and vascular lumen diameter and increase in tunica intima thickness starting from 14 weeks after irradiation (highest total dose of 23.6 Gy, total follow up 26 weeks) measured by dynamic histomorphometry and histology assessment.²⁷ In their study bone necrosis only followed after surgical intervention post-IR, which might indicate a less severe impact of IR-dose alone when compared to our findings after a single fraction of 30 Gy. A significant decrease in osteocytes and increase in empty lacunae (osteocyte death) in the bone of irradiated rabbit mandibles was correspondingly demonstrated in another study after administration of a total dose varying between 35 Gy and 45 Gy (in 5 fractions).³⁹ Additionally, an increase of myofibroblasts invading osteocytes and surrounding sequesters was noted corresponding with the known chronic fibrotic state associated with RT.^{8,39} Finally, group IV showed a lack of osteoblast lining (periosteum), increased resorption by osteoclast activity and decreased vascularization, which is in line with observations describing human ORN mandibles.⁶ The absence of periosteum might be the first step preceding soft tissue ulceration that eventually succumbs to bone necrosis and exposure. However, bone necrosis and exposure were not observed in our model.

Previous rabbit models studying IR effects in the HN region applied different treatment approaches such as total radiation dose, duration and number of fractions administered and technique of IR (X-ray tube, linear accelerator, cobalt therapy).^{1,7,16-18,24,26,28,29,38,39} After dosimetry calculation and comparisons with previous investigations a cumulative dose ranging between 22.4 to 32 Gy was chosen for this pilot study with the purpose to select a clinically relevant spectrum of IR therapy approaches. Because cell and tissue turnover occurs 3 times faster in rabbits compared to humans,^{7,38} emerging and recovery of IR damage may occur at different times. We hypothesized that a minimum period



of 8 weeks would correspond with a period of 24 weeks (6 months) in humans and therefore would be sufficient to detect late IR injury in the microvasculature. However, the effects of RT might have manifested in a milder form in bone as damaged cells would be replaced by osteoprogenitor cells in a higher turnover rate.³⁸ It may have been advantageous to prolong the observation period of post-IR beyond 11 weeks to determine if there may be a delayed response in the microcirculation corresponding to late IR injury as observed in human HN cancer patients.

Several points need to be considered in view of this pilot investigation. First, the small sample size per groups was very small and may not be sufficient in order to validate and ascertain adequate detection of late IR injury. Second, compared to other animal studies 11 weeks is relatively short and might therefore have been too soon to detect vascular and histology changes characteristic of late IR injury. Finally, it is difficult to scale IR doses adequately for rabbits and perhaps a higher dose may have been required in order to achieve clinically comparable tissue pathophysiology associated with mandibular IR injury.

In conclusion, the present pilot study described for the first time a model in which in vivo oral microcirculatory response after HN IR was monitored and quantified prospectively. Within the scope of this study, no significant lasting effect in terms of perfused vessel density or clinical late IR damage could be detected in the different groups after 11 weeks. In general, acute changes in vessel density and platelet counts were observed at 5 weeks after initiating IR in all groups. Marked changes in architecture (telangiectasia) and histology (loss of periosteum and vasculature) were observed after a single dose of 30 Gy. Future studies should prolong the observation period and examine injury dose-response prevalence by correlating the microcirculation, telangiectasia and histopathology findings with the progression of IR side effects.

Acknowledgements

We would like to acknowledge and thank the staff of the Department of Experimental RT for their support and Sanne Hackmann from the Animal Research Institute Academic Medical Center (ARIA) for her biotechnical support.

REFERENCES

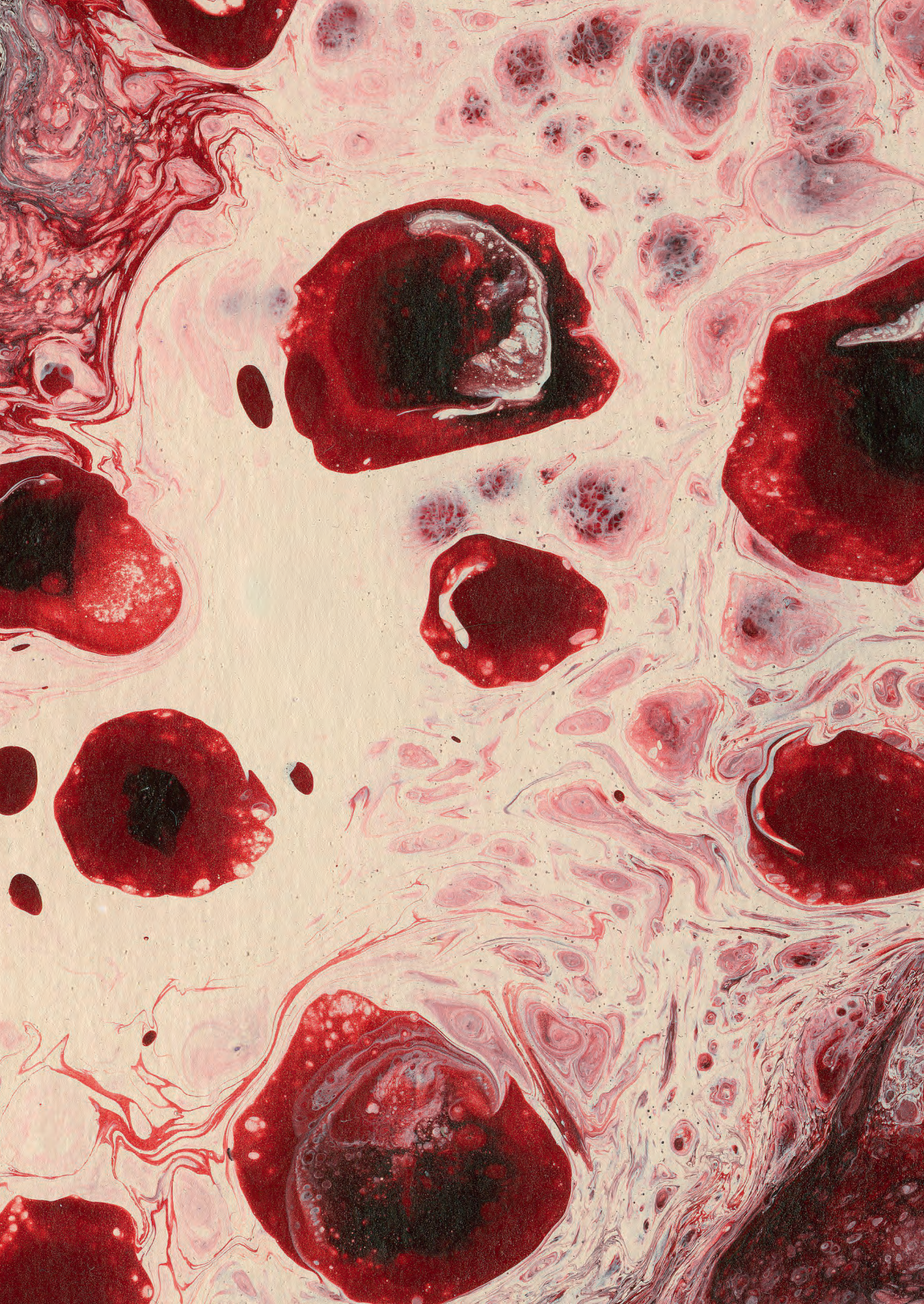
1. Aygenc E, Celikkanat S, Bilgili H, et al. Pentoxifylline effects on acute and late complications after radiotherapy in rabbit. *Otolaryngol Head Neck Surg.* 2001;124(6):669–673.
2. De Backer D, Creteur J, Preiser JC, Dubois MJ, Vincent JL. Microvascular blood flow is altered in patients with sepsis. *Am J Respir Crit Care Med.* 2002;166(1):98–104.
3. De Backer D, Hollenberg S, Boerma C, et al. How to evaluate the microcirculation: Report of a round table conference. *Crit Care.* 2007;11(5):R101.
4. Bennett MH, Feldmeier J, Hampson NB, Smee R, Milross C. Hyperbaric oxygen therapy for late radiation tissue injury. *Cochrane Database Syst Rev.* 2016;4(4):CD005005.
5. Boerma EC, Mathura KR, van der Voort PH, Spronk PE, Ince C. Quantifying bedside-derived imaging of microcirculatory abnormalities in septic patients: a prospective validation study. *Crit Care.* 2005;9(6):R601–R606.
6. Bras J, De Jonge HK, Van Merkesteyn JP. Osteoradionecrosis of the mandible: pathogenesis. *Am J Otolaryngol.* 1990;11(4):244–250.
7. Clark CL, Strider J, Hall C, et al. Distraction osteogenesis in irradiated rabbit mandibles with adjunctive hyperbaric oxygen therapy. *J Oral Maxillofac Surg.* 2006;64(4):589–593.
8. Delanian S, Lefaix JL. The radiation-induced fibroatrophic process: Therapeutic perspective via the antioxidant pathway. *Radiother Oncol.* 2004;73(2):119–131.
9. Gillett CS. Selected drug dosages and clinical reference data. In: Manning PJ, Ringler DH, Newcomer CE, editors. *The Biology of the Laboratory Rabbit.* San Diego, USA: Academic Press. 1994;(2nd ed.):467–472.
10. Goedhart PT, Khalilzada M, Bezemer R, Merza J, Ince C. Sidestream dark field (SDF) imaging: a novel stroboscopic LED ring-based imaging modality for clinical assessment of the microcirculation. *Opt Express.* 2007;15(23):15101–15114.
11. Granström G. Radiotherapy, osseointegration and hyperbaric oxygen therapy. *Periodontol* 2000. 2003;33:145–162.
12. Helmers R, Milstein DMJ, van Hulst RA, de Lange J. Hyperbaric oxygen therapy accelerates vascularization in keratinized oral mucosal surgical flaps. *Head Neck.* 2014;36(9):1241–1247.
13. Helmers R, Straat NF, Navran A, et al. Patient-side appraisal of late radiation-induced oral microvascular changes. *Int J Radiat Oncol Biol Phys.* 2018;102(4):1299–1307.
14. Hewitt CD, Innes DJ, Savory J, Wills MR. Normal biochemical and hematological values in New Zealand White rabbits. *Clin Chem.* 1989;35(8):1777–1779.
15. Hutchings S, Watts S, Kirkman E. The Cytocam video microscope. A new method for visualising the microcirculation using incident dark field technology. *Clin Hemorheol Microcirc.* 2016;62(3):261–271.
16. Jegoux F, Aguado E, Cognet R, et al. Alveolar ridge augmentation in irradiated rabbit mandibles. *J Biomed Mater Res A.* 2010;93(4):1519–1526.
17. Ma Y, Shen G. Distraction osteogenesis after irradiation in rabbit mandibles. *Br J Oral Maxillofac Surg.* 2012;50:662–667.
18. Marx RE, Ehler WJ, Tayapongsak P, Pierce LW. Relationship of oxygen dose to angiogenesis induction in irradiated tissue. *Am J Surg.* 1990;160(5):519–524.
19. Marx RE, Johnson RP. Studies in the radiobiology of osteoradionecrosis and their clinical significance. *Oral Surg Oral Med Oral Pathol.* 1987;64(4):379–390.
20. Marx RE. Osteoradionecrosis: a new concept of its pathophysiology. *J Oral Maxillofac Surg.* 1983;41(5):283–288.
21. Milstein DM, Bezemer R, Ince C. Sidestream dark-field (SDF) video microscopy for clinical imaging of the microcirculation. In: Leahy MJ, editor. *Microcirculation Imaging.* Weinheim, Germany: Wiley-VCH Verlag GmbH & Co. KGaA. 2012;(1st ed.):37–52.
22. Milstein DM, Lindeboom JA, Ince C. The influence of zoledronic acid and cyclophosphamide on microcirculation regeneration in healing oral mucosal flaps. *Arch Oral Biol.* 2011;56(6):599–606.
23. Moon DH, Moon SH, Wang K, et al. Incidence of, and risk factors for, mandibular osteoradionecrosis in patients with oral cavity and oropharynx cancers. *Oral Oncol.* 2017;72:98–103.



24. Muhonen A, Haaparanta M, Grönroos T, et al. Osteoblastic activity and neoangiogenesis in distracted bone of irradiated rabbit mandible with or without hyperbaric oxygen treatment. *Int J Oral Maxillofac Surg.* 2004;33(2):173–178.
25. Nabil S, Samman N. Incidence and prevention of osteoradionecrosis after dental extraction in irradiated patients: a systematic review. *Int J Oral Maxillofac Surg.* 2011;40(3):229–243.
26. O'Donovan DA, Yeung I, Zeman V, Neligan PC, Pang CY, Forrest CR. Radiation-induced craniofacial bone growth inhibition: development of an animal model. *J Craniofac Surg.* 2001;12(6):533–543.
27. Poort LJ, Ludlage JHB, Lie N, et al. The histological and histomorphometric changes in the mandible after radiotherapy: An animal model. *J Craniomaxillofac Surg.* 2017;45(5):716–721.
28. Price DL, Moore EJ, Friedman O, Garces YI, Kee AY, Furutani KM. Effect of Radiation on Segmental Distraction Osteogenesis in Rabbits. *Arch Facial Plast Surg.* 2008;10(3):159–163.
29. Rabelo GD, Beletti ME, Dechichi P. Histological analysis of the alterations on cortical bone channels network after radiotherapy : A rabbit study. 2010;73(11):1015–1018.
30. Semple JW, Italiano JE Jr, Freedman J. Platelets and the immune continuum. *Nat Rev Immunol.* 2011;11(4):264–274.
31. Sønstevoid T, Johannessen AC, Stühr L. A rat model of radiation injury in the mandibular area. *Radiat Oncol.* 2015;10:129.
32. Spronk PE, Ince C, Gardien MJ, Mathura KR, Oudemans-van Straaten HM, Zandstra DF. Nitroglycerin in septic shock after intravascular volume resuscitation. *Lancet.* 2002;360(9343):1395–1396.
33. Stone HB, Coleman CN, Anscher MS, McBride WH. Effects of radiation on normal tissue: consequences and mechanisms. *Lancet Oncol.* 2003;4(9):529–536.
34. Strojjan P, Hutcheson KA, Eisbruch A, et al. Treatment of late sequelae after radiotherapy for head and neck cancer. *Cancer Treat Rev.* 2017;59:79–92.
35. Vissink A, Jansma J, Spijkervet FKL, Burlage FR, Coppes RP. Oral sequelae of head and neck radiotherapy. *Crit Rev Oral Biol Med.* 2003;14(3):199–212.
36. Ye L, Oei RW, Kong F, et al. Prognostic values of hematological biomarkers in nasopharyngeal carcinoma patients treated with intensity-modulated radiotherapy. *Eur Arch Otorhinolaryngol.* 2018;275(5):1309–1317.
37. Zachariah B, Jacob SS, Gwede C, et al. Effect of fractionated regional external beam radiotherapy on peripheral blood cell count. *Int J Radiat Oncol Biol Phys.* 2001;50(2):465–472.
38. Zhang WB, Zheng LW, Chua D, Cheung LK. Bone Regeneration after radiotherapy in an animal model. *J Oral Maxillofac Surg.* 2010;68(11):2802–2809.
39. Zong C, Cai B, Wen X, et al. The role of myofibroblasts in the development of osteoradionecrosis in a newly established rabbit model. *J Craniomaxillofac Surg.* 2016;44(6):725–733.

PART II

CLINICAL STUDIES





CHAPTER 5

Patient-side appraisal of late radiation-induced oral microvascular changes

Renée Helmers

Nina F. Straat

Arash Navran

Tim A.P. Nai Chung Tong

David N. Teguh

Robert A. van Hulst

Jan de Lange

Dan M.J. Milstein

Edited version of: Int J Radiat Oncol Biol Phys. 2018;102(4):1299–1307.

ABSTRACT

Objectives: Late radiation-induced tissue toxicity in the head and neck (HN) region is associated with ulceration and osteoradionecrosis as a result of a detrimental effect on the underlying tissue microvasculature. The aim of this investigation was to determine the clinical feasibility of examining and measuring late irradiation changes in the oral microcirculation of HN cancer patients using the novel CytoCam video microscope system.

Materials and methods: In 30 HN cancer patients and 30 age-matched controls, bilateral video images were recorded noninvasively of the oral microcirculation of the buccal mucosa and mandibular gingiva. Tissue perfusion parameters such as functional capillary density (FCD), buccal blood vessel diameter (\emptyset_{bv}), and microcirculatory flow index (MFI) were analyzed.

Results: No difference was observed for mean buccal mucosa FCD in irradiated vs. healthy tissue, whereas a lower mean gingival FCD in irradiated vs. healthy tissue was observed (34 ± 17 cpll/mm² vs. 68 ± 19 cpll/mm²; $p < 0.001$). A significant difference in mean buccal \emptyset_{bv} of 16 ± 3 μ m was measured compared to 14 ± 1 μ m in control buccal mucosa ($p < 0.001$). No significant difference in MFI was observed between the two groups.

Conclusion: Quantifying oral microcirculatory injury associated with late irradiation effects using the CytoCam was feasible in HN cancer patients. Results indicate that marked differences in tissue-specific microcirculatory measurements of angioarchitecture, diminished capillary density, and extensively dilated blood vessel diameters are associated with late irradiation effects in HN cancer patients.

INTRODUCTION

Irradiation of malignancies in the anatomically complex head and neck (HN) region inevitably results in collateral damage to vital tissues.^{13,32} Vascular damage in the oral mucosa is a late sequela following acute mucosal injury. Mucositis develops in 80% of patients during the course of curative HN irradiation and manifests as atrophy of epithelial cells and inflammatory infiltrates.^{26,32} Subsequent release of vasoactive cytokines results in fibrin leakage into surrounding tissues followed by vascular lumen blockage that can ultimately reduce tissue vascular perfusion and regional hypoxia.³² Late irradiation sequelae associated with irradiation dosages of 50–65 Gy⁶ can emerge several months after completing RT and can lead to problems with mastication and speech (due to trismus and/or xerostomia), atrophy and fibrosis with ulceration of the oral mucosa, and in some advanced cases as osteoradionecrosis (ORN) of the jaw.^{6,18,27}

Late irradiation side effects vary in severity and pathology among patients. As severity of late sequelae associated with RT is not proven to correlate with the degree of acute effects,^{4,23,34} it is difficult to predict the course of late radiation damage. Most tissues do not reveal late side effects clinically before a stage of severe tissue breakdown becomes apparent in the form of soft tissue necrosis or ORN. Understanding late irradiation pathophysiology in the microcirculation can provide a way of subclinical diagnostics to bring to light clinically relevant information on early onset of side effects and their severity. Tissue inspection and monitoring provides an opportunity for planning ahead strategies to improve patient quality of life by preventing progression of pathology. Hyperbaric oxygen is an example of such a strategy that could potentially improve tissue resistance to injury and maintenance of health by reducing avascularity.^{3,11,21,27}

To date several reports on vascular irradiation were published using different techniques. Early in the 1970s studies based on histology and intravital microscopy were conducted, describing degeneration of capillaries after irradiation as telangiectasia and microaneurysms.²³ Transcutaneous oxygen measurements and laser Doppler flowmetry (LDF) were each used to assess microcirculation functionally in irradiated skin and oral mucosa but failed to yield consistency in results.^{10,12,24,28,29} Direct observation of angioarchitecture and morphology in irradiated tissue can provide additional evidence-based



support on pathophysiology that was otherwise absent using techniques such as LDF. Doppler optical coherence tomography (DOCT) combined with speckle variance OCT (svOCT) was used to examine angiomorphology and blood flow in the oral mucosa with late irradiation injury.⁸ Orthogonal polarization spectral imaging (OPSI) and sidestream dark-field imaging (SDFI) have previously been used to describe the microcirculation of oral squamous cell carcinoma¹⁹, microvascular inflammation associated with irradiation-induced oral mucositis in HN cancer patients (HNCP)¹⁴, and the effects of chemotherapy on buccal mucosa in patients with hematological malignancies.^{19,20} To perform chairside evaluation of the late effects of RT in the oral microcirculation a CytoCam video microscope system, a successor of the OPSI and SDFI instruments, was used.

The aims of this study were to examine whether a chairside assessment approach was feasible to identify and quantify the late effects of RT on the oral microcirculation in patients treated for malignant HN disease. We tested the hypothesis that irradiation elicits detectable (late) oral microcirculatory derangements such as capillary rarefaction, altered angiomorphology, and vessel diameters.

MATERIALS AND METHODS

This single-center observational study was conducted between June 2014 and July 2016 in the Department of Oral and Maxillofacial Surgery of the Academic Medical Center of the University of Amsterdam. The procedures and guidelines for this study were reviewed and approved by the Institutional Medical Ethics Committee of the Academic Medical Center of the University of Amsterdam (Ref. Nos. NL49017.018.14, NL57131.018.16). Signed informed consent was obtained from all participants. This investigation was performed in accordance with the principles established in the Declaration of Helsinki (Fortaleza, October 2013).

Study participants

HNCP referred to the Department of Hyperbaric Medicine (for prophylactic or therapeutic indications) whom previously (>6 months) received uni- or bilateral HN irradiation with >50 Gy were eligible for participation. Patients were excluded if they received hyperbaric baric oxygen therapy in the past, had

undergone surgery in the HN region in <6 months (which both may influence vascularization), or had severe trismus preventing intraoral measurements. History of general health and past irradiation dose were obtained with patient approval. Dentate or edentulous status was noted. A group of healthy age-matched volunteers (ASA 1; including smokers, social drinkers, and $19 < \text{BMI} < 30$) was included and used as a control group. To obtain an indication of systemic health and to exclude unknown cardiovascular disease, basic hemodynamic parameters (heart rate, systolic, diastolic, and mean arterial blood pressures) and body temperature were recorded for each control subject.

Microvascular imaging

Microcirculation measurements were performed using a CytoCam (CC) Microscope System (Braedius Medical, Huizen, The Netherlands); details on the CC instrument are described elsewhere.^{1,15} Using incident dark-field illumination and CMOS sensor-based imaging technology, the commercially available CC is a lightweight handheld imaging instrument that operates by epilluminate a tissue of interest with pulsed (2 ms) 530 nm wavelength green light through light-emitting diodes (LEDs) located around the tip of the probe lens. As hemoglobin from erythrocytes absorb the green light, the remaining light scatters into the surrounding tissue. Using a 4× objective lens system (237× onscreen magnification), the imaging sensor records and processes the relayed tissue light and produces a clear and high-resolution image (14 megapixel, 25 fps) of dark circulating erythrocytes in the lumen of blood vessels contrasted by a bright background in a field of view (FOV) equal to 1.55×1.16 mm (1.80 mm^2). The CC is connected to a fanless medical grade panel PC (Braedius Medical, Huizen, The Netherlands) equipped with the CCTools software (CytoCamTools Camera Manager v1.7.12, Braedius Medical, Huizen, The Netherlands) for camera operation and video data processing.

Measurement procedures

Microcirculation measurements were performed in the same examination room kept at a constant temperature of $20 \pm 2^\circ\text{C}$. Participants were seated upright in a chair with their head resting against the wall to limit head movement. Prior to measurements the participants were requested to refrain from eating, drinking (other than water), and any oral hygiene practices for at least 30 min. Participants were asked to briefly rinse their mouth with lukewarm ($\sim 40^\circ\text{C}$) water since most HNCP have a dry mouth; the same procedure was performed



in controls to maintain standardization. Before each measurement, a barrier to prevent direct contact between the probe and patient saliva during intraoral measurements was prepared using a disposable cap (CytoCam Protection Caps, Braedius Medical, Huizen, The Netherlands) placed on the CC and draped with a large Latex and powder free examination glove (Klinion® Protection, Medico BV, Oud-Beijerland, The Netherlands) with the tip of the middle finger cut off.

Participants were instructed to open their mouth slightly to measure the buccal mucosa and to put the teeth in occlusion to measure the mandibular gingiva. The tip of the handheld unit was placed in gentle contact with 4 regions of interest (ROIs) and always in the same sequential order for each measurement, i.e. the left and right cheek parallel to the upper premolar region, the left and right gingiva in the lower premolar region. The probe was kept exactly perpendicular to the targeted tissue locations with the lens of the probe placed flat over the epithelium of the mucosa. A modified pen grip, a precision grip used by dentists, was applied for stability during gingiva recordings using the adjacent teeth for support. After adjusting proper focus and contrast settings each measurement was performed during careful probe advancement and retraction maneuvers while in contact with the mucosa to ensure maximizing the presence of capillaries and avoiding pressure induced artefacts in the FOV. All image recordings were performed by an investigator (I) trained to manage the handheld device by an experienced researcher (II). An assistant (III) operated the CC PC manually for clip recordings, adjustments of contrast and focus settings, and recording of focal depth (Fd; μm). For each measurement 4 different clips of adjacent sites of 4 s each were recorded and averaged to represent each anatomic ROI. For the control group, all basic hemodynamic data was obtained by the same examiner (IV) prior to performing microcirculation imaging.

Data analysis

Microcirculation recordings were converted into two .avi file formats (full screen and Automated Vascular Analysis (AVA) software compatible) and exported using CCTools for analysis. Data was analyzed for Fd, classification of angioarchitecture, total and functional capillary density (TCD and FCD respectively), microvascular flow index (MFI), and buccal blood vessel diameter (\emptyset_{bv}). Three types of classes can be distinguished in angioarchitecture³³: an array of capillary loops (score 1), both capillary loops and vascular network

(score 2), and vascular network without any loops (score 3). Capillary density was analyzed by selecting a still frame from each recorded clip according to the former established criteria considering image resolution, clarity, and potential pressure artefacts.⁹ TCD and FCD assessment was carried out by counting the total and functional capillary loops per visual field in each frame (area of 1.80 mm²). Intra-class correlation coefficient (ICC) was performed on a sample dataset to ascertain inter-rater reproducibility agreement between examiners (I, II, and III) for buccal and gingiva FCD (ICC=0.982; $p<0.001$). After completing capillary enumeration for each density dataset, the results were divided by 1.80 to standardize and present findings as the mean number of capillaries per millimeter squared (cpl/mm²). MFI was scored as the predominant flow type in each quadrant as being absent (score 0), intermittent (score 1), sluggish (score 2), or normal (continuous) (score 3).⁵

The AVA software package (AVA v3.02, Microscan BV, Amsterdam, The Netherlands), calibrated for analysis of the CC-derived images (horizontal pitch=1.306944, vertical pitch=1.289930), was used to obtain samples of diameter measurements from CC exported recordings of our study participants. After performing a full vascular segmentation procedure and selecting a series of vascular diameters using AVA, a digital overlay \emptyset_{bv} measuring tool (containing magnitudes of 5, 10, 20, 30, 40 and 50 μm) was prepared in Adobe Photoshop (Adobe Photoshop CC 2017, Adobe Systems Incorporated, San Jose, California, USA). In each of the 4 isolated frames from the buccal mucosa, 5 of the largest vessels per quadrant (20 total) were measured for \emptyset_{bv} and averaged to represent the mean \emptyset_{bv} in each frame.

For each parameter (Fd, angioarchitecture, TCD, FCD, MFI, and buccal \emptyset_{bv}) four datasets were obtained, analyzed at random by two independent investigators (I and III), and averaged to represent the measurement mean at each targeted ROI.

Statistical analysis

Based on a two-tailed independent-samples t-test, a total sample size of 60 (N=30 per group) was computed with an alpha set at 5%, a power of 90%, and a large effect size of 0.86. Normality distribution of all data parameters was assessed by the Shapiro-Wilk test. Comparisons between irradiated and healthy tissue capillary density and \emptyset_{bv} were examined using an independent-samples t-test. As only Fd data was not normally distributed, the Mann-Whitney U test



was used for this data. IBM SPSS Statistics software package (IBM® SPSS® Statistics version 24, IBM Corp. Armonk, NY, USA) was used to perform all data analyses. All data are presented as means±standard deviation (SD) and significance level was confirmed if *p*-values were <0.05.

RESULTS

Both patients and control subjects easily complied with microcirculation measurements, as they were noninvasive and painless. Even patients that experienced preexisting discomfort associated with their underlying pathology, such as trismus, were able to tolerate the measurements well. Patient and control participant demographics and hemodynamic parameters are presented in Table 1. The images acquired with the CC were of excellent quality as the buccal and gingival tissues were able to provide sufficient contrast with the microcirculation to gain clear high-resolution images (CC brightness=450 in all measurements). Four clips were obtained per ROI (16 total) in each participant, a total of 960 clips were analyzed in this study.

Table 1. Patient and control demographics and hemodynamic parameters for controls.

Patient demographics [N=30]		Mean	SD
Age	[yrs]	61	± 10
Gender	[F:M]	8:22	
Dental status	[edent.:dentate]	9:21	
<i>Site of radiation</i>		N (%)	
Oral cavity		10 (33%)	
Oropharynx		8 (27%)	
Hypopharynx		1 (3%)	
Nasopharynx		4 (13%)	
Larynx		5 (17%)	
Other		2 (7%)	
Oral lesion presence		5 (17%)	
<i>Co-morbidities</i>		N (%)	
Diabetes		1 (3%)	
Hypertension		3 (10%)	
COPD		3 (10%)	

Table 1. Continued

Patient demographics [N=30]		Mean	SD
Intoxication	N (%)		
Smoking history	4 (13%)		
<i>Cancer therapy</i>			
Chemoradiation	N (%)		
Only RT	12 (40%)		
	18 (60%)		
Mean RT dosage buccal mucosa	[Gy]	34	± 12
Mean RT dosage gingiva	[Gy]	49	± 17
Time since RT	[yrs]	4	± 5
Healthy controls [N=30]		Mean	SD
Age	[yrs]	51	± 4
Gender	[F:M]	11:19	
Dental status	[edent.:dentate]	0:30	
<i>Basic hemodynamics</i>			
HR	[bpm]	73	± 2
SBP	[mmHg]	132	± 14
DBP	[mmHg]	82	± 8
MAP	[mmHg]	99	± 9

COPD = chronic obstructive pulmonary disease; DBP = diastolic blood pressure; HR = heart rate; MAP = mean arterial pressure; RT = radiation therapy; SBP = systolic blood pressure; SD = standard deviation

Angioarchitecture

Buccal and gingival angioarchitecture classifications are presented in Figure 1. Only class 1 was observed in control subject tissues. Irradiated sites presented all class types [Table 2]. Sample images of healthy buccal and gingiva microcirculation are presented in Figure 2. The observed differences in irradiated buccal mucosa were altered capillary loops with telangiectasia-like (ballooning) and loss in normal arrangement of capillary loop organization [Fig. 3]. All observed pathologic microvasculature appeared hemodynamically functional with good blood circulation present in all vessels of the buccal mucosa and gingiva.



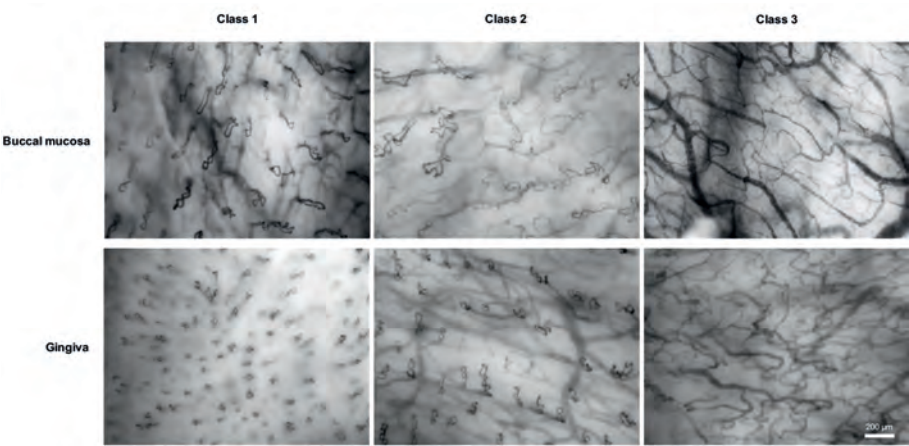


Figure 1. Classification of angioarchitecture in images obtained from buccal mucosa and mandibular gingiva in HN irradiated cancer patients: class 1 (only capillary loops), class 2 (both capillary loops and vascular network) (supplementary videoclip available online), and class 3 (vascular network without any loops).

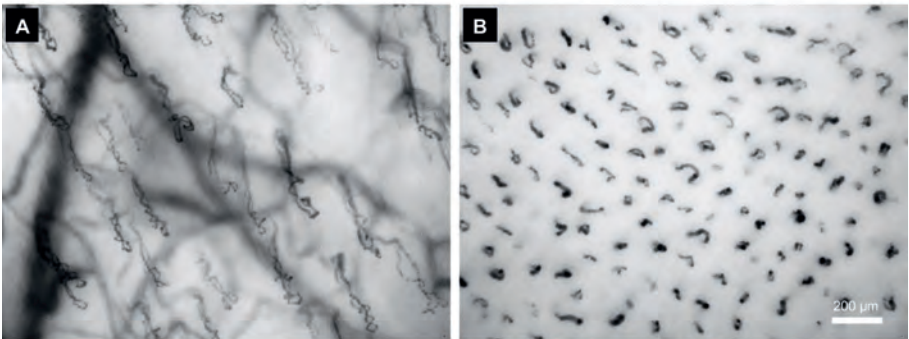


Figure 2. Sample images of normal (non-irradiated) tissue from the buccal mucosa (A) and mandibular gingiva (B) in control subjects.

Table 2. Classification of angioarchitecture of the buccal mucosa and mandibular gingiva in controls and HN irradiated (RT) patients: class 1 (only capillary loops), class 2 (both capillary loops and vascular network) and class 3 (vascular network without any loops).

	Buccal mucosa		Mandibular gingiva	
	Control	RT	Control	RT
Class 1	100%	77%	100%	64%
Class 2	0%	18%	0%	34%
Class 3	0%	5%	0%	2%

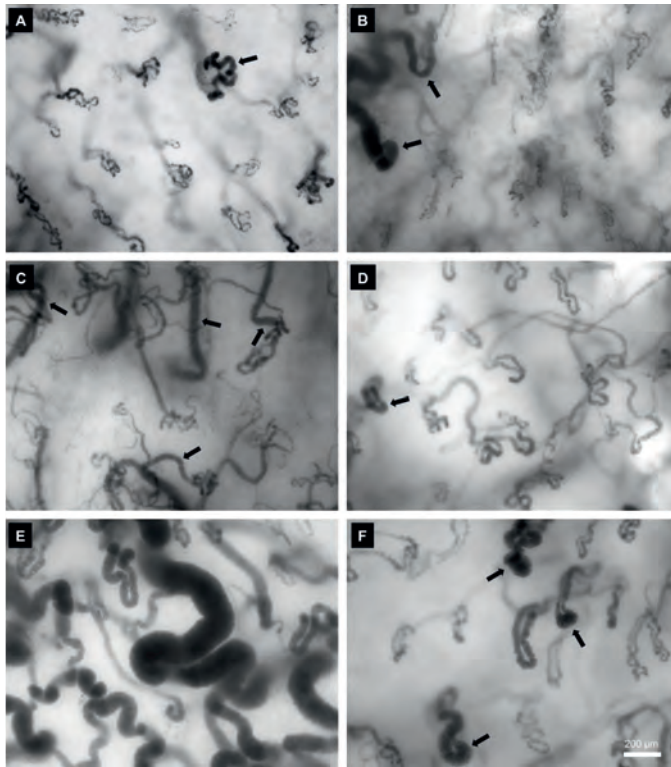


Figure 3. Typical CytoCam images illustrating alterations in irradiated buccal mucosa in HNCP. Telangiectasia or ‘ballooning’ of vessels (black arrows) can be seen in panels A-D and F, chaotic arrangement and malformation of loops can be observed in panels C-E with panel E demonstrating in one case an intense combination of telangiectasia with irregular capillaries and chaotic microvascular (supplementary videoclip available online). The black arrows in panel F show distinctly the ‘ballooning’ phenomenon in the subepithelial capillary loops (supplementary videoclip available online). Similar observations matching microvascular irregularities (black arrows) from panel A and F were also presented by Tsuya et al. in atomic bomb survivors.³⁰

Capillary density and blood vessel diameters

Table 3 summarizes the distribution of registered Fd and the data for capillary density and buccal \emptyset_{bv} . Mean buccal and gingiva TCD was equal to FCD in both control subjects and HNCP, there were no observed difference in hemodynamic functionality in vessels. A statistically significant decrease in mean FCD in irradiated mandibular gingiva was found compared to control gingiva, 34 ± 17 cpl/mm² vs. 68 ± 19 cpl/mm² ($p < 0.001$) respectively. No significant difference was found between irradiated edentulous and dentate gingival FCD.

Irradiated buccal mucosa presented in general a larger mean \emptyset_{bv} of 16 ± 3 μ m vs. 14 ± 1 μ m for control buccal mucosa ($p < 0.001$). No significant difference

in mean buccal FCD was found between control subjects (20 ± 5 cpl/mm²) and irradiated buccal mucosa (19 ± 7 cpl/mm²). MFI was 3 (continuous blood flow present) for both buccal and gingival microcirculation in both groups.

Table 3. Summary of focus depth (Fd) and microcirculation measurement for both control and irradiated tissue (RT). Data is presented in means \pm SD.

		Buccal mucosa						Mandibular gingiva					
		Control				RT		Control				RT	
Fd	[μm]	197	±	39	157	±	54*	147	±	40	123	±	53
TCD	[cpl/mm ²]	20	±	5	20	±	7	68	±	19	34	±	17*
MFI	[AU]	3	±	0	3	±	0	3	±	0	3	±	0
Ø _{bw}	[μm]	14	±	1	16	±	3*						

MFI microvascular flow index, TCD total capillary density, ϕ_{bv} blood vessel diameter * $p < 0.001$ vs control.

DISCUSSION

The purpose of this study was to examine the feasibility of a chairside approach in detecting and measuring late microvascular irradiation pathology in the oral mucosa of HNCP. Differences in microcirculatory parameters, such as capillary density and ϕ_{bv} , between healthy and irradiated tissue can be easily detected using the CC, demonstrating its clinical applicability for chairside patient assessments. The results suggest no altered microvasculature morphology occurred in irradiated mandibular gingiva although a generalized reduction in gingival FCD was present. Despite the close proximity between the gingiva and buccal mucosa, FCD of the buccal mucosa was relatively unhindered despite angiomorphologic differences.

Reduced vascularity due to fibrosis is a known long-term adverse effect after therapeutic RT.^{3,32} Several techniques (biopsy, transcutaneous oxygen measurement, LDF) have been applied in the past to study this phenomenon in oral and cutaneous tissues, but inconsistent findings were reported. Doll et al. found a decrease of blood flow in irradiated skin of breast cancer patients and a normalization after 36 months compared to control sites using LDF.¹² Another study, using cutaneous laser Doppler, reported increased subcutaneous microcirculation associated with thermal stimulation in irradiated breast skin compared to a non-irradiated contralateral side¹⁰; the investigators argue

that these observations in the RT area could be a result of impairment of endothelial function and telangiectatic neocapillaries. Transcutaneous oxygen pressure was reported unaffected after irradiation even after several years.²⁴ Histopathologic studies reported vascular loss and fibrosis over time after RT in HNCP.^{7,22,25} Irradiated HNCP oral mucosal punch biopsies (3 mm cross-sectional thickness) showed that vessel lumen diameters in buccal mucosa did not differ in subepithelial capillaries, whereas a marked increase in vascular lumens in deeper connective tissue was observed.²² Interestingly, our results indicate that patterns of angioarchitecture can be used to identify (subclinically) epithelial thickness changes such as atrophy. A difference between control tissue and irradiated tissue was observed, indicated by a decreased Fd paired with epithelial atrophy represented by class 3 angioarchitecture in irradiated tissue vs. an increased Fd and intact epithelium with class 1 capillary loop patterns in control tissue. The findings from our study confirm a loss in capillary loops in buccal mucosa, represented by a class 3 angioarchitecture, and a marked increase in \emptyset_{bv} was measured in irradiated buccal mucosa compared to healthy mucosa. Our results confirm previous histopathological observations.^{7,22,25} The presence of flow is potentially necessary to discover increases in lumen diameter that are otherwise overlooked in histologic specimens; for this reason, in vivo measurements are most veracious in reflecting actual pathology.

A clear observation during the assessment of irradiated tissue microcirculation in this study was the manifestation of telangiectasias [Fig. 3]. In other studies, telangiectasias were frequently described in different areas of irradiated cutaneous tissue and were attributed to impaired vasoregulatory mechanisms that resulted in altered hemodynamics and stasis.^{2,22,23} The observed distended vascular effect might be due to breakdown of downstream capillaries²³ and the potential irradiation damage to small diameter nerves that regulate blood flow distribution.² Another proposed pathophysiological mechanism associated with RT is that the radiation injured endothelial cells and oxygen deprived extracellular environment around capillaries stimulate proliferation of neocapillaries of irregular calibers and morphology.² Figure 3 (panels e and f) illustrates potentially an example of such an oxygen deprived site as described by Baker et al. showing disorganized, irregularly formed capillaries. Interestingly, early in the 1950s in atomic bomb survivors similar distorted loops in the labial mucosa was observed using intravital microscopy.²



To our knowledge, Davoudi et al. performed the first clinical study that considered in vivo oral microcirculation parameters by looking at late irradiation effects. The investigators presented their concept using DOCT and svOCT for the first time to investigate blood flow and morphology parameters and demonstrated technical feasibility by comparing data of one late radiation toxicity patient to a healthy volunteer. Their data showed a significantly higher blood flow velocity ($\times 1.8$) and increased vessel volume density in irradiated tissue. Although it can be an advantage to measure blood flow and create reconstructed 3D images, the clinical application of DOCT and svOCT is currently cumbersome.⁸

Discrepancies in reports regarding microcirculatory alterations after RT make it difficult to compare data between studies directed at understanding the adverse effects of HN irradiation. Standardized data acquisition procedures are necessary for providing reliable clinical assessments of irradiation-induced side effects and facilitates identifying correlations associated with different pathologies, i.e. mucositis, atrophy and tissue necrosis. Ideally a future scoring system should include systematic clinical assessments of irradiation injury severity based on microcirculatory parameters.

A limitation of this study was not correlating microcirculatory parameters to clinical pathology. In our study, 5 (17%) out of 30 patients presented with oral lesions, unfortunately these numbers are too small to detect any robust correlations. Comparing microcirculatory parameters of irradiated tissue with no clinically visible signs of pathology and tissue with clinical pathology (e.g. ulceration, dry mouth, osteoradionecrosis) could expose a transition phase in microcirculation between the two. Identifying microcirculatory differences in this transition phase could offer a window of opportunity in which potential adjunctive therapies (e.g. hyperbaric oxygen therapy) could ameliorate altered irradiated tissue states. As a clear difference in oral microcirculatory parameters between irradiated tissue and control tissue was presented in this study, further research should be aimed at exposing this microcirculatory transition phase between irradiated tissue with and without clinical pathology in which the CytoCam can serve an important diagnostic role for monitoring microcirculation parameters at patient side.

Next to the opportunity for determining tissue state in a chairside setting, therapy can be targeted towards these subclinical parameters and equally monitored for treatment response. In this light, it is important to describe the microcirculation to further identify its value as a clinical parameter.

Inasmuch as microvascular pathologies are studied, it must be considered that systemic conditions such as hypertension and diabetes mellitus may increase adverse effects on microcirculation since vascular health is already potentially compromised. Comorbidities should therefore be reported as has been performed in this study. To this end, it can be argued that in our study no distinction was made between patients that received chemoradiotherapy (CRT) or RT alone. Although the effect of CRT on long-term side effects is not entirely clear, a systematic review conducted by Nabil et al. found no increased risk of ORN compared to only RT.²¹ However, subtle effects on the microcirculation might be overseen when no distinction is made. With respect to ORN, the measurements in this study were only conducted on the mandibular gingiva. The rationale behind this restriction in site lies in the higher prevalence of ORN in the mandible due to differences in blood perfusion compared with the maxilla.^{16,21} Moreover, HNCP referred for hyperbaric oxygen therapy had a higher prevalence of irradiation on the mandible due to the highest predilection of HN squamous cell carcinoma on tongue and the floor of the mouth.³¹ Another interesting point to consider is that dental status may be an influencing factor on gingival capillary density as edentulous areas may differ compared to dentate areas. The role of plaque accumulation and microorganism load may further influence gingival capillary density. Currently, no data linking gingival capillary density measurements and microbial status and/or edentulous vs. dentate areas exist. Further microcirculatory investigations are warranted before insightful conclusions can be drawn.

CONCLUSIONS

This study shows the clinical feasibility in detecting tissue-specific microcirculatory alterations in irradiated oral tissues in HNCP. Unique to this study is the capability of subclinically measuring reduced capillary density and large blood vessel diameters in HNCP in relation to late irradiation pathology. Further studies should be aimed at developing a systematic scoring system for identifying the severity of late microcirculatory irradiation damage in correlation with clinical radiation injury. Describing in vivo parameters of different stages of disease could be more valuable if microcirculatory measurements were included to support diagnosis involving pathophysiological processes and evaluations of therapeutic efficacy.

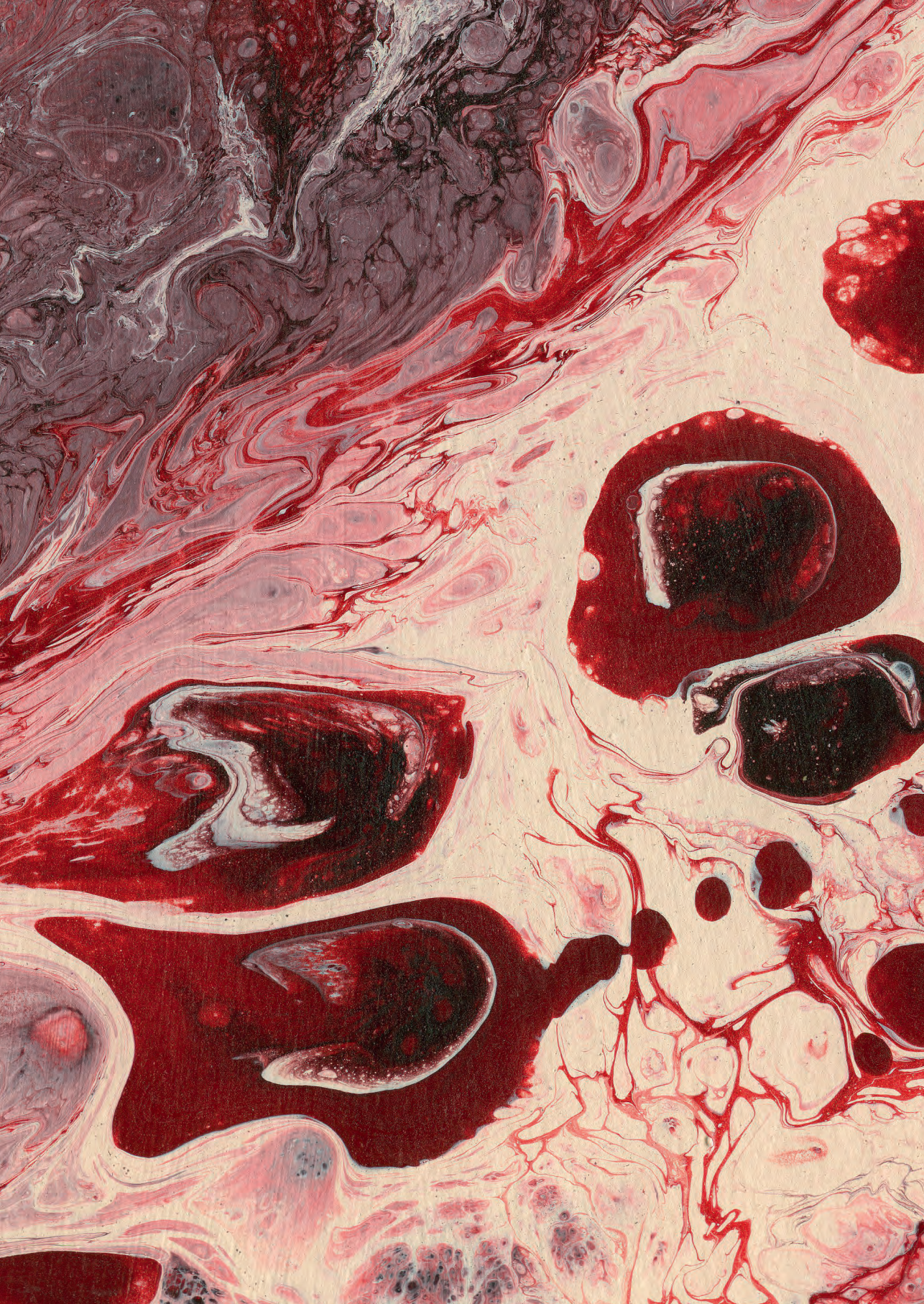


REFERENCES

1. Aykut G, Veenstra G, Scorcella C, Ince C, Boerema C. Cytocam-IDF (incident dark field illumination) imaging for bedside monitoring of the microcirculation. *Intensive Care Med* 2015;3(1):40.
2. Baker DG, Krochak RJ. The response of the microvascular system to radiation: a review. *Cancer Invest* 1989;7(3):287–94.
3. Bennett MH, Feldmeier J, Hampson NB, Smee R, Milross C. Hyperbaric oxygen therapy for late irradiation injury. *Cochrane database Syst Rev* 2016;4:CD005005.
4. Berry RJ, Wiernik G, Patterson TJ, Hopewell JW. Excess late subcutaneous fibrosis after irradiation of pig skin, consequent upon the application of the NSD formula. *Br J Radiol* 1974;47:277–81.
5. Boerema EC, Mathura KR, van der Voort PH, Spronk OE, Ince C. Quantifying bedside derived imaging of microcirculatory abnormalities in septic patients: a prospective validation study. *Crit Care* 2005;9:R601–6.
6. Cooper JS, Fu K, Marks J, Silverman S. Late effects of radiation therapy in the head and neck region. *Int J Radiation Oncology Biol Phys* 1995;31:1141–64.
7. Curi MM, Cardoso CL, de Lima HC, Kowalski LP, Martins MD. Histopathologic and histomorphometric analysis of irradiation injury in bone and the surrounding soft tissues of the jaws. *J Oral Maxillofac Surg* 2016;74(1):190–9.
8. Davoudi B, Morrison M, Bizheva K, Yang VX, Dinniwell R, Levin W, et al. Optical coherence tomography platform for microvascular imaging and quantification: initial experience in late oral radiation toxicity patients. *J of Biomed Opt* 2013;18:76008.
9. De Backer D, Hollenberg S, Boerma C, Goedhart P, Büchele G, Ospina-Tascon G, et al. How to evaluate the microcirculation: report of a round table conference. *Crit Care* 2007; 11(5):R101.
10. Delanian S, Lefaix JL. Evaluation of late radiation induced changes of the superficial microcirculation. I. Clinical benefit of the cutaneous Doppler laser. *Cancer Radiother* 2000;4:408–414.
11. Dieleman FJ, Phan TTT, van den Hoogen FJA, Kaanders JHAM, Merks MAW. The efficacy of hyperbaric oxygen therapy related to the clinical stage of osteoradionecrosis of the mandible. *Int J Oral Maxillofac Surg* 2017;428–433.
12. Doll C, Durand R, Grulkey W, Sayer S, Olivetto I. Functional assessment of cutaneous microvasculature after radiation. *Radiother Oncol* 1999;51:67–70.
13. Granstrom G. Radiotherapy, osseointegration and hyperbaric oxygen therapy. *Periodontol* 2000 2003;33:145–62.
14. Hamilton S, Yoo J, Hammond A, Read N, Venkatesan V, Franklin J, et al. Microvascular changes in radiation-induced oral mucositis. *J Otolaryngol Head Neck Surg* 2008;37:730–737.
15. Hutchings SD, Watts S, Kirkman E. The Cytocam video microscope. A new method for visualising the microcirculation using Incident Dark Field technology. *Clin Hemorheol Microcirc* 2016;62:261–271.
16. Kerdvongbundit V, Vongsavan N, Soo-ampon S, Phankosol P, Hasegawa A. Microcirculation of the healthy human gingiva. *Odontology* 2002;90(1):48–51.
17. Lindeboom JA, Mathura KR, Ince C. Orthogonal polarization spectral (OPS) imaging and topographical characteristics of oral squamous cell carcinoma. *Oral Oncol* 2006;42:581–585.
18. Marx RE, Johnson RP. Studies in the radiobiology of osteoradionecrosis and their clinical significance. *Oral Surg Oral Med Oral Pathol* 1987;64:379–90.
19. Milstein DM, Raber-Durlacher JE, Lindeboom JA, Biemond BJ, de Lange J. Different oral mucosal microcirculatory response in two separate chemotherapy regimens. *Supportive Care Cancer* 2012;20:S219.
20. Milstein DM, te Boome LC, Cheung YW, Lindeboom JA, van den Akker HP, Biemond BJ, et al. Use of sidestream dark-field (SDF) imaging for assessing the effects of high-dose melphalan and autologous stem cell transplantation on oral mucosal microcirculation in myeloma patients. *Oral Surg Oral Med Oral Pathol Oral Radiol Endod* 2010;109:91–97.
21. Nabil S, Samman N. Risk factors for osteoradionecrosis after head and neck radiation: a systematic review. *Oral Surg Oral Med Oral Pathol Oral Radiol* 2012;113:54–69.

22. Prott JF, Handschel J, Micke O, Sunderkötter, Meyer U, Pifko J. Long-term alterations of oral mucosa in radiotherapy patients. *Int J Radiat Oncol Biol Phys* 2002;54(1):203–210.
23. Reinhold HS. The influence of radiation on blood vessels and circulation. Chapter IV. Structural changes in blood vessels. *Curr Top Radiat Res Q* 1974;10:58–74.
24. Rudolph R, Tripuraneni P, Koziol JA, McKean-Matthews M, Frutos A. Normal transcutaneous oxygen pressure in skin after radiation therapy for cancer. *Cancer* 1994;74:3063–3070.
25. Schultze-Mosgau S, Grabenhauer GG, Radespiel-Tröger M, Wiltfang J, Ries J, Neukam FW, et al. Vascularization in the transition area between free grafted soft tissues and pre-irradiated graft bed tissues following preoperative radiotherapy in the head and neck region. *Head Neck* 2002;24(1):42–51.
26. Sonis ST. The pathobiology of mucositis. *Nat Rev Cancer* 2004;4:277–284.
27. Stone HB, Coleman CN, Anscher MS, McBride WH. Effects of radiation on normal tissue: consequences and mechanisms. *Lancet Oncol* 2003;4:529–536.
28. Svalestad J, Hellem S, Vaagbo G, Irgens A, Thorsen E. Reproducibility of transcutaneous oximetry and laser Doppler flowmetry in facial skin and gingival tissue. *Microvasc Res* 2010;79:29–33.
29. Svalestad J, Thorsen E, Vaagbø G, Hellem S. Effect of hyperbaric oxygen treatment on oxygen tension and vascular capacity in irradiated skin and mucosa. *Int J Oral Maxillofac Surg* 2014;43:107–112.
30. Tsuya A, Wakano Y, Otake M. Capillary microscopic observation on the superficial minute vessels of atomic bomb survivors, 1956–1957. *Radiat Res* 1971;46(1):199–216.
31. Vigneswaran N, Williams MD. Epidemiological trends in head and neck cancer and aids in diagnosis. *Oral Maxillofac Surg Clin North Am* 2014;26(2):123–141.
32. Vissink A, Jansma J, Spijkervet FK, Burlage FR, Coppes RP. Oral sequelae of head and neck radiotherapy. *Crit Rev Oral Biol Med* 2013;14:199–212.
33. Weber MA, Milstein DM, Ince C, Oude Rengerink K, Roovers JP. Vaginal microcirculation: non-invasive anatomical examination of the micro-vessel architecture, tortuosity and capillary density. *NeuroUrol Urodyn* 2015;34(8):723–729.
34. Withers HR, Peters LJ, Taylor JM, Owen JB, Morrison WH, Schultheiss TE, et al. Late normal tissue sequelae from radiation therapy for carcinoma of the tonsil: patterns of fractionation study of radiobiology. *Int J Radiat Oncol Biol Phys* 1995;33:563–568.







CHAPTER 6

Hyperbaric oxygen therapy redirects late irradiation injury in oral microcirculation towards healthy microvascular tissue state

Renée Helmers

Dan M.J. Milstein

Nina F. Straat

Arash Navran

David N. Teguh

Robert A. van Hulst

Ludi E. Smeele

Jan de Lange

Submitted

ABSTRACT

Objectives: Late side effects of radiotherapy in head and neck cancer patients (HNCs) result in long-term decreased tissue vascularity and a compromised healing capacity. The aim of this study was to examine the *in vivo* effect of hyperbaric oxygen therapy (HBOT) on the individual vessels of the microcirculation in irradiated oral tissue.

Materials and methods: Using a handheld vital microscope system the effect of HBOT on oral mucosal microcirculation parameters concerning microvascular flow index, gingival and buccal vessel density and buccal vessel diameter were measured in 34 previously irradiated HNCs. Measurements were obtained prior to HBOT (T0) and then at 4 weeks (T4) and 24 weeks (6 months; T24) posttreatment.

Results: A significant increase in mean buccal vessel density and decrease in buccal vessel diameter was found 6 months after HBOT (T24) compared to baseline (T0), 22 ± 11 cpl/mm² vs. 25 ± 7 cpl/mm² ($p < 0.05$) and 20 ± 4 μ m vs. 16 ± 5 μ m ($p < 0.05$) respectively. Altered microvascular morphology was observed to be present throughout all time points.

Conclusion: Our results indicate that microcirculation histopathology associated with late irradiation injury in oral mucosa is able to respond to HBOT by redirecting oral microcirculation parameters towards values consistent with healthy tissue.

INTRODUCTION

Late radiation tissue injury (LRTI) is an inevitable and potentially progressive side effect that becomes clinically apparent after 6 months to years and is associated with radiotherapy (RT) in the treatment of cancer. Tissue hypoxia that results from RT-induced vascular hypoperfusion has a negative effect on the quality of tissue and prevents an adequate healing response after tissue injury or elicits spontaneous breakdown. This can ultimately lead to necrosis of bone, cartilage and soft tissues which are difficult to treat conditions. Consequently, functional and aesthetic problems can arise that have a major impact on quality of life.^{7,16} It is difficult to make a prediction on whether and when late irradiation (IR) side effects will occur and evolve to clinical pathology as the degree of acute effects does not correlate with the severity of late effects.^{5,23,39} However, fraction dose and individual patient related factors are identified as potential risk factors.^{8,21,30} The underlying detrimental effects of LRTI only become clinically evident when tissue breakdown occurs with no tendency to heal.

Hyperbaric oxygen therapy (HBOT) is directed at improving IR tissue quality by increasing oxygen tension in hypovascular tissues to promote neoangiogenesis.^{10,18} Although several studies show beneficial effects of HBOT on IR HN tissue, the mechanisms remain largely elusive and very limited evidence for preventing and managing ORN exists.^{4,26} However, administering HBOT is often used curatively or prophylactically in IR tissues and the existing treatment protocols are still based on research performed in the 1970s.²⁶ In 2019 the first randomized controlled trial was published in the HN region in which data based on 100 patients showed a low occurrence rate of mandibular ORN 6 months after dentoalveolar surgery in both the HBOT group and the control group (6.4 % vs. 5.7 %); such results would not justify an indication of HBOT to prevent ORN after dentoalveolar surgery. However, it remains uncertain whether iatrogenic trauma causes or accelerates tissue breakdown that would otherwise emerge on the long-term due to poor tissue quality as a result of IR.²⁵

Microcirculation monitoring can give insight in the pathophysiology of LRTI and provide functional and anatomic feedback on treatment effects of supporting therapies. Recently the late effect on oral microcirculation parameters was measured in IR oral mucosa when compared to healthy oral mucosa in a chairside setting using a CytoCam (CC) microscope system based



on incident dark-field illumination imaging (IDFI). Large vessel diameters in buccal mucosa and a reduction in vessel density in mandibular gingiva was observed and morphologic observations showed telangiectasias in the oral mucosa consistent with injured microvascular endothelium.¹² The *in vivo* net effect of HBOT over time on reconstitution of adequate tissue perfusion and tissue vitality associated with irradiated oral tissue has not yet been elucidated on the level of individual vessels. In this study the aim was to monitor *in vivo* the effects of HBOT prospectively on irradiated oral microcirculation with the use of the CC microscope system. We tested the hypothesis that HBOT redirects microcirculation parameters such as functional capillary density (FCD), blood vessel diameters (\emptyset_{bv}) and angiomorphology towards levels corresponding with healthy tissue.

MATERIALS AND METHODS

A prospective observational study was conducted between November 2014 and July 2017 in the Department of Hyperbaric Medicine and the Department of Oral and Maxillofacial Surgery of the Amsterdam University Medical Centre (UMC), location AMC. The institutional medical ethics committee of the Amsterdam UMC/AMC (Ref. Nr. NL49017.018.14) approved all procedures and guidelines of the study, which were performed in accordance with the principles established in the Declaration of Helsinki (Fortaleza, October 2013).

Patients

Head and neck cancer patients (HNCs), previously treated with RT, that were referred to the Department of Hyperbaric Medicine for either prophylactic or therapeutic HBOT indications were included in this study. Inclusion criteria were a minimum dose of 50 Gy RT received >6 months prior to participation. Exclusion criteria were surgery in the HN region or HBOT 6 months previous to the study and severe trismus preventing adequate mouth opening for measuring intraorally. Furthermore, patients that received <20 HBOT sessions in total were excluded from the study. History of general health and IR-dose was acquired from medical records after patient approval. Smoking status was based on information provided by the patient. Dentate or edentulous state was noted.

HBOT

Hyperbaric treatment sessions were carried out in a multiple person hyperbaric chamber and had a total duration of 110 min; 100% oxygen was administered through an oronasal mask during 75 min total at 2.4 ATA.³⁴ HBOT was planned on weekdays from Monday to Friday. Patients receiving HBOT sessions concerning pre-extraction osteoradionecrosis prophylaxis (20 sessions prior and 10 sessions postoperative, total of 30 sessions) and patients receiving HBOT therapeutically (≥ 20 sessions) were pooled.

Microvascular imaging

To visualize the oral microcirculation a CytoCam (CC) Microscope System (Braedius Medical, Huizen, The Netherlands) was used; details on this vital handheld imaging instrument are described elsewhere.^{1,15,20} In brief, a clear and high-resolution image (14-megapixel, 25 fps) with a field of view (FOV) equal to 1.55x1.16mm (1.80 mm²) is created of the microcirculation displaying the lumen of blood vessels filled with dark circulating erythrocytes contrasted by a bright background. A medical PC (Braedius Medical, Huizen, The Netherlands) is connected with the CC which is set with the CCTools software (CytoCamTools Camera Manager v1.7.12, Braedius Medical, Huizen, The Netherlands) for camera operation and video data processing.

Measurement procedures

Microcirculation measurements were performed at baseline (T0), 4 weeks after start of HBOT (T4) and 24 weeks (6 months) after start of HBOT (T24). The measurement procedures followed protocolled patient instruction and microscope handling as described in a previous study of our group.¹² An allocated examination room maintained at a constant 20 \pm 2°C was used for performing the microcirculation measurements at all time points. A trained investigator (RH) performed all measurements together with an assistant (NFS) who controlled the CC PC to adjust contrast, focus and focal depth (Fd; μ m) and recorded the images. Four regions of interest (ROIs) were measured: the left and right cheek parallel to the upper premolar region and the left and right gingiva in the lower premolar region. In each region 4 different clips of 4 s each were recorded of adjacent sites. The average of the 4 clips represented the ROI.



Data analysis

The CCTools software was used to export image recordings in .avi file format. The following parameters were analyzed from the exported clips: Fd, classification of angioarchitecture, total and functional capillary density (TCD and FCD respectively), microvascular flow index (MFI), and buccal blood vessel diameter (\emptyset_{bv}). Angioarchitecture was divided into 3 class types³⁸: an array of capillary loops (score 1), both capillary loops and vascular network (score 2) and vascular network without any loops (score 3). Frame selection for capillary density assessment was based on clarity, resolution and the absence of pressure artifacts.² To determine TCD and FCD the capillary loops in each frame (area of 1.80 mm²) were counted. At completion of the density dataset the results were divided by 1.80 to convert to mean number of capillaries per millimeter squared (cpl/mm²). The type of flow per quadrant was described using the MFI scoring system: absent (score 0), intermittent (score 1), sluggish (score 2), or normal (score 3).⁶ Blood vessel diameter (\emptyset_{bv}) was analyzed in Adobe Photoshop (Adobe Photoshop CC 2020, Adobe Systems Incorporated, San Jose, California, USA) using a digital overlay diameter measuring tool (containing magnitudes of 5, 10, 20, 30, 40 and 50 μ m) that was previously described elsewhere.¹² The diameter magnitude of the 5 largest vessels per quadrant (20 total) were measured and averaged as \emptyset_{bv} per frame. Vessel morphology was screened throughout all time points for IR induced alterations in the form of telangiectasias and/or disorganization of vessel loops. An intraclass correlation coefficient of 0.982 ($p < 0.001$) was computed from a sample subset of data on buccal and gingiva FCD to ascertain interrater reproducibility agreement between examiners (RH, NFS, and DMJM). Remaining datasets were randomized and analyzed at random for each parameter (Fd, angioarchitecture, MFI, and buccal \emptyset_{bv}) by the same investigator (RH).

Statistical analysis

Previous capillary density mean comparisons between healthy and irradiated oral mucosa demonstrated a large effect size of 0.86.¹² In the present study comparative analysis of capillary density between each time point was performed using generalized linear model approach. With a total sample size of 32, a single-group repeated measures analysis of variance (ANOVA) with a 5% significance level has an 80% power to detect an effect size of 0.22. Finally, 34 patients were included in this study [Fig. 1]. Normality distribution of all data parameters (FCD, TCD, \emptyset_{bv} , Fd) was assessed by the Shapiro-Wilk test. Based on the outcome of the Shapiro-Wilk test, repeated measures

ANOVA or Friedman test was used to detect overall time effects. Significant main effects were subsequently analyzed using paired samples t-test with Bonferroni correction. A linear regression analysis was performed to detect whether (previous) smoking, chemotherapy or dentition state (dentate vs. edentulous) had a significant association on the outcome of microcirculation parameters. McNemar test was used to check whether proportion of healthy tissue (class I type angioarchitecture) was significant different over time. Descriptive and statistical analyses were performed using the SPSS Statistics software package (IBM SPSS Statistics version 27, IBM Corp. Armonk, NY, USA). All data are presented as mean \pm standard deviation (SD). A p -value of <0.05 was considered statistically significant.

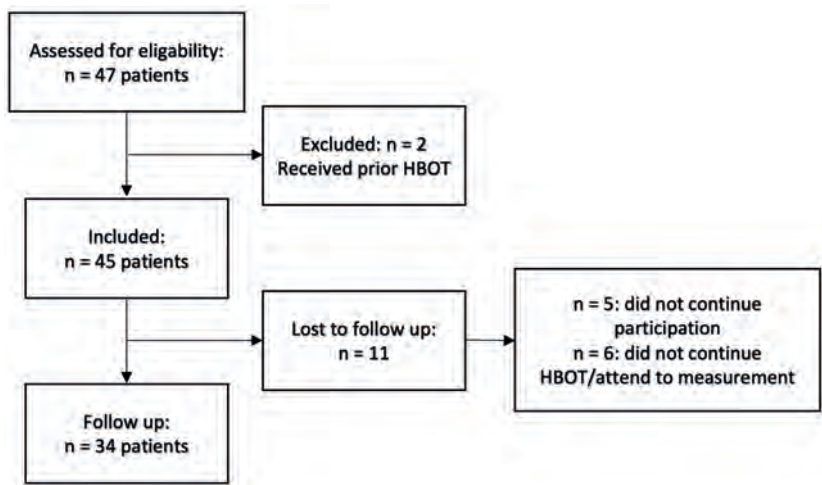


Figure 1. Patient selection flowchart.

RESULTS

The noninvasive oral microcirculation measurements were well tolerated by all patients and no pain or discomfort was experienced or reported. Radiation dose, indications for HBOT (prophylactic or therapeutic) and patient demographics are presented in Table 1. Microcirculation image quality recorded from the buccal and gingival tissue with the CC was excellent with sharp high-resolution and sufficient contrast (CC brightness=450 in all measurements) to observe the



tissue microvasculature and luminal blood flow. 16 clips were acquired from each patient, 4 clips per ROI. A total of 1632 clips were analyzed. No significant difference in Fd was observed between the time points [Table 2].

Table 1. Patient demographics.

Patient demographics [N=34]		Mean	±	SD
Age	[yrs]	59	±	12
Gender	[F:M]	12:22		
Dental status	[edentulous:dentate]	10:14		
<i>Co-morbidities</i>				
Diabetes	N (%)			
	1 (3%)			
Hypertension	2 (6%)			
COPD	2 (6%)			
<i>Intoxication</i>				
Smoking history	4 (12%)			
Smoker	8 (24%)			
<i>Cancer therapy</i>				
CRT	14 (41%)			
Only RT	20 (59%)			
<i>Site of radiation</i>				
Oral cavity	12 (35%)			
Oropharynx	12 (35%)			
Hypopharynx	0 (0%)			
Nasopharynx	4 (12%)			
Larynx	2 (6%)			
Other	4 (12%)			
Oral lesion presence	9 (26%)			
<i>RT</i>				
Mean RT dosage buccal mucosa	[Cy]	38	±	13
Mean RT dosage gingiva	[Cy]	51	±	12
Time since RT	[yrs]	4	±	5
<i>HBOT</i>				
Prophylactic indication	N (%)			
	16 (47%)			
Therapeutic indication	18 (53%)			
Number of sessions		32	±	7

CRT chemoradiotherapy; COPD chronic obstructive pulmonary disease; HBOT hyperbaric oxygen therapy; RT radiotherapy; SD standard deviation

Table 2. Focus depth during CytoCam microcirculation measurement. Data is presented in means \pm SD.

	Buccal angioarchitecture						Gingival angioarchitecture					
	T0		T4		T24		T0		T4		T24	
Focus depth [μ m]	136 \pm 74	146 \pm 70	141 \pm 53	130 \pm 52	116 \pm 57	84 \pm 95						

Angioarchitecture

Temporal classification of buccal and gingival tissue angioarchitecture is presented in Table 3. Overall, the proportion of class 1 angioarchitecture increases overtime although no significant difference was detected ($p>0.05$).

Table 3. Classification of angioarchitecture of the buccal mucosa and mandibular gingiva in HNCP; class 1 (only capillary loops), class 2 (both capillary loops and vascular network) and class 3 (vascular network without any loops).

	Buccal mucosa			Mandibular gingiva		
	T0	T4	T24	T0	T4	T24
Class I	59%	74%	76%	79%	69%	81%
Class II	37%	26%	24%	17%	31%	19%
Class III	3%	0%	0%	4%	0%	1%

Vessel morphology

Altered vessel morphology associated with IR, i.e. telangiectasias in the form of distortion or “ballooning” of vessels loops, was observed at all time points in both buccal and gingival mucosa. Furthermore, disorganization of vessel loops remained present at T4 and T24. Figure 2 illustrates images of these microvascular alterations in IR buccal mucosa. Normal (continuous; MFI=3) blood flow was present in all observed vessels.

Capillary density and blood vessel diameters

An overview of capillary density and buccal \emptyset_{bv} is presented in Table 4. Mean TCD and FCD was the same in all patients and no difference in MFI was observed. A statistically significant decrease in mean \emptyset_{bv} was found between T0 and T24 (20 ± 4 μ m vs. 16 ± 5 μ m) ($p<0.001$) and T4 and T24 (20 ± 6 μ m vs. 16 ± 5 μ m) ($p<0.05$). No significant difference was detected in mean FCD of the mandibular gingiva between the time points T0, T4 and T24 (respectively 33 ± 16 cpll/mm², 46 ± 36 cpll/mm² and 27 ± 36 cpll/mm²). An overall statistically significant increase in mean buccal mucosa FCD was found overtime (T0: 20 ± 11 cpll/mm², T4: 24 ± 10 cpll/mm² and T24: 25 ± 07 cpll/mm²) ($p<0.05$).



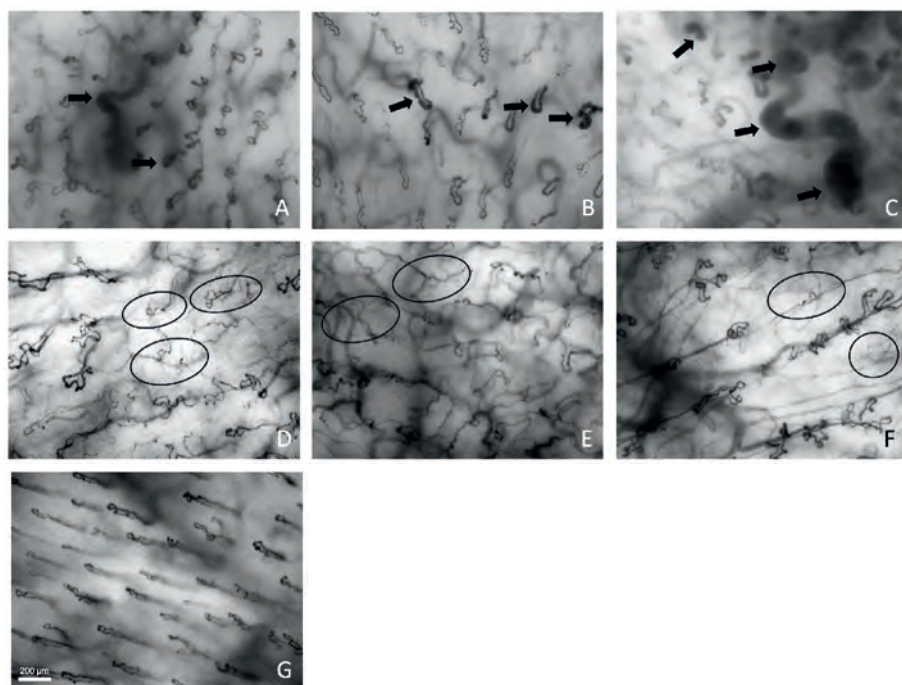


Figure 2. CytoCam images illustrating microvascular alterations in IR buccal mucosa observed across all time points: morphologic alterations in the form of telangiectasias or “ballooning” of vessels (black arrows) at T0 (a), T4 (b) and T24 (c), disorganization, malformation and loss of vessel loops (encircled) at T0 (d), T4 (e) and T24 (f). As a comparison, similar to healthy buccal mucosa, an example of organized vessel loops of the buccal mucosa observed at T24 weeks (6 months) after start of HBOT (g).

However, the difference between the time points was not significant in the post hoc analysis based on the Bonferroni correction. Sample images of buccal and gingiva microcirculation at baseline (T0), after 4 weeks (T4) and after 24 weeks (6 months; T24) are presented in Figure 3. The difference in \emptyset_{bv} and FCD overtime was not statistically significant different between the following groups: (previous) smokers and non-smokers, patients that received CRT and patients that only received RT and between edentulous and dentate patients. An exception to this was a significantly higher \emptyset_{bv} at T4 that was observed in previous smokers compared to non-smokers ($22 \pm 6 \mu\text{m}$ vs. $18 \pm 5 \mu\text{m}$) ($p < 0.05$). Having a history of smoking showed a significant increasing effect ($p < 0.05$) on the change of \emptyset_{bv} between T0 and T4 (unstandardized coefficient B; $B = 3.88$). MFI for both buccal and gingival microcirculations was scored as 3 (normal, continuous blood flow) throughout all time points.

Table 4. Summary of microcirculation measurement in irradiated oral tissue (HNCP). Data is presented in means±SD.

		Buccal mucosa						Mandibular gingival mucosa					
		T0		T4		T24		T0		T4		T24	
FCD	[cpl/mm ²]	20	± 11	24	± 10	25	± 7	33	± 16	46	± 36	26	± 36
MFI	[AU]	3	± 0	3	± 0	3	± 0	3	± 0	3	± 0	3	± 0
Ø _{BV}	[µm]	20	± 4	20	± 6	16	± 5**						

FCD: functional capillary density, MFI: microvascular flow index, Ø_{BV}: blood vessel diameter.

*p<0.05 vs. T4, #p<0.001 vs. T0.

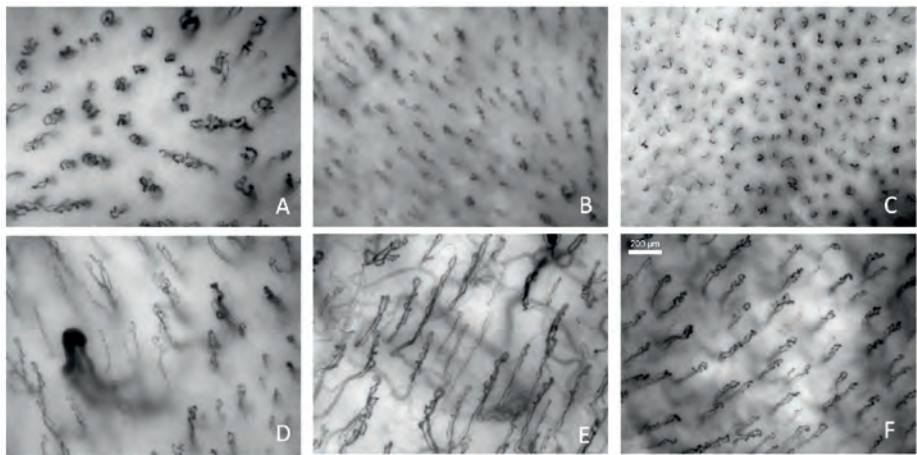


Figure 3. CytoCam images illustrating buccal mucosa at T0 (a), T4 (b) and T24 (c) and mandibular gingival at T0 (d), T4 (e), and T24 (f).

DISCUSSION

The aim of this study was to monitor (over time) the influence of HBOT on irradiated oral mucosal microcirculation in HNCPs using a vital handheld microscope system. The results indicate that HBOT may initiate changes to the IR oral mucosal microcirculation that shift in the direction of healthy tissue microcirculation values by raising vessel density and reducing vessel diameter. A general increase in FCD and a decrease in Ø_{BV} was observed in buccal mucosa 6 months after the start of HBOT. Interestingly, no increase in FCD in mandibular gingival microcirculation was observed. Furthermore, morphological aspects associated with IR microvasculature (telangiectasias, disorganization and loss

of capillary loops) remained present after HBOT. Based on these findings, the hypothesis that HBOT redirects the examined microcirculation parameters towards levels corresponding to healthy tissue could only be partially supported.

Late IR changes in oral microcirculation of HNCP show an increased vessel diameter in irradiated buccal mucosa compared to that of healthy, age-matched control.¹² In the present study a significant decrease of irradiated buccal mucosal \emptyset_{bv} was observed 6 months after HBOT, which indicates a trend consistent with previous measurements of \emptyset_{bv} in healthy buccal tissue.¹² Additionally, the marginally increased percentage of buccal mucosal angioarchitecture to a class 1 was observed 6 months after HBOT which represents a gain of capillary loops akin to normal subepithelial anatomy. Unfortunately, the overall observed expression of class 1 angioarchitecture was not found to be significant after 6 months, nor was the difference in Fd. In our previous study, a described lower mean mandibular gingiva FCD in irradiated tissue compared to healthy tissue might drive the hypothesis of an increase in FCD after HBOT because of its alleged angiogenic potential.¹² The data of the present study did not show a rise of FCD in the mandibular gingiva of HNCP in a follow up period of 6 months after start of HBOT. IR dose history showed that the mandibular mucosa received a higher mean dose compared to the mean dose received on the buccal mucosa. In the view of this finding, the microcirculation in the mandibular mucosa may have been injured to a greater extent and therefore be more difficult to resuscitate with HBOT. Furthermore, there is a great variability in individual response to HBOT of the mandibular tissue shown by the large standard deviations in FCD. This could also explain the varying individual efficacy of HBOT on the underlying etiopathology associated with ORN of the jaw. Although previous microcirculation measurements could not detect a significant difference in mean buccal FCD between irradiated and healthy tissue¹², the present study does show a significant increase in mean buccal FCD measured 6 months after HBOT.

Angiopathies such as telangiectasias has frequently been described in tissue that was subject to IR.^{3,12,13,22,23,35} Altered capillary loops, presenting as telangiectasia-like (ballooning) vessels, were observed at all time points after HBOT. Therefore, it cannot be concluded that HBOT is able to restore capillary loop vascular morphology and reverse pathology associated with microvascular endothelium. However, the degree of “ballooning” of vessels was effectively decreased after HBOT as represented by the measured decreased \emptyset_{bv} . This

could suggest an adaptation in flow dynamics and intravascular pressures in which bulging would be limited in the oral microcirculation.

HBOT has shown to induce neoangiogenesis and increase vascularity in wound healing models and compromised tissues.^{11,14,27} Marx et al. described an eight- to ninefold increase in microangiographically determined vascular density after hyperbaric oxygen (20 sessions, 2.4 ATA) compared to both normobaric oxygen and air-breathing controls in an irradiated rabbit jaw model.¹⁸ Earlier, he described increased microvascular density when obtained and assessed before and after receiving HBOT (20 sessions, 2.4 ATA) in tissue biopsies of 50 irradiated HNCP.¹⁷ In another clinical study looking at buccal mucosal biopsies (3–4 mm depth) of 20 irradiated HNCP, blood vessel density was increased by HBOT after 6 months.³¹ Svaalestad et al. also reported significant increase in blood flow after heat provocation at 3 and 6 months after HBOT when compared to controls. Furthermore, an increased oxygen tension was observed in facial skin after HBOT using transcutaneous oximetry.³² Transmucosal oximetry in ORN patients demonstrated an increase in gingival oxygen tension values from a mean of 50% to a mean of 86% of the oxygen tension of healthy controls after HBOT (30 sessions, 2.4 ATA).³⁶ In the present study the assessment of multiple microcirculation parameters (i.e., vascular function (flow), vascular morphology, angioarchitecture and vascular density) were captured using IDFI and the results revealed an increased mean FCD in irradiated buccal mucosa 6 months after HBOT.

Contradicting results were published by an experimental study that did not observe an effect of HBOT on histological vascular density in the irradiated mandibular skin of rats after different HBOT regimes (18 and 30 sessions, 2.5 ATA) over a period of 12 weeks.²⁸ Furthermore, an increased vessel diameter was noted after irradiation that did not change after HBOT. The results of the present study did show a reversible effect of HBOT on vessel diameter in buccal mucosa with a significant decrease towards healthy tissue values that appear consistent with datasets described in our previous study.¹² It is possible that a delayed effect of HBOT is not detected in studies with a shorter follow up period. However, another experimental study did show histologically increased vascular density in irradiated salivary gland in a mouse model in a short period of 10 weeks after HBOT (20 sessions, 2.4 ATA).²⁹

There are some points of consideration concerning the present study. HNCP often have known comorbidities such as hypertension, diabetes mellitus and



often are (former) smokers. Awareness of the influence of these comorbidities and their compromising effect on the microvascular state and tissue perfusion ahead of enduring (chemo-) radiotherapy (CRT) should be considered and interpreted in context with clinical outcomes and potential supportive care. Measurable effects of (former) smoking and diabetes on oral microcirculation were previously described.^{9,24} The potential resuscitating effect associated with HBOT on late IR injury of the microcirculation could therefore be altered or even latent. The percentage of former smokers in this study was notably low compared with other reports and therefore might concern an underreported observation.^{19,33} However, our results did not show an association of former smoking and the effect of HBOT on microvascular IR injury over a period of 6 months. Additionally, no significant difference in patients with CRT compared with RT alone was found between the time points for all microcirculation parameters. Another point of consideration is that the number of patients in this study are not sufficient to divide into subgroups based on comorbidities to extract potential subtle differences in adverse effects on the microcirculation. Furthermore, the maxillary gingiva was excluded from observation as prevalence of substantial IR on the maxilla was scarce in the HNCP that were referred for HBOT. A further explanation indicates that the highest predilection of squamous cell carcinoma in the HN region is on the tongue and floor of the mouth.³⁷ Finally, although accumulation of plaque could hypothetically influence observed gingival capillary density, no significant association with edentulism and effect of HBOT on gingival FCD was detected in our study.

The present study reports a measurable effect of HBOT in the oral microcirculation of previously irradiated tissue. Future studies should be directed at correlating microvascular parameters to clinical appearance of IR tissue injury. Stages of emerging oral tissue necrosis linked to the state of the microcirculation should be identified and scored. Chairside appraisal of the oral microcirculation in an individual patient could determine *in-vivo* the severity of vascular IR injury that is present, monitor the efficacy of HBOT and consequently direct timing and duration specified to response of the oral tissue requiring supportive care or treatment. Therefore, monitoring microcirculation provides an opportunity to detect emerging pathophysiology in an early state so that supportive therapies could prevent progression of late IR tissue injury to the mutilating and difficult to treat ORN in the HN region. Time-consuming and (relatively) costly HBOT (~€5,000 – €10,000 per patient; average of 30

sessions) could only be committed to selected cases instead of the current potential overtreatment of the general patient population. At the same time a firm decrease in patient quality of life could be avoided by timely clinical monitoring and intervention.

In conclusion, the results of this study indicate that HBOT partially redirects irradiated oral mucosal microcirculation parameters towards healthy tissue state. This could ameliorate the healing capacity of the oral cavity and its surrounding tissues.

ACKNOWLEDGEMENTS

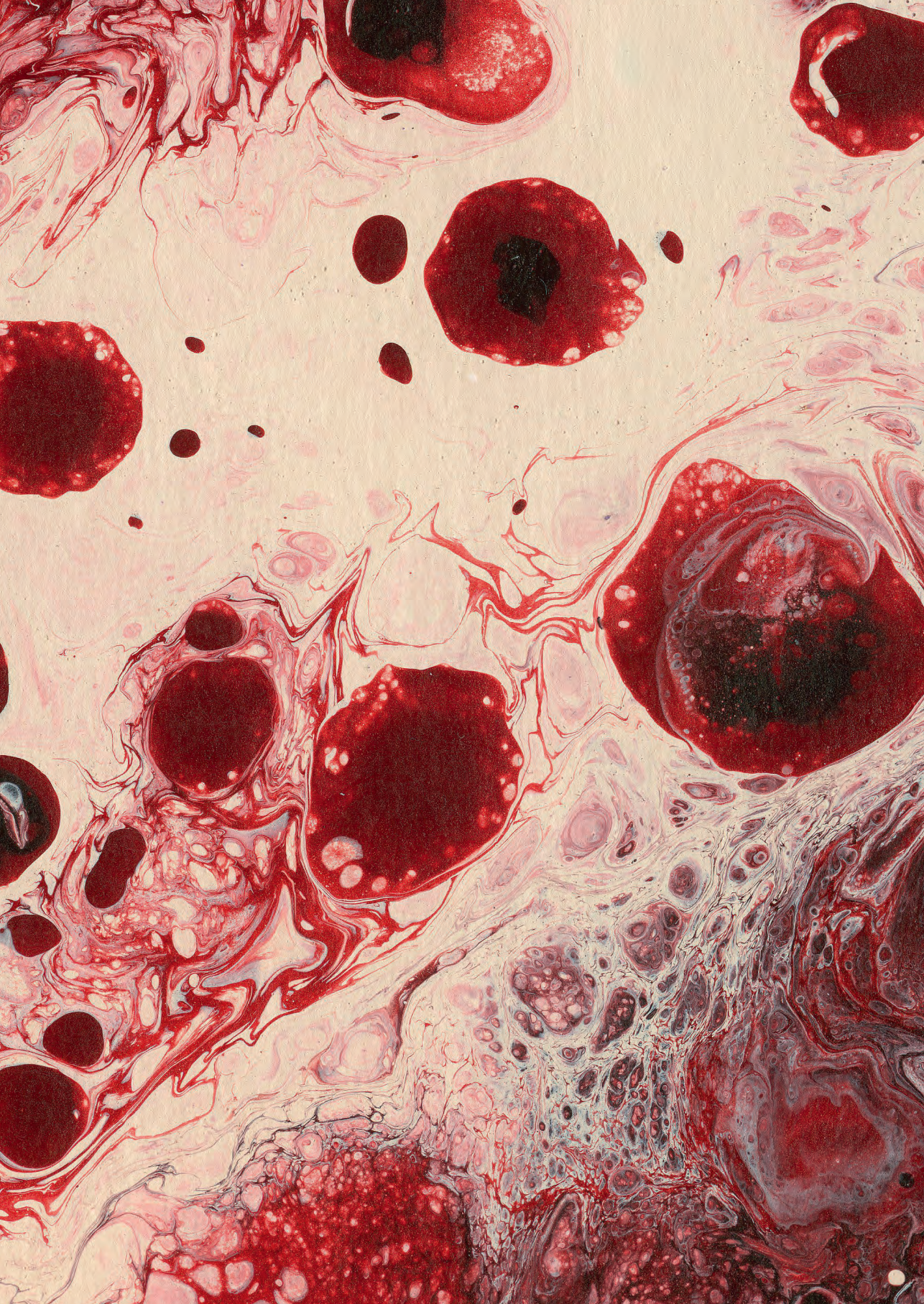
We would like to thank all patients for participating in this investigation. Also, we greatly appreciate the broad support and cooperation regarding the staff of the Hyperbaric Medicine Department. This research was supported by a grant from Fonds NutsOHRA [Nr. 1303-014].

REFERENCES

1. Aykut G, Veenstra G, Scorcella C, Ince C, Boerma C. Cytocam-IDF (incident dark field illumination) imaging for bedside monitoring of the microcirculation. *Intensive Care Med* 2015;3(1):40.
2. De Backer D, Hollenberg S, Boerma C, Goedhart P, Büchele G, Ospina-Tascon G, et al. How to evaluate the microcirculation: report of a round table conference. *Crit Care* 2007; 11(5):R101.
3. Baker DG, Krochak RJ. The response of the microvascular system to radiation: a review. *Cancer Invest* 1989;7(3):287-94.
4. Bennett MH, Feldmeier J, Hampson NB, Smee R, Milross C. Hyperbaric oxygen therapy for late irradiation injury. *Cochrane database Syst Rev* 2016;4:CD005005.
5. Berry RJ, Wiernik G, Patterson TJ, Hopewell JW. Excess late subcutaneous fibrosis after irradiation of pig skin, consequent upon the application of the NSD formula. *Br J Radiol* 1974;47:277-81.
6. Boerma EC, Mathura KR, van der Voort PH, Spronk OE, Ince C. Quantifying bedside derived imaging of microcirculatory abnormalities in septic patients: a prospective validation study. *Crit Care* 2005;9,R601-6.
7. Chang EI, Leon P, Hoffman WY, Schmidt BL. Quality of life for patients requiring surgical resection and reconstruction for mandibular osteoradionecrosis: 10-year experience at the University of California San Francisco. *Head Neck* 2012;34(2):207-12.
8. Dörr W. Radiobiology of tissue reactions. *Ann ICRP* 2015;44(1 Suppl):58-68.
9. Djaberi R, Schuijff JD, de Koning EJ, Wijewickrama DC, Pereira AM, Smit JW, Kroft LJ, Roos Ad, Bax JJ, Rabelink TJ, Jukema JW. Non-invasive assessment of microcirculation by sidestream dark field imaging as a marker of coronary artery disease in diabetes. *Diab Vasc Dis Res* 2013;10(2):123-34.
10. Feldmeier JJ. Hyperbaric oxygen therapy and delayed radiation injuries (soft tissue and bony necrosis): 2012 update. *Undersea Hyperb Med* 2012;39(6):1121-39.
11. Helmers R, Milstein DM, van Hulst RA, de Lange J. Hyperbaric oxygen therapy accelerates vascularization in keratinized oral mucosal surgical flaps. *Head Neck* 2014;36(9):1241-7.
12. Helmers R, Straat NF, Navran A, Nai Chung Tong TAP, Teguh DN, van Hulst RA, de Lange J, Milstein DMJ. Patient-Side Appraisal of Late Radiation-Induced Oral Microvascular Changes. *Int J Radiat Oncol Biol Phys* 2018;102(4):1299-1307.
13. Helmers R, Milstein DM, Straat NF, Rodermond HM, Franken NAP, Savci-Heijink CD, de Boer HH, de Lange J. Outcome of a rabbit model for late irradiation effects in mandibular oral mucosa and bone: A pilot study. *J Clin Transl Res* 2020;6(6):225-235.
14. Hopf HW, Gibson JJ, Angeles AP, Constant JS, Feng JJ, Rollins MD, Zamirul Hussain M, Hunt TK. Hyperoxia and angiogenesis. *Wound Repair Regen* 2005;13(6):558-64.
15. Hutchings SD, Watts S, Kirkman E. The Cytocam video microscope. A new method for visualizing the microcirculation using Incident Dark Field technology. *Clin Hemorheol Microcirc* 2016;62:261-71.
16. Jacobson AS, Zevallos J, Smith M, Lazarus CL, Husaini H, Okay D, et al. Quality of life after management of advanced osteoradionecrosis of the mandible. *Int J Oral Maxillofac Surg* 2013;42:1121-8.
17. Marx RE, Johnson RP. Studies in the radiobiology of osteoradionecrosis and their clinical significance. *Oral Surg Oral Med Oral Pathol* 1987;64:379-90.
18. Marx RE, Ehler WJ, Tayapongsak P, Pierce LW. Relationship of oxygen dose to angiogenesis induction in irradiated tissue. *Am J Surg* 1990;160(5):519-24.
19. Mayer DK, Carlson J. Smoking patterns in cancer survivors. *Nicotine Tob Res* 2011;13(1):34-40.
20. Milstein DM, Romay E, Ince C. A novel computer-controlled high resolution video microscopy system enables measuring mucosal subsurface focal depth for rapid acquisition of oral microcirculation video images. *Intensive Care Med* 2012;38:S271.
21. Mortensen HR, Overgaard J, Specht L, Overgaard M, Johansen J, Evensen JF, Andersen LJ, Andersen E, Grau C. Prevalence and peak incidence of acute and late normal tissue morbidity in the DAHANCA 6&7 randomised trial with accelerated radiotherapy for head and neck cancer. *Radiother Oncol* 2012;103(1):69-75.

22. Prott JF, Handschel J, Micke O, Sunderkötter, Meyer U, Pifko J. Long-term alterations of oral mucosa in radiotherapy patients. *Int J Radiat Oncol Biol Phys* 2002;54(1):203-10.
23. Reinhold HS. The influence of radiation on blood vessels and circulation. Chapter IV. Structural changes in blood vessels. *Curr Top Radiat Res Q* 1974;10:58-74.
24. Scardina GA, Messina M, Melilli D, Cumbo E, Carini F, Tomasello G, Messina P. Permanence of Modifications in Oral Microcirculation in Ex-Smokers. *Med Sci Monit.* 2019 Jan 30;25:866-871.
25. Shaw RJ, Butterworth CJ, Silcocks P, Tesfaye BT, Bickerstaff M, Jackson R, Kanatas A, Nixon P, McCaul J, Praveen P, Lowe T, Blanco-Guzman M, Forner L, Brennan P, Fardy M, Parkin R, Smerdon G, Stephenson R, Cope T, Glover M. HOPON (Hyperbaric Oxygen for the Prevention of Osteoradionecrosis): A Randomized Controlled Trial of Hyperbaric Oxygen to Prevent Osteoradionecrosis of the Irradiated Mandible After Dentoalveolar Surgery. *Int J Radiat Oncol Biol Phys* 2019;104(3):530-9.
26. Shaw RJ, Dhanda J. Hyperbaric oxygen in the management of late radiation injury to the head and neck. Part I: treatment. *Br J Oral Maxillofac Surg* 2011;49(1):2-8.
27. Sheikh AY, Rollins MD, Hopf HW, Hunt TK. Hyperoxia improves microvascular perfusion in a murine wound model. *Wound Repair Regen* 2005;13(3):303-8.
28. Sønstevold T, Johannessen AC, Reed RK, Salvesen GS, Stuhr L. Hyperbaric oxygen treatment did not significantly affect radiation injury in the mandibular area of rats. *Oral Surg Oral Med Oral Pathol Oral Radiol* 2018;125(2):112-9.
29. Spiegelberg L, Braks JA, Groeneveldt LC, Djasim UM, van der Wal KG, Wolvius EB. Hyperbaric oxygen therapy as a prevention modality for radiation damage in the mandibles of mice. *J Craniomaxillofac Surg* 2015;43(2):214-9.
30. Stone HB, Coleman CN, Anscher MS, McBride WH. Effects of radiation on normal tissue: consequences and mechanisms. *Lancet Oncol* 2003;4(9):529-36.
31. Svaalestad J, Hellem S, Thorsen E, Johannessen AC. Effect of hyperbaric oxygen treatment on irradiated oral mucosa: microvessel density. *Int J Oral Maxillofac Surg* 2015;44(3):301-7.
32. Svaalestad J, Thorsen E, Vaagbø G, Hellem S. Effect of hyperbaric oxygen treatment on oxygen tension and vascular capacity in irradiated skin and mucosa. *Int J Oral Maxillofac Surg* 2014;43:107-12.
33. Swoboda CM, Walker DM, Huerta TR. Likelihood of Smoking Among Cancer Survivors: An Updated Health Information National Trends Survey Analysis. *Nicotine Tob Res* 2019; 21(12):1636-1643.
34. Teguh DN, Bol Raap R, Koole A, Knippenberg B, Smit C, Oomen J, van Hulst RA. Hyperbaric oxygen therapy for nonhealing wounds: Treatment results of a single center. *Wound Repair Regen* 202;29(2):254-260.
35. Tsuya A, Wakano Y, Otake M. Capillary microscopic observation on the superficial minute vessels of atomic bomb survivors, 1956-1957. *Radiat Res* 1971;46(1):199-216.
36. Thorn JJ, Kallehave F, Westergaard P, Hansen EH, Gottrup F. The effect of hyperbaric oxygen on irradiated oral tissues: transmucosal oxygen tension measurements. *J Oral Maxillofac Surg* 1997;55(10):1103-7.
37. Vigneswaran N, Williams MD. Epidemiological trends in head and neck cancer and aids in diagnosis. *Oral Maxillofac Surg Clin North Am* 2014;26(2):123-41.
38. Weber MA, Milstein DM, Ince C, Oude Rengerink K, Roovers JP. Vaginal microcirculation: Non-invasive anatomical examination of the micro-vessel architecture, tortuosity and capillary density. *Neurourol Urodyn.* 2015 Nov;34(8):723-729.
39. Withers HR, Peters LJ, Taylor JM, Owen JB, Morrison WH, Schultheiss TE, et al. Late normal tissue sequelae from radiation therapy for carcinoma of the tonsil: patterns of fractionation study of radiobiology. *Int J Radiat Oncol Biol Phys* 1995;33:563-8.







CHAPTER 7

GENERAL DISCUSSION

The pathophysiological process of LRTI remains a significant clinical problem and an ongoing topic of debate given the different theories discussed in the literature.^{1,5,8} Progression and degree of LRTI differs per individual and no scoring index based on (vascular) tissue state is available to classify the onset of tissue injury before clinical symptoms emerge. HBOT is being applied prophylactically prior to oral surgery to prevent disturbed healing in IR tissues, without solid evidence from the current literature and based on differing clinical judgement of the treating physician.¹³ For therapeutic indication, HBOT is administered in cases of tissue necrosis where deterioration is already in a far progressed state and therefore difficult to reverse.

The work presented in this thesis aimed to extend knowledge on development and treatment of LRTI in oral tissue by elucidating the effects of RT and HBOT independently on the oral microcirculation. Additionally, the data aimed to provide more clarity regarding the effects and resuscitating potential of HBOT in previously IR oral tissues in HNCs. Furthermore, the feasibility of using HVM devices (SDF and CC device) in chairside observation of HNCs to identify RT and HBOT induced changes in the microcirculation was examined.

NB and HB hyperoxia-driven microcirculatory changes

Supplemental oxygen is administered to treat tissues with inadequate oxygen saturation levels that are subject to infection or hypoxia due to an underlying pathology and suffer from compromised microvascular blood perfusion. HBOT additionally dissolves O₂ in blood plasma due to pressure causing a higher oxygen tension aside from fully saturated hemoglobin in RBCs. The steep O₂ gradient next to distressed tissue promotes the forming of new capillaries aiding the vascularization process. An experimental model was developed in which sublingual microvascular alterations in response to hyperoxia under NB and HB circumstances was described (Chapter 2). SDFI has proven to be a feasible technique for continuous intrabarochamber microcirculation measurements. Furthermore, in healthy subjects the NB/HB hyperoxia-driven changes in the sublingual microcirculation were observed to be reversible and hyperoxic microvascular response (vasoconstriction) seemed absent in HB conditions as blood vessel diameter did not alter compared to NB normoxia. The latter might indicate a beneficial physiological adaptation to maintain optimal tissue perfusion.



HBOT and wound healing

In an experimental model it was demonstrated for the first time that continuous microcirculation measurements using SDF imaging enabled evaluating wound status by quantifying the vascular regeneration during the healing process over time. The results in Chapter 3 suggested that HBOT positively influenced vascular regeneration as indicated by the elevated FCD in surgically raised oral mucosal flaps in comparison to healing under normal conditions. The findings of this study support the available evidence that HBOT has a beneficial effect on vascularization and wound blood perfusion.^{7,11,12,14,16}

Onset of late IR injury in oral mucosa and bone

LRTI develops in months to years after RT and the progression to tissue necrosis becomes clinically apparent when tissue breakdown occurs. Elucidating the onset of late microvascular IR injury might aid the early detection of tissue deterioration and thereby could promote early diagnosis and the effectuation of timely (preventive) therapies. In Chapter 4 a translational model was introduced that aimed to capture early microvascular alterations associated with the onset of late IR injury. Noninvasive and prospective (11 weeks after RT) measurements of the IR oral mucosal microcirculation with the use of the SDF-device did not show lasting microvascular density changes compared to baseline. However, when angiomorphology was considered, telangiectasias were clearly observed after a single dose of 30 Gy corresponding with post-IR microcirculatory effects as described in other scientific reports.^{2,9,10,15} Gradually with cumulative doses of 22.4 Gy, 26 Gy, 30 Gy and 32 Gy, histological changes developed that presented in the form of decreased vascularity, fibrosis of soft tissue and bone. Moreover, a single dose of 30 Gy histologically provoked necrosis of teeth and bone tissue and a lack of osteoblast lining (periosteum) was observed. These histological findings are in line with previous reports in the literature associated with ORN in human mandibles.⁴

The discrepancy between observations in oral mucosal microcirculation and the histological alterations in the underlying bone suggests that soft tissue microcirculation remains unhindered until LRTI progresses in the underlying bone. It might implicate a process where soft tissue secondarily succumbs to underlying bone necrosis. The histologically observed absence of periosteum might be a precursor to soft tissue ulceration. However, the model presented

in Chapter 4 may not have sufficiently undergone a time period to merit late irradiation injury in general and it might have been too early to observe evolution to the actual late phase in the microcirculation or to clinically develop bone exposure akin to ORN. The observed side effects after 5 weeks (reduced vessel density and decreased platelet count) might involve vascular alterations reflecting the onset of IR injury in a transition phase to late IR injury. Therefore, in future experimental studies the observation period should be prolonged and microvascular injury dose-response prevalence should be assessed by correlation of microcirculation alterations, microvascular morphology and histopathology with progression of IR side effects.

Late IR induced oral microvascular changes

The CC video microscope system, based on IDF illumination imaging, has shown to be feasible in examining and detecting late IR induced changes in the oral microcirculation. HNCPs that received RT at least 6 months prior to measurement show observable changes in their oral microcirculation that could be identified and quantified with a chairside assessment approach. The parameters that express the functionality of the microcirculation such as capillary density, morphology, vessel diameter and flow were captured by a simple outpatient clinic procedure that was well tolerated by the patients. A substantial advantage for *in-vivo* monitoring of the microcirculation is that the presence of flow presents the individual vessels in their functional status, which might reflect the vessel diameter and morphology more accurately than in a histologic specimen. The study presented in Chapter 4 confirms the decreased vascularity corresponding with general findings known to occur in irradiated tissue in the majority of previous studies.^{3,6,9} Compared to healthy oral tissue, angiomorphology changes were predominantly observed in buccal mucosa whereas decreased functional capillary density (FCD) was present in mandibular gingival mucosa.

The observation of telangiectasias was a recurrent phenomenon in IR oral microcirculation in the studies presented in Chapters 4, 5 and 6, which were underreported in the literature by others^{2,9,10,15} and were attributed to compromised vasoregulation that affects hemodynamic function and results in blood stasis.^{2,9,10}



Oral microcirculatory response to HBOT in HN cancer patients

The effect of HBOT on previously established late IR alterations in oral microcirculation was subsequently monitored prospectively *in vivo* with the use of the CC microscope system. The results presented in Chapter 6 indicate that HBOT partially redirects microcirculation parameters towards healthy tissue values by increasing vessel density and reducing vessel diameter. Although these observations might confirm the angiogenic potential of HBOT, the clinical relevance remains undetermined. To which extent IR oral tissue quality needs to be revived to be resistant to further breakdown and to successfully endure future surgical events remains unclear. In other words: when will the tissue arrive to the point of equilibrium that facilitates undisturbed wound healing and that is beneficial for future tissue stability? When this injury resistant state of tissue quality is well-defined, therapy can be adapted to this need and the efficacy of a therapy can be determined.

FUTURE PERSPECTIVES

Although RT and HBOT induced microcirculatory changes can be measured, they have not yet been correlated to clinical findings. Future studies should be focused at grouping patients in categories based on clinical symptoms (for example: no clinical signs, soft tissue ulceration, stages of ORN) and total received RT dose and subsequently correlate these to observed microcirculatory parameters. Comparing the mean values of these microcirculatory parameters between groups and development of an additional scoring system could eventually aid in pinpointing stages of emerging disease and expose a transition phase between no clinical appearance and clinically visible IR pathology. Exposing a transition phase to clinical pathology could offer a window of opportunity for timely tissue supportive treatment (e.g., HBOT, pharmacologic management) and aid in the selection of patients that are in need of treatment. Furthermore, chairside monitoring of microcirculation tissue state (underlying vascular status) during therapy could enhance knowledge on treatment response and desired duration of treatment based on therapeutic efficacy (optimization of treatment protocols). With accurate patient selection for HBOT the general patient population is alleviated from potential overtreatment with lengthy and expensive therapy (approx. €5,000 – €10,000

per patient; average of 30 sessions) that lacks an indisputable scientific basis for the prevention and treatment of ORN and is itself not free of side-effects (temporary visual problems, Eustachian tube problems, claustrophobia and seizure).¹⁷ Furthermore, cost-efficacy of HBOT could be determined when true indication and efficacy of treatment are identified.

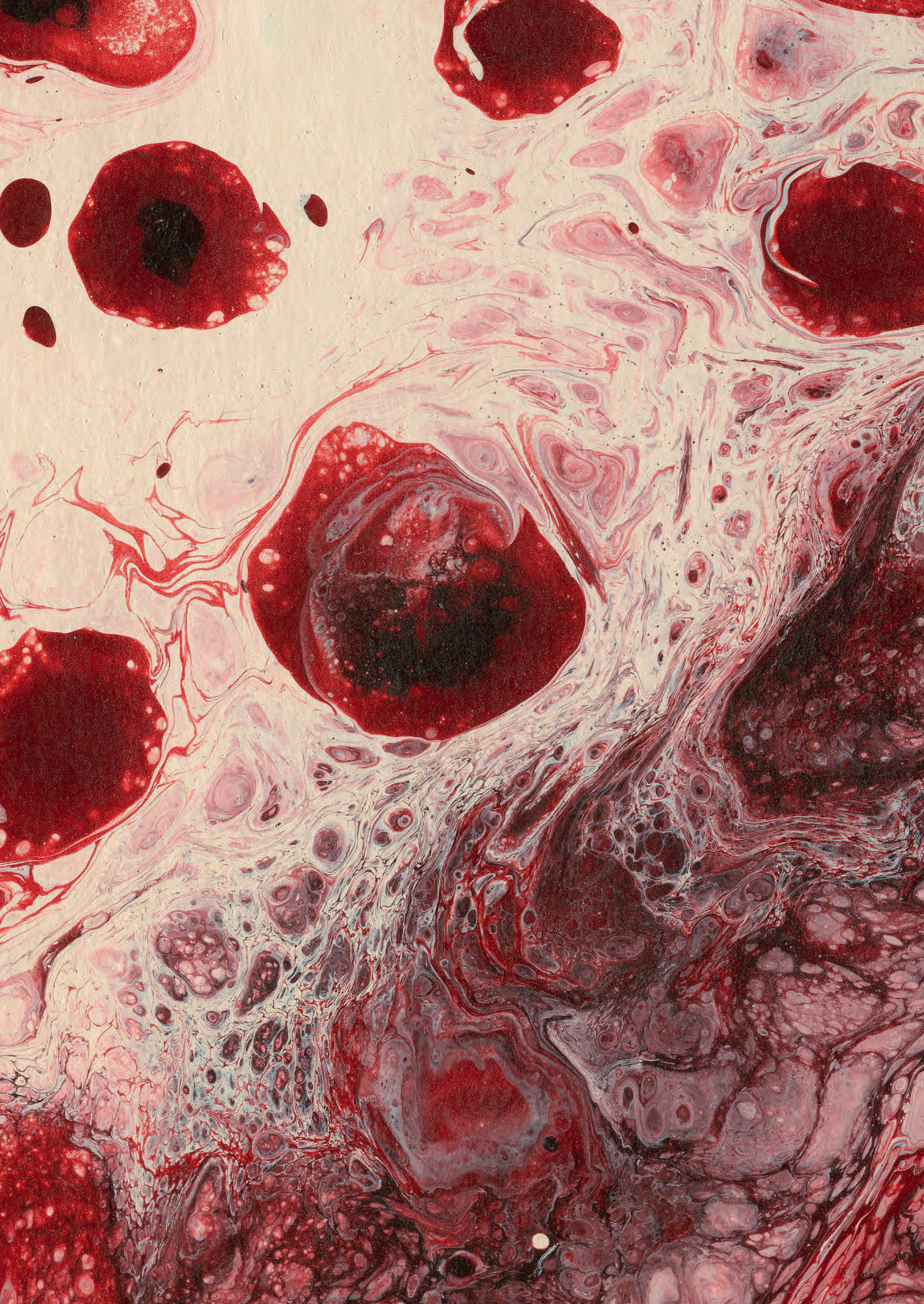
The CC has proven to be clinically feasible for chairside monitoring of the microcirculation. However, quantification of the microcirculation parameters is time consuming and future development of fully automated chairside assessment with instant value calculation of oral microcirculation parameters could aid in the previously described objectives for stage of tissue pathology appraisal and evaluation of efficacy of therapy.

In conclusion, this thesis revealed that microcirculatory changes can be measured and attributed to RT and HBOT. HBOT has shown to partially redirect microcirculatory parameters in IR tissue towards healthy tissue values. Development of a future scoring system for “late radiation microcirculation injury” in oral mucosa would additionally benefit and sharpen the understanding of the pathophysiology related to ORN. A chairside IR injury severity score of a patient’s underlying microvascular status could aid in patient selection and allocation timing and duration of HBOT or other microvascular tissue resuscitating therapies.



REFERENCES

1. Al-Nawas B, Duschner H, Grötz KA. Early cellular alterations in bone after radiation therapy and its relation to osteoradionecrosis. *J Oral Maxillofac Surg* 2004;62:1045.
2. Baker DG, Krochak RJ. The response of the microvascular system to radiation: a review. *Cancer Invest* 1989;7(3):287–294.
3. Bennett MH, Feldmeier J, Hampson NB, Smee R, Milross C. Hyperbaric oxygen therapy for late irradiation injury. *Cochrane database Syst Rev* 2016;4:CD005005.
4. Bras J, De Jonge HK, Van Merkesteyn JP. Osteoradionecrosis of the mandible: pathogenesis. *Am J Otolaryngol* 1990;11(4):244–250.
5. Delanian S, Lefaix JL. The radiation-induced fibroatrophic process: Therapeutic perspective via the antioxidant pathway. *Radiother Oncol*. 2004;73:119–131.
6. Doll C, Durand R, Grulkey W, Sayer S, Olivetto I. Functional assessment of cutaneous microvasculature after radiation. *Radiother Oncol* 1999;51:67–70.
7. Hopf HW, Gibson JJ, Angeles AP et al. Hyperoxia and angiogenesis. *Wound Rep Reg* 2005;13:558–564.
8. Marx RE. Osteoradionecrosis: a new concept of its pathophysiology. *J Oral Maxillofac Surg* 1983;41:283–288.
9. Prott JF, Handschel J, Micke O, Sunderkötter, Meyer U, Pifko J. Long-term alterations of oral mucosa in radiotherapy patients. *Int J Radiat Oncol Biol Phys* 2002;54:203–210.
10. Reinhold HS. The influence of radiation on blood vessels and circulation. Chapter IV. Structural changes in blood vessels. *Curr Top Radiat Res Q* 1974;10:58–74.
11. Rodríguez PG, Felix FN, Woodley DT, Shim EK. The role of oxygen in wound healing: A review of the literature. *Dermatol Surg* 2008; 34:1159–1169.
12. Sander AL, Henrich D, Muth CM, Marzi I, Barker JH, Frank JM. In vivo effect of hyperbaric oxygen on wound angiogenesis and epithelialization. *Wound Repair Regen* 2009;17:179–184.
13. Shaw RJ, Dhanda J. Hyperbaric oxygen in the management of late radiation injury to the head and neck. Part I: treatment. *Br J Oral Maxillofac Surg* 2011;49:2–8.
14. Sheikh AY, Rollins MD, Hopf HW, Hunt TK. Hyperoxia improves microvascular perfusion in a murine wound model. *Wound Rep Reg* 2005;13:303–308.
15. Tsuya A, Wakano Y, Otake M. Capillary microscopic observation on the superficial minute vessels of atomic bomb survivors, 1956–1957. *Radiat Res* 1971;46:199–216
16. Uhl E, Sirsjo A, Haapaniemi T, Nilsson G, Nylander G. Hyperbaric oxygen improves wound healing in normal and ischemic skin tissue. *Plast Reconstr Surg* 1994; 4:835–841.
17. Vudiniabola S, Pirone C, Williamson J, Goss AN. Hyperbaric oxygen in the prevention of osteoradionecrosis of the jaws. *Aust Dent J* 1999;44:243–247.





CHAPTER 8

SUMMARY

Radiotherapy (RT) plays an important part in the treatment of head and neck cancer patients. A late side effect of RT is the progressive process of reduced blood flow and fibrosis of the irradiated tissues, which can result in a compromised healing tendency. In an advanced stage this can lead to necrosis of soft tissue and bone (osteoradionecrosis). This process can emerge several months to years after radiotherapy, either spontaneously or after surgery or wounding. The patient's health status and the amount of radiation dose influence the risk of late side effects. However, based on the previous, it is not possible to fully predict which individual patient will develop osteoradionecrosis over time.

Hyperbaric oxygen therapy (HBOT) is used both preventively and curatively to support healing in irradiated tissue. Previous research has shown that hyperbaric oxygen promotes blood flow in irradiated tissues. However, the precise working mechanism and the type of patients that benefit from therapy remains unclear.

Previous studies have shown that microcirculation assessment is of additional value in diagnosing diseases and predicting their course. With the use of “handheld vital microscopy” (HVM), an imaging technique in the form of a hand-held microscope, it is possible to image the microcirculation down to the level of the red blood cells and to assign a value to the density, diameter, blood flow and shape of the capillaries. The studies in this thesis were performed with the use of this technique.

Chapters 2 and 3 describe experimental studies which demonstrate that the effect of HBOT can be measured in the oral microcirculation directly (in a hyperbaric tank) and over time. It was observed that the direct effect of hyperbaric oxygen in the microcirculation (decrease in vessel density) is immediately restored upon return to normal pressure and oxygen (**chapter 2**). The usual vasoconstriction in response to higher oxygen tension was not observed under pressure in this experiment. This aberrant vascular response under pressure could facilitate oxygen transport to hypoxic tissues (e.g. chronic wound, irradiated tissue). In **chapter 3**, an experimental wound healing model investigates the effects of hyperbaric oxygen on the duration of wound healing in the mouth using repeated microcirculation measurements. A faster healing



tendency was observed in a group exposed to hyperbaric oxygen compared to a control group.

Subsequently, this thesis showed that changes in oral mucosal microcirculation of previously irradiated head and neck cancer patients are measurable and significantly different from oral mucosal microcirculation values of healthy volunteers in the same age group (**chapter 5**). An additional study measured the effect of hyperbaric oxygen on these changes, observing a partial return to the values of healthy oral mucosa six months after treatment (**chapter 6**). This confirms the previously reported observation in the literature that HBOT promotes blood flow. However, it remains unclear at what level of improvement in blood flow a clinical benefit is actually achieved: complete wound healing and the prevention of necrosis. Future studies that correlate the underlying status of the microcirculation with the development of clinical symptoms may contribute to early detection of the severity of late radiation damage. This way timely administration of HBOT could be applied and the effectiveness of the therapy could be monitored in the microcirculation. This way, an unnecessary, costly and extensive hyperbaric oxygen treatment could be spared to a part of the patients, while the therapy can be more accurately focused on a selection of patients who actually benefit from it.

SAMENVATTING

Radiotherapie (RT) speelt een belangrijke rol in de behandeling van patiënten met hoofd-halskanker. Een late bijwerking van bestraling kan zich uiten in een progressief proces van verminderde doorbloeding en verlittekening (fibrose) van de bestraalde weefsels en hiermee zorgen voor een verminderde genezingstendens. In een ver gevorderd stadium kan dit leiden tot het afsterven (necrose) van weke delen en bot (osteoradionecrose). Dit proces kan gedurende maanden tot jaren na radiotherapie ontstaan, zowel spontaan als na een chirurgische ingreep of het ontstaan van een wond. De gezondheidsstatus van de patiënt en de hoogte van bestralingsdosis beïnvloeden het risico op late bijwerkingen. Echter is het op basis hiervan niet volledig te voorspellen welk individu na verloop van tijd osteoradionecrose zal ontwikkelen.

Hyperbare zuurstoftherapie (HBOT) wordt zowel preventief als curatief toegepast ter ondersteuning van de genezing in bestraald weefsel. Uit eerder onderzoek blijkt dat hyperbare zuurstof de doorbloeding in bestraald weefsel bevordert. Het precieze werkingsmechanisme en welk type patiënt baat heeft bij de therapie blijft echter onduidelijk.

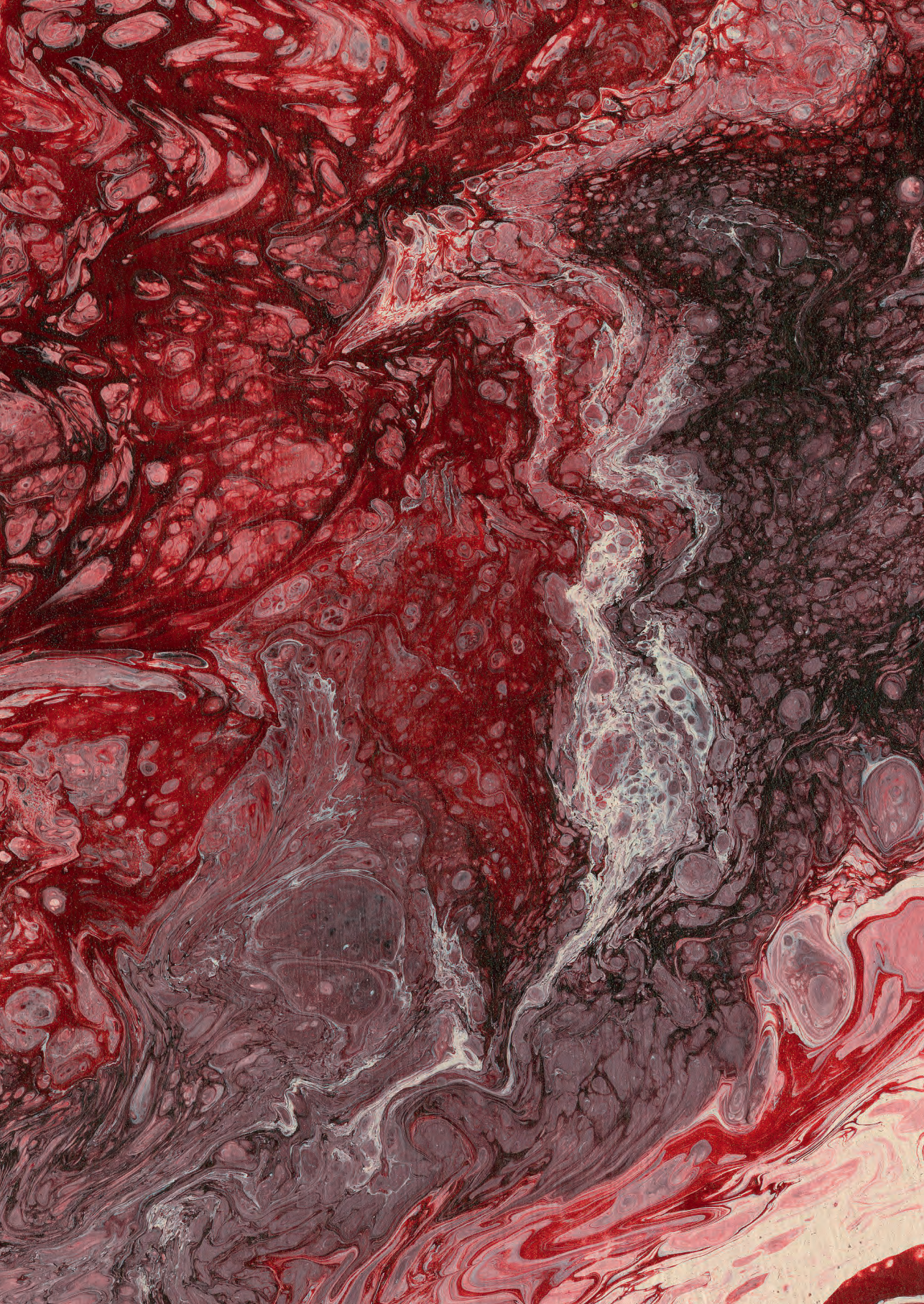
Eerder onderzoek heeft aangetoond dat het monitoren van de haarvaten (microcirculatie) van aanvullende waarde is bij het diagnosticeren van ziektes en de voorspelling van het beloop daarvan. Met de toepassing van “handheld vital microscopy” (HVM), een beeldvormende techniek in de vorm van een handmicroscop, is het mogelijk de microcirculatie in beeld te brengen tot op het niveau van de rode bloedcellen en een waarde toe te kennen aan de dichtheid, diameter, doorbloeding en vorm van de haarvaten. Met behulp van deze techniek zijn de studies in dit proefschrift uitgevoerd.

Hoofdstuk 2 en **3** beschrijven experimentele onderzoeken die aantonen dat de effecten van HBOT te meten zijn in de orale microcirculatie op directe wijze (in een hyperbare tank) en in verloop van tijd. Hierbij wordt gezien dat het directe effect van hyperbare zuurstof in de microcirculatie (het afnemen van de vaatdensiteit) direct herstellen bij terugkeren naar normale druk en zuurstof (**hoofdstuk 2**). De gebruikelijke vasoconstrictie als reactie op een hogere zuurstofspanning wordt in dit onderzoek onder druk niet waargenomen. Deze



afwijkende vaatreactie onder druk zou het zuurstoftransport naar hypoxische weefsels (bijv. chronische wond, bestraald weefsel) kunnen faciliteren. In **hoofdstuk 3** wordt in een experimenteel wondgenezing model gekeken naar de effecten van hyperbare zuurstof op de duur van de wondgenezing in de mond middels herhaaldelijke microcirculatie metingen. Hierbij werd een snellere genezigstendens geobserveerd in een groep blootgesteld aan hyperbare zuurstof in vergelijking met een controlegroep.

Vervolgens heeft dit proefschrift aangetoond dat er veranderingen in de microcirculatie in het mondslijmvlies van in het verleden bestraalde hoofd-hals kankerpatiënten meetbaar zijn en significant verschillen van de microcirculatie waarden in het mondslijmvlies van gezonde vrijwilligers in dezelfde leeftijdsgroep (**hoofdstuk 5**). In een aanvullende studie is het effect van hyperbare zuurstof op deze veranderingen gemeten, waarbij een half jaar na behandeling een gedeeltelijke terugkeer richting de waarden van gezond mondslijmvlies wordt geobserveerd (**hoofdstuk 6**). Hiermee wordt de eerder in de literatuur beschreven observatie dat HBOT de doorbloeding bevordert, bevestigd. Echter blijft onduidelijk bij welke mate van verbetering van de doorbloeding ook daadwerkelijk een klinische winst behaald wordt: een volledige wondgenezing en het voorkomen van necrose. Toekomstige studies die de onderliggende status van de microcirculatie correleren aan het ontwikkelen van klinische symptomen kunnen mogelijk bijdragen aan een vroege detectie van de ernst van de late radiatie schade. Op deze manier zou HBOT tijdig kunnen worden toegepast en de effectiviteit van deze therapie gemonitord kunnen worden in de microcirculatie. Een onnodige, dure en intensieve hyperbare zuurstof behandeling kan op deze manier een deel van de patiënten bespaard blijven terwijl de toepassing nauwkeuriger gericht kan worden op een selectie van patiënten die er daadwerkelijk baat bij hebben.





APPENDICES

CONTRIBUTING AUTHORS

C.N.W. Belterman (CB)

Department of Experimental Cardiology, Amsterdam University Medical Centre (UMC), University of Amsterdam, Amsterdam, The Netherlands

H.H. de Boer (HB)

Department of Pathology, Amsterdam University Medical Centre (UMC), University of Amsterdam, Amsterdam, The Netherlands

N.A.P. Franken (NF)

Laboratory of Experimental Oncology and Radiobiology, Department of Radiation Oncology, Amsterdam University Medical Centre (UMC), University of Amsterdam, Amsterdam, The Netherlands

S. Hackmann (SH)

Department of Large Laboratory Animals, Animal Research Institute Academic Medical Center (ARIA), Amsterdam University Medical Centre (UMC), University of Amsterdam, Amsterdam, The Netherlands

R.A. van Hulst (RvH)

Department of Surgery/Hyperbaric Medicine, Amsterdam University Medical Centre (UMC), University of Amsterdam, Amsterdam, The Netherlands

J. de Lange (JL)

Department of Oral & Maxillofacial Surgery, Amsterdam University Medical Centre (UMC), Academic Centre for Dentistry Amsterdam (ACTA), University of Amsterdam, Amsterdam, The Netherlands

D.M.J. Milstein (DM)

Department of Oral & Maxillofacial Surgery, Amsterdam University Medical Centre (UMC), University of Amsterdam, Amsterdam, The Netherlands

T.A.P. Nai Chung Tong (TT)

Academic Centre for Dentistry Amsterdam (ACTA), University of Amsterdam and VU University Amsterdam

A. Navran (AN)

Department of Radiation Oncology, Netherlands Cancer Institute/Antoni van Leeuwenhoek Hospital, Amsterdam, The Netherlands

H.M. Rodermond (HR)

Laboratory of Experimental Oncology and Radiobiology, Department of Radiation Oncology, Amsterdam University Medical Centre (UMC), University of Amsterdam, Amsterdam, The Netherlands

C.D. Savci-Heijink (CS)

Department of Pathology, Amsterdam University Medical Centre (UMC), University of Amsterdam, Amsterdam, The Netherlands

L.E. Smeele (LS)

Department of Oral & Maxillofacial Surgery, Amsterdam University Medical Centre (UMC), University of Amsterdam, Department of Head and Neck Oncology and Surgery, Netherlands Cancer Institute/Antoni van Leeuwenhoek Hospital, Amsterdam, The Netherlands

N.F. Straat (NS)

Department of Oral & Maxillofacial Surgery, Amsterdam University Medical Centre (UMC), University of Amsterdam, Amsterdam, The Netherlands

D.N. Teguh (DT)

Department of Surgery/Hyperbaric Medicine, Amsterdam University Medical Centre (UMC), University of Amsterdam, Amsterdam, The Netherlands



CHAPTER INFORMATION

Chapter 2

Published as:

Sublingual microvascular perfusion is altered during normobaric and hyperbaric hyperoxia

Authors:

D.M.J. Milstein, R. Helmers, S. Hackmann, C.N.W. Belterman, R.A. van Hulst, J. de Lange

Author contributions:

Study design:	DM, RvH, JL
Conduct of study:	DM, RH, SH, CB
Collection of data:	DM, RH, SH, CB
Analysis and management of data:	DM
Preparation of manuscript:	DM, RH
Review of manuscript:	SH, CB, RvH, JL

Funding sources:

Department and institutional funds.

Conflicts of interest:

None

Chapter 3

Published as:

Hyperbaric oxygen therapy accelerates vascularization in keratinized oral mucosal surgical flaps

Authors:

R. Helmers, D.M.J. Milstein, R.A. van Hulst, J. de Lange

Author contributions:

Study design:	RH, DM, RvH, JL
Conduct of study:	RH, DM, RvH
Collection of data:	RH, DM
Analysis and management of data:	RH
Preparation of manuscript:	RH, DM
Review of manuscript:	RvH, JL

Funding sources:

Department and institutional funds.

Conflicts of interest:

None



Chapter 4

Published as:

Outcome of a rabbit model for late irradiation effects in mandibular oral mucosa and bone: a pilot study

Authors:

R. Helmers, D.M.J. Milstein, N.F. Straat, H.M. Rodermond, N.A.P. Franken, C.D. Savci-Heijink, H.H. de Boer, J. de Lange

Author contributions:

Study design:	RH, DM, HR, NF
Conduct of study:	RH, DM
Collection of data:	RH, HR, NF
Analysis and management of data:	RH, NS, HB
Preparation of manuscript:	RH
Review of manuscript:	DM, NS, HR, NF, CS, HB, JL

Funding sources:

Fonds NutsOHRA [Nr. 1303-014].

Conflicts of interest:

None

Chapter 5

Published as:

Appraisal of late radiation-induced oral microvascular changes at the patient-side

Authors:

R. Helmers, N.F. Straat, A. Navran, T.A.P. Nai Chung Tong, D.N. Teguh, R.A. van Hulst, J. de Lange, D.M.J. Milstein

Author contributions:

Study design:	RH, RvH, JL, DM
Conduct of study:	RH, DM
Collection of data:	RH, NS, TT, DM
Analysis and management of data:	RH, NS, TT
Preparation of manuscript:	RH
Review of manuscript:	NS, AN, DT, RvH, JL, DM

Funding sources:

Fonds NutsOHRA [Nr. 1303-014].

Conflicts of interest:

None



Chapter 6

Submitted as:

Hyperbaric oxygen therapy redirects late irradiation injury in oral microcirculation towards healthy microvascular tissue state

Authors:

R. Helmers, D.M.J. Milstein, N.F. Straat, A. Navran, D.N. Teguh, R.A. van Hulst, L.E. Smeele, J. de Lange

Author contributions:

Study design:	RH, DM, RvH, LS, JL
Conduct of study:	RH, DM
Collection of data:	RH, NS, AN
Analysis and management of data:	RH, NS, AN
Preparation of manuscript:	RH
Review of manuscript:	DM, NS, AN, DT, RvH, LS, JL

Funding sources:

Fonds NutsOHRA [Nr. 1303-014].

Conflicts of interest:

None

LIST OF PUBLICATIONS

In this thesis

Helmers R, Milstein DMJ, van Hulst RA, de Lange J. Hyperbaric oxygen therapy accelerates vascularization in keratinized oral mucosal surgical flaps. *Head Neck*. 2014;36(9):1241-7.

Milstein DMJ, Helmers R, Hackmann S, Belterman CN, van Hulst RA, de Lange J. Sublingual microvascular perfusion is altered during normobaric and hyperbaric hyperoxia. *Microvasc Res*. 2016;105:93-102.

Helmers R, Straat NF, Navran A, Nai Chung Tong TAP, Teguh DN, van Hulst RA, de Lange J, Milstein DMJ. Patient-Side Appraisal of Late Radiation-Induced Oral Microvascular Changes. *Int J Radiat Oncol Biol Phys*. 2018;102(4):1299-1307.

Helmers R, Milstein DMJ, Straat NF, Rodermond HM, Franken NAP, Savci-Heijink CD, de Boer HH, de Lange J. Outcome of a rabbit model for late irradiation effects in mandibular oral mucosa and bone: A pilot study. *J Clin Transl Res*. 2020;6:225-235.

Helmers R, Milstein DMJ, Straat NF, Navran A, Teguh DN, van Hulst RA, Smeele LE, de Lange J. Hyperbaric oxygen therapy redirects late irradiation injury in oral microcirculation towards healthy microvascular tissue state.
(Submitted for publication)

Other

Korfage JA, Helmers R, Matignon Mde G, van Wessel T, Langenbach GE, van Eijden TM. Postnatal development of fiber type composition in rabbit jaw and leg muscles. *Cells Tissues Organs*. 2009;190(1):42-52.

Dubois L, Helmers R, Braun AK. Het belang van triage bij tandletsel: de verschillen tussen het ziekenhuis en de tandartspraktijk [The importance of triage in dental trauma. The differences between the hospital and dental practice]. *Ned Tijdschr Tandheelkd*. 2020;127(5):302-308. Dutch.

Helmers R, Klop C, Schreurs R, de Lange J, Dubois L. Minimally invasive treatment with a patient specific implant in reconstruction of isolated anterior wall fracture of the frontal sinus. *J Craniofac Surg*. 2021;32(1):341-344.



ACKNOWLEDGEMENTS / DANKWOORD

In dit dankwoord wil ik de mensen bedanken die gedurende mijn lange promotietraject wetenschappelijk en sociaal ondersteunend zijn geweest om dit tot een goed eind te brengen.

In de eerste plaats dank aan alle gezonde proefpersonen en patiënten die vaak al na maanden van uitgebreide oncologische zorg toch de tijd hebben willen nemen om voor of na een lange hyperbare tank sessie mee te werken aan dit onderzoek. Daarnaast kan ik de kleine harige proefpersonen (**Bas, Barend, Billy, Björn, Bobby, Casper, Charles, Christiaan, Constantijn, Coos, Bonnie, Clyde, Jackle, Hyde, Butch, the Kid, Mickey en Mallory**) hierbij niet vergeten. Zonder hen was het niet mogelijk geweest om een gestandaardiseerd model te onderzoeken.

Prof. dr. J. de Lange, hooggeleerde promotor, beste Jan. Dank voor het vertrouwen om met mij dit promotietraject aan te gaan. Ongetwijfeld had je vooraf niet gedacht dat ik er zo lang over zou doen en zeker zal je een paar keer gedacht hebben dat ik de handdoek in de ring zou gooien. Wat voor mij begon als een ticket voor de opleiding tot MKA-chirurg heeft zich ontwikkeld in een super leerzaam proces waarbij jij de tijdsdruk nooit hebt opgevoerd (hooguit heb je het je 100x hardop afgevraagd). Al heeft dit misschien voor twee, drie jaar extra gezorgd, het heeft het mij de kans gegeven om mij naast dit promotietraject te ontwikkelen als MKA-chirurg, organisatorisch talent ;) en mijn sociale skills nog enigszins op peil te houden. Toch heb ik een kritische stelling (7) die ook al van toepassing was in 1971 bijgevoegd. Ik bewonder jouw manier van leidinggeven waarbij veel ruimte is voor de ontwikkeling en inbreng van het individu en het team en ik leer dagelijks van jouw delegerende capaciteiten.

Prof. dr. L.E. Smeele, hooggeleerde promotor, beste Ludi. Aan het begin van mijn promotietraject ben jij van grote waarde geweest bij het opstarten van de projecten en mijn introductie in het Antoni van Leeuwenhoekziekenhuis. Hieruit zijn vruchtbare contacten ontstaan die van belang zijn geweest gedurende mijn gehele promotietraject. Naast je wetenschappelijke bijdrage moet ik je nogmaals bedanken voor het kopwerk tijdens de twee Zuiderzee klassiekers



die we met de afdeling gereden hebben. Met jouw steady snelheid waren we ondanks een verlate start weer snel bij de kopgroep!

Dr. D.M.J. Milstein, beste Dan. We hebben elkaar erg goed leren kennen gedurende mijn promotiejaren en veel van elkaar mogen leren. Ik bewonder je onuitputtelijke geest met een mate van wetenschappelijke nieuwsgierigheid die ik nog niet eerder heb gezien. Hierdoor was het soms een uitdaging ons te beperken tot de daadwerkelijke vraagstelling. Waar jij mij leerde notebooks bij te houden van alle onderzoeksprojecten en de vergaarde data met precisie te analyseren en bediscussiëren, leerde ik jou de sandwich methode. Jij hebt me daadwerkelijk wetenschappelijk leren schrijven waarbij ik niets aan de verbeelding mocht overlaten. Ik ben je zeer dankbaar voor de aandacht en nauwkeurigheid waarmee je mijn stukken hebt nagekeken en hebt voorzien van commentaar. Wees altijd welkom voor een glas wijn!

Graag wil ik de leden van de promotiecommissie bedanken voor het kritisch lezen en beoordelen van dit proefschrift. Ik zie uit naar een leerzame gedachtewisseling tijdens mijn verdediging.

De co-auteurs wil ik bedanken voor hun waardevolle bijdrage en betrokkenheid bij dit proefschrift. Tevens veel dank aan de onderzoeks-studenten, tank- en ARIA medewerkers voor hun onmisbare inzet.

Lieve paranimfen **Jessica en Marie-Chris!** Wat ben ik blij dat deze chicks naast mij willen staan tijdens mijn verdediging. Jessie, aangezien we al zo veel fasen van het leven met elkaar gedeeld hebben mag jouw aanwezigheid op deze bijzondere dag niet ontbreken. Jouw humor, onuitputtelijke energie en sprankelende persoonlijkheid zijn een voorbeeld en maken mij altijd vrolijk. Al hebben we geen tijd meer voor duizenden koffietjes en borreltjes tussendoor, onze quality time weekendjes in Antwerpen/Ardennen zijn heel dierbaar voor mij.

MC, partner in crime. Nagenoeg samen gestart in het AMC, samen de opleiding doorlopen en die eindeloze promotie doorstaan. Fijn om altijd samen te kunnen spuien, relativeren, vloeken, roddelen en beeldend de ware aard te bespreken van alle gekkies om ons heen. Ik denk altijd met een glimlach terug aan kamertje A1-116 die we samen met JP ziel hebben gegeven. Ik mis je als

naaste collega, maar ben blij dat we straks samen in de Lutherse Kerk mogen staan!

Beste AMC staf/3D, **Eddy, Fred, Ronald, Jacco, Leander, Pim, Jitske, JP, Tom, Ruud, Juliana en Niels**. Wat een fijne groep mensen om mee te werken. Ondertussen kennen we elkaar door en door en weten we precies wat we aan elkaar hebben. Een mooie verzameling van mensen met aanvullende kwaliteiten die ons als groep sterk maken. De humor, ambitie, gezelligheid en eerlijkheid waardeer ik erg. Veel dank voor het meenemen van dit jonge staflid in de gezamenlijke ambities en de aansporing waar nodig. Ik kijk uit naar de voortzetting van de afdeling als AmsterdamUMC en heb alle vertrouwen in een synergistische samenvloeiing.

Beste A(N)IOS, **Simone, Sophie, Johan, Willem, Jesper, Karel, Jorrit en Brandaan**. Als jong staflid leer ik mogelijk meer van jullie dan jullie van mij. Ik ben trots op jullie als individu en als groep. Het is superleuk om jullie zo snel te zien ontwikkelen in het vak en ik hoop dat mijn vertrouwen in jullie daarin bijdraagt. Stiekem ben ik nog jaloers op jullie AIOS-uitjes en ik ben blij dat we als staf nog af en toe getolereerd worden op de tennis avondjes. Ik ga ervan uit dat jullie mijn promotiefeest een beetje uit de hand laten lopen.

Polikliniek MKA, Beste **Simone, Inge, Drikje, Ingrid, Ingrid, Mandy, Lotte, Samira, Erica, Dennis, Esmee, Annemiek, Yvonne, Yvonne, Ilse, Rachel, Guido, Willemijn, Antoinette en Kasper**. In de afgelopen 2 jaar heb ik me als chef de policlinique mogen bemoeien met het reilen en zeilen van de poli. Een functie waar ik nogal blauw in ging maar met wat klappen van de zweep denk ik wel langzaam ingegroeid ben. Een groep mooie, karakteristieke mensen die ik in de loop van de jaren goed heb leren kennen en ben gaan waarderen. Met het hart op de tong zoals het in Amsterdam hoort. Dat gaat soms ook gepaard met de nodige strubbelingen, maar ik ben trots op jullie persoonlijke groei en ontwikkeling wat bijdraagt aan een hecht team. Op naar de lateraliserie!

Inge, Mireille, Ilse, Riekje en Roel, wat een gezellig team op de dinsdag in Volendam! Een dag waar ik altijd met plezier naar uit kijk! De kibbeling smaakt me maar al te goed en langzaam begin ik zelfs de Volendamse taal mij eigen



te maken. Maatschap NHN, poli MKA Alkmaar en Hoorn, veel dank voor de prettige samenwerking!

Lieve vrienden, we leerden elkaar kennen in de mooiste stad van het land en wat hebben we ondertussen al veel meegemaakt. Het is superfijn om zulke lieve en leuke vrienden te hebben om mooie momenten mee te maken, te vieren en steun te vinden bij de downs. Ik ben supertrots om te zien wat voor sterke mensen ik om mij heen heb en ik leer iedere dag heel veel van jullie. En de grootste gemeenschappelijke deler is dat er bij iedereen wel een steekje los zit. Mijn grootste wens is dat dat zo blijft.

Lieve **mama, papa, Yvonne en Miro**. Jullie staan aan de basis. Dank voor het eindeloze vertrouwen in mij en alles wat ik weer bedenken te gaan doen. Jullie staan altijd voor mij klaar in voor- en tegenspoed en zonder jullie oppas-kwaliteiten zou het allemaal helemaal niet lukken.

Lieve **Lenny**, jij bent mijn thuis. Jij leerde mij kennen als een uithuizig en bezig bijtje en maakt je nu soms een beetje zorgen of ik me niet ga vervelen als dit promotietraject eindelijk klaar is. Je kent me tenslotte ook niet anders. Don't worry, hierna verander ik eindelijk in een zorgzame vrouw die iedere zondagochtend pannenkoeken en appeltaart bakt ;).... Laat ik in ieder geval zeggen dat je er nog wel een aantal tegoed hebt. Zonder jou was me dit niet gelukt. Ik ben heel blij om jou aan mijn zij te hebben en nog trotser op wat voor vader jij bent voor Mila. Haar papa is haar alles. En tenslotte lieve, vrolijke **Mila**, in mijn buik voelde ik al dat je een force of nature zou worden. Jij leert mij het meest over mezelf door me letterlijk een spiegel voor te houden. Geduld heb ik niet en die stel jij nou juist zo graag met je eigenwijsheid en sterke wil op de proef. Maar ik zou het niet anders willen, je bent mijn zonnetje! Ik hou van jullie.

ABOUT THE AUTHOR / CURRICULUM VITAE

Renée Helmers was born on August 31st, 1986 in Amsterdam. She spent her childhood in Amsterdam and attended secondary school at the Vossius gymnasium. At the age of 13 she moved to Hollandsche Rading and graduated in 2004 at the Alberdingk Thijm College in Hilversum. After graduation she moved back to Amsterdam to study Dentistry at the University of Amsterdam in 2004 and subsequently Medicine in 2010 at the Vrije Universiteit Amsterdam. During her medicine studies she worked as a dentist in the evening and at a dentistry emergency post in the weekends in Amsterdam. After finishing her bachelor, she started her PhD simultaneously with her master in Medicine.

After graduating from Medicine in 2014 she started her training in Oral and Maxillofacial surgery at the Amsterdam Medical Centre (head of department: Prof. dr. J. de Lange). In the beginning of 2019, she was registered as an Oral and Maxillofacial surgeon and that same year she started as a consultant at the department of Oral and Maxillofacial surgery at the AmsterdamUMC. Her special interest goes out to oral implantology and trauma. From 2020 she combined her work at the Academic hospital with working in a peripheral hospital (Northwest Clinics).

Renée lives in Amsterdam with Lennart Spaans and their daughter Mila.



